STRUCTURE OF RADIO SOURCES FROM INTERPLANETARY SCINTILLATIONS*

BY

SATYENDRA M. BHANDARI

PHYSICAL RESEARCH LABORATORY

AHMEDABAD- 380009

INDIA

A THESIS SUBMITTED TO THE GUJARAT UNIVERSITY

FOR THE DEGREE OF DOCTOR OF PHILOSOPHY

IN PHYSICS

17 MARCH 1978

---

*Based on observations carried out using the OOTY RADIO TELESCOPE

C O N T E N T S

STATEMENT OF ORIGINALITY

The work presented in this thesis is original and is the result of new investigations carried out by the author. References are given in appropriate places in the text whenever use has been made of the work of others.
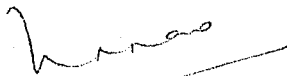
No part of the work presented in this thesis has been submitted previously for any degree or academic award in the Gujarat University or any other University or Institution.

Author

S.M. Bhandari
Physical Research Laboratory
Ahmedabad 380 009, INDIA

Certified by.
Professor-in-charge

Prof. U.R. Rao
Director
ISRO Satellite Centre
Bangalore 562 140, INDIA
         and

Professor
Physical Research Laboratory
Ahmedabad 380 009, INDIA

ABSTRACT OF THE THESIS

STRUCTURE OF RADIO SOURCES FROM INTERPLANETARY SCINTILLATIONS

Understanding the origin and evolution of extra-galactic radio sources, emitting energies of the order of $\sim 10^{60}$ ergs over their lifetime, has been one of the outstanding problems in radio astronomy eversince the identification of radio sources with radio galaxies and QSOs were made. Recent theoretical and observational studies of the structure and morphology of extragalactic radio sources have suggested that the relativistic particles responsible for radio emission are continually produced or accelerated in bright compact 'hot-spots' having angular sizes less than about a second of arc and located near the outer extremeties of the extended components. It is obviously important to study these regions in as much detail as possible with angular resolutions finer than a second of arc.

Observations of the rapid fluctuations in the intensity of a radio source, caused by the presence of electron density inhomogeneities in the interplanetary space, referred to as interplanetary scintillations (IPS), provide a convenient means of obtaining angular resolution of the order of $0''.1$ arc, mostly independent of the wave-

length of observations. The IPS technique has been used extensively to examine the fine sub-arc second structure of radio sources in the northern sky. Comparatively little attention has been paid to high resolution studies of a large number of radio sources catalogued in the southern sky regions. Furthermore, no detailed study of the relationship between compact and extended features of radio source structures has been carried out. The aim of the present work is to extend the IPS studies to radio sources in the southern sky and to use IPS data to investigate the role of compact scintillating components in extended extragalactic radio sources.

The author undertook an IPS survey of a large number of radio sources stronger than about 1.5 Jy in the southern sky, at 327 MHz using the Ooty Radio Telescope. Results on the angular size and fractional flux densities of scintillating compact components in about 200 Parkes and 4C sources in the declination range $0°$ to $-30°$ are presented. We have combined high resolution information on a large number of radio sources at meter wavelengths available from IPS surveys made at Arecibo, Cambridge and Ooty to study the relationship between the fine structure in radio sources revealed by IPS and the overall structure and morphology known from high resolution aperture synthesis observations.

It is shown, for the first time, that clear correlations exist between scintillation visibility μ and

the overall angular extent θ on the one hand and μ and the
flux density S of radio sources on the other. These correla-
tions between μ, θ and S could be interpreted as a distance
effect - weaker sources on the average are located farther
away so as to have smaller overall angular extent and higher
scintillation visibility compared to the stronger sources.
Implications of these results on the estimation of angular
sizes of scintillating components in radio sources are
discussed.

The Thesis is divided into seven chapters.

The first chapter contains a general description
of our present knowledge of the structure of extragalactic
radio sources. Existing IPS studies of the solar wind
plasma and the fine structure of radio sources are briefly
summarized. Objectives and scope of the present work on IPS
studies of southern sky sources are outlined at the end of
this chapter.

The second chapter briefly reviews the theory of
IPS for a point source in the thin-screen approximation used
for interpreting the present IPS observations. Expressions
for calculation of expected scintillation visibility for
simplified models of brightness distribution representing
the observed structures of strong nearby sources are
developed for comparison with observations.

Chapter 3 starts with a brief description of the characteristics of the antenna and the receiver system used for IPS observations and then describes in detail the method of observation and analysis of IPS data obtained at 327 MHz using the Ooty Radio Telescope. Systematic IPS observations of a few strong, compact point-like sources are used to determine the average characteristics of small scale plasma density irregularities in the interplanetary medium. Procedure for estimating the angular size and fractional flux density of scintillating components in extended radio sources is outlined.

In Chapter 4 we present the results on the fine structure of 188 Parkes and 4C radio sources from the southern sky IPS survey. The criteria for selection of sources for IPS observations are listed and an unbiased random sample of stronger 149 sources is defined for the purpose of statistical studies. Incidence of compact scintillating components in different classes of identified and unidentified sources as well as with spectral index and redshift is studied. Comments on the fine structure of a few individual sources of interest are also included in this chapter.

Study of statistical correlations between scintillation visibility and other parameters of radio sources and their interpretations forms the subject matter of Chapters 5 and 6. An attempt is made to understand the IPS data in terms of known multicomponent structure of extended extragalactic radio sources.

Using the presently available IPS data on radio sources covering a wide range of flux density we have first investigated the dependence of scintillation visibility μ on flux density S. Although large statistical uncertainties are present, a correlation between median values of μ and S, free from observational biases, is shown to exist. Weaker sources on the average have larger values of μ compared to the stronger ones.

For the statistically complete sample of 3CR sources we have established a clear correlation between scintillation visibility μ and overall angular extent θ. Model curves for variation of expected μ with decreasing θ were computed for two simplified model brightness distributions representing high resolution structures of 3C33 and Cygnus A using the method outlined in Chapter 2. The observed increase in μ with decreasing θ, when compared with model curves suggests that at meter wavelengths most sources at 3CR flux density level should have multicomponent structures intermediate between those observed in 3C33 and Cygnus A. Also, at meter wavelengths, a significant fraction of total flux density of many 3C sources originates in components with sizes as small as 1/10 to 1/50th of the overall size of the source.

These statistical relations between μ, θ and S clearly provide a strong evidence that weaker sources are located farther away than the stronger ones.

In Chapter 6 the suggestion concerning the use of angular size of compact 'hot-spots' in strongly scintillating radio sources as 'rigid rods' for cosmological studies by Hewish and coworkers at Cambridge, is critically examined. We suggest that due to the presence of multicomponent structure in extended radio sources, the measurement of angular size of scintillating component based on the slope of the scintillation index-elongation curve would lead to an overestimate of the angular size of hot-spots. The estimated angular size is likely to be weighted by larger and larger scintillating substructures in radio sources located at increasing redshifts z. This explains the absence of small diameter scintillating components at large z and provides a non-cosmological interpretation of the $\gamma - z$ relation observed by Cambridge workers.

The main conclusions of the present study are summarized and discussed in the last chapter.

The work described in this thesis is based on the following publications of the author made jointly with other members of the IPS group. Most of the observations, analyses and interpretations described in this thesis are, however, made by the author.

1. Diameter of PKS 1514-24 ($\equiv$ AP Lib)
   S. Ananthakrishnan, A.P. Rao and S.M. Bhandari
   Nature (PS) (1972) 235, 167.

2. Observations of Interplanetary Scintillations at 327 MHz
   A. Pramesh Rao, S.M. Bhandari and S. Ananthakrishnan
   Aust. J. Phys. (1974) 27, 105.

3. Structure of 194 Southern Declination Radio Sources
   from Interplanetary Scintillations
   S.M. Bhandari, S. Ananthakrishnan and A. Pramesh Rao
   Aust. J. Phys. (1974) 27, 121.

4. Correlation of Scintillation Visibility with Flux Density
   and Angular Extent of Extragalactic Radio Sources
   G. Swarup and S.M. Bhandari
   Astrophys. Lett. (1976) 17, 31.

In addition to the above work, the author has also made the following contributions in x-ray astronomy and the study of comets which do not form part of the present thesis.

1. Time variation of the X-ray spectrum and Optical
   Luminosity of SCO X-1
   T. Kitamura, M. Matsuoka, S.Miyamoto, M.Nakagawa, M. Oda,
   Y. Ogawara, K. Takagishi, U.R. Rao, E.V. Chitnis, U.B.
   Jayanthi, A.S. Prakasarao and S.M. Bhandari
   Astrophys. and Sp. Sc. (1971) 12, 378.

2. Occultation of Radio Source PKS 2025-15 by Comet Kohoutek
   (1973f)
   S. Ananthakrishnan, S.M. Bhandari and A. Pramesh Rao
   Astrophys. and Sp. Sc. (1975) 37, 275.

ACKNOWLEDGEMENTS

To begin, I would like to express my sincere debt of gratitude to Professor U.R. Rao, my thesis supervisor, for his inspiring guidance, keen interest and unwavering support throughout the course of the present study. It is indeed a great privilege for me to have been closely associated with him from the very beginning of my research career at the Physical Research Laboratory (PRL), Ahmedabad. I am also grateful to him for giving me the opportunity to independently pursue the present research program of interplanetary scintillation (IPS) studies using the newly built giant Ooty Radio Telescope and for his critical appraisal of the work from time to time.

The IPS program at the Radio Astronomy Centre (RAC), Ooty was carried out by the author in collaboration with Dr.S. Ananthakrishnan and Dr.A. Pramesh Rao and under the guidance of Professor G. Swarup of Tata Institute of Fundamental Research (TIFR), Bombay.

I am deeply indebted to Prof. Swarup, who patiently and most unselfishly directed the course of my research, for his extremely valuable guidance, advice and encouragement. The completion of the present thesis owes much to his increasing enthusiasm for IPS studies. I sincerely

stenciling the thesis in a consistent format in spite of the fact that different unconnected pieces of the manuscript were made available at widely separated times and places.

I wish to thank the personnel at various supporting facilities, in particular the library staff, for their enthusiastic help and cooperation. I should also acknowledge the care with which Mr. Ghanshyam Patel has cyclostyled the thesis.

It will be an important omission if I fail to use this opportunity to record my thanks to Professor Bambang Hidajat of Bosscha Observatory, Indonesia who aroused my interest in the study of comets which led me to suggest a novel "cometary radio source occultation" technique of probing the plasma density structure of comets. The first successful observation of the resulting "cometary scintillations" was made at Ooty by the author in collaboration with his IPS colleagues. This small excursion, though harmful as far as the progress of the present thesis was concerned, has neverthless been highly provocative and absorbing for me. Fruitful discussions and correspondence with Professor Asoka Mendis of University of California, San Diego on various aspects of cometary physics are gratefully acknowledged.

Finally, I dedicate this thesis to my mother who, while encouraging me in my endeavours, silently bore the burden of my long absence from financial and other responsibilities.

AUTHOR

S.M. BHANDARI

STRUCTURE OF RADIO SOURCES FROM

INTERPLANETARY SCINTILLATIONS

CHAPTER 1

INTRODUCTION

1.1 EXTRAGALACTIC RADIO ASTRONOMY

Understanding the origin and evolution of discrete cosmic radio sources has been a fascinating and challenging problem eversince the optical identification of some of the brightest radio sources, e.g. Cygnus A and Fornax A, with external galaxies established their extragalactic nature. Measurements of redshifts and distances of the associated galaxies provided estimates of radio luminosites and characteristic source dimensions. From the observed non-thermal spectrum and linear polarization of radio emission, the radiation mechanism in these radio sources was correctly identified as the incoherent synchroton process. Assuming rough energy equipartition between relativistic electrons and magnetic field, the minimum total energy required to explain the observed radio emission was calculated to be in excess of $\sim 10^{58}$ ergs. Explanation of such enormous energy content of radio sources led to many speculations concerning the primary energy sources in galaxies.

Due to lack of our knowledge of the structure of radio sources, the initial radio observations with poor angular resolutions contributed little towards understanding the origin of radio sources. Photographs of some of the

associated galaxies taken with large optical telescopes, on the other hand, showed a wealth of structure reminiscent of some kind of catastrophic activity in their nuclei. Quite naturally, therefore, all initial attempts to explain the highly energetic phenomenon of extragalactic radio sources were largely governed by the appearance of their optical counterparts. A variety of exotic suggestions e.g. direct collision between two galaxies in motion in a cluster, an accelerated chain reaction of supernova explosions in dense central regions of a galaxy, explosive gravitational collapse of a supermassive stellar body in the nucleus of a galaxy etc., were advanced to explain the generation of radio sources.

Improvements in radio astronomical techniques during the last two decades have resulted in more than a million fold increase in sensitivity and resolving power obtainable at radio wavelengths. Extensive observations with ingeneous application of interferometric, aperture synthesis and lunar occultation techniques have provided accurate positions, optical identifications and structural details of hundreds of radio sources.

Most of the newly identified radio sources are found to be associated either with radio galaxies of E, D or N type or with QSOs. In contrast to galaxies, QSOs appear stellar and their emission and absorption line spectra show high redshifts. In some cases emissions line redshifts exceeding 3 have been observed. On the other hand, the

largest redshift measured for a galaxy associated with a
radio source is only about 0.8. If, as is conventional,
the redshifts of both radio galaxies and QSOs are interpreted
to be wholly due to cosmological expansion of the Universe,
the intrinsic properties of radio sources are observed to
span a wide range of values; their radio luminosities range
from $\sim 10^{41}$ to 10^{46} ergs/sec and their linear sizes range from
less than a kpc to a few Mpc.

The very first interferometric observations of
radio sources revealed a peculiar radio morphology. There
appeared to be no direct correlation between the distribution
of radio and optical emissions. The radio emission, most
surprisingly, was observed to come from two extended regions
straddling the optical galaxy. Subsequent high resolution
studies of the detailed structure of these radio emitting
regions and the discovery of compact non-thermal radio
structures within the nuclei of some of the radio galaxies
have stimulated fresh efforts to understand the physics
of radio sources. A variety of new theoretical models have
been developed. While none of the existing models is
capable of satisfactorily accounting for all known chara-
cteristics of radio sources, the new approach, based on
observed structure and morphology of radio emitting regions,
has been quite fruitful. It is now generally considered
that the origin of radio sources is related to a continuous
or recurrent generation of energy in the nucleus of the parent

galaxy or QSO, rather than in a single catastrophic explosion releasing all the required energy instantaneously. The nature of the ultimate source of energy and details of how the central nucleus energises the compact and extended radio components situated far outside the associated galaxy or QSO are far from understood.

Observations of the fine structure of increasingly large and statistically complete samples of radio sources and a study of the relationship between compact and extended components in them are likely to provide clues for an improved understanding of the physical processes occurring in radio sources. The determination of angular sizes and structures of extragalactic radio sources also provides considerable input to observational cosmology. Recent studies of variation of overall angular sizes of radio sources with redshift and with flux density have shown that a comparison of structure of radio sources over a wide range of flux densities contains useful information on the evolutionary nature of the Universe.

In this thesis we investigate the nature of compact sub-arc second components in a large number of radio sources as revealed by their interplanetary scintillation (IPS) observations at meter wavelengths. In Section 1.2 we first summarize the present knowledge of the structure of radio sources and point out the diverse theoretical explanations that have been proposed to explain the presence of compact scintillating components in them. A brief account of the

existing IPS studies of the plasma density irregularities in the interplanetary medium and of the fine structure of extragalactic radio sources is presented in Section 1.3. The aims and objectives of the present study are outlined in Section 1.4, where a brief description of the organization of the subsequent chapters of the thesis is also provided.

1.2 STRUCTURE OF EXTRAGALACTIC RADIO SOURCES

Extragalactic radio sources have invariably shown structural details down to the finest angular resolution with which they have been examined. The most comprehensive data on their overall structure and morphology come from high frequency aperture synthesis observations of sources from the "3CR complete sample" with angular resolutions upward of a few seconds of arc (Mackay 1971, Jenkins et al. 1977 and references therein).

From lower resolution aperture synthesis maps at 1.4 GHz Mackay (1971) showed that a large majority of sources which could be adequately resolved show a prominent double structure with components placed more or less symmetrically about the associated galaxy or QSO, where identified. These components are found to be extended along the line joining them and remain unresolved perpendicular to it. The brightness distribution is sharply peaked near their outer edges with low brightness 'tails' extending inwards. Sometimes these diffused tails are observed to extend all the way to the

central optical object forming a 'bridge' of emission between the outer components. In some cases a third weak component coincident with the optical object is also detected. The remaining sources show more complex structures e.g. with a pair of components on either side of the optical object etc. However, in nearly all sources the radio emission is observed to come from a narrow, straight or smoothly curved, band in the sky containing all the peaks of emission.

Recently, observations with the Cambridge 5-km aperture synthesis telescope have provided detailed high sensitivity maps of a complete sample of 167 3CR sources at 5 GHz with an order of magnitude better resolution of 2"x2" cosec δ arc (Jenkins et al. 1977 and references therein). These maps reveal much fine structure within the extended components. The bright outermost regions of each of the extended components are now known to contain one or more compact high brightness regions called 'hot-spots'. In addition to such compact regions near the heads, the low brightness tails and bridges often show complex structure with intermediate angular scales. In an increasing fraction of identified sources highly compact radio components coincident with the nucleus of the associated optical object are observed.

The hot-spots usually subtend an angle smaller than about a second of arc and except in a few nearby sources, it has not been possible to directly resolve and study their

structure. Cygnus A and 3C33, being strong and nearby, have been examined in great spatial detail. Cygnus A has been mapped at 5 and 15 GHz with angular resolution of ~2" and ≲ 1" arc respectively (Hargrave and Ryle 1974, 1976). Cygnus A beautifully illustrates most morphological features of powerful extragalactic radio sources and later in this thesis (Fig. 5.7) we have included its brightness distribution map at 5 GHz. 3C33 has been studied with comparable high resolution using lunar occultation and interplanetary scintillation techniques at 327 MHz (Gopal-Krishna et al. 1976) and by aperture synthesis at 5 GHz along with a few other sources (Hargrave and McEllin 1975). These observations are of importance in that most of the emission from these sources, including the compact hot-spots with sizes ranging from about half a kpc to ~ 10 kpc, has been resolved. The hot-spots in these sources represent structures on scales about a factor of 40 to 700 times smaller than their total linear extents.

The central components have been investigated using very long baseline interferometry (VLBI) technique at short cm wavelengths and have been found to contain structures on angular scales of 1-10 milliseconds of arc. It is extremely interesting to note that in a few cases (e.g. 3C111, 154, 236 and Cygnus A), the central components exhibit double or elongated structures which are oriented in roughly the same position angle as the outer extended

doubles (Kellermann et al. 1975, Fomalont and Miley 1975, Menon 1975, Pauliny-Toth et al. 1976). The concurrent presence of central and outer components in a large fraction of radio sources identified with giant elliptical galaxies was also noted earlier by Ekers and Ekers (1973).

The central components have extremely flat or inverted radio spectra at cm wavelengths and are generally self-absorbed at decimeter wavelengths. Hot-spots, on the other hand, usually have normal steep spectra down to meter wavelengths. Thus the compact features that contribute at meter wavelengths are mainly the hot-spots located near the outer extremeties of double radio sources. Extensive lunar occultation studies of the structure of radio sources at 327 MHz at Ooty have indeed shown that, down to about 1 Jy, a majority of sources display a basic double morphology (Kapahi 1975b).

Theoretical Models:

The presence of compact hot-spots in radio sources, in regions farthest from the optical nucleus pose a number of difficulties for many theoretical models of radio sources. Both De Young-Axford and inertial confinement mechanisms require unreasonably large component velocities and thermal plasma density within the components in order to confine the hot-spots to small volumes for the lifetime of the source. This is also supported by the observed

lack of steepening in the radio spectra of hot-spots out to 5 GHz which implies that the lifetime of electrons in the hot-spots is much less than the likely age of the source. Relativistic particles responsible for radio emission from hot-spots must therefore be replenished frequently or must be accelerated continuously (Longair et al. 1973, Hargrave and Ryle 1974).

There are three general types of explanations for the presence of highly relativistic particles at or near the outer boundaries of radio sources. A detailed discussion of various theoretical schemes in relation to the energetics, structure and morphology of radio sources has been provided in many recent reviews on the subject (Longair et al. 1973, Blandford and Rees 1975, De Young 1976). In the following we simply note the interesting diversity of physical conditions involved in the formation of the hot-spots suggested by each of the models.

In one class of models the double radio sources are generated as a result of repeated ejection of relativistic plasma clouds from the associated galaxy or QSO in two opposite directions which are confined by the ram pressure of the external medium (Christiansen et al. 1976). Hot-spots in these models are identified with the fluid-dynamic instabilities which develop near the leading edge of the plasma cloud as it is decelerated by the external medium. These instabilities generate turbulence leading to in-situ particle

acceleration by Fermi mechanism (Pacholczyk and Scott 1976).

The second type of models suppose that the nucleus of the associated galaxy ejects compact massive objects, e.g. spinars or black holes, in two opposite directions to form the double radio structures (Burbidge 1967, Saslaw et al. 1974, Rees and Saslaw 1975). These active massive objects then provide continuous in-situ generation of energy within the outer components. Hot-spots represent these massive objects or regions surrounding them. In another variation of these models the hot-spots have been identified as the discrete clouds ejected by the massive magnetised rotating body located at the outer edges of each of the components (Flasar and Morrison 1976).

In the third class of models the energy is produced in the active nucleus of the optical object and transferred continuously to the outer components in the form of highly collimated beams of low frequency electromagnetic waves or relativistic plasma. The beam pushes out and escavates a cavity in the intergalactic medium (Rees 1971, 1976, Blandford and Rees 1975). Hot-spots are the regions at the ends of the beam where it interacts with the intergalactic medium and accelerates particles to relativistic energies.

These models differ in that they prescribe altogether different processes for transferring energy from the central nucleus to the outer components and for the

formation of hot-spots. However, it is interesting to note that in all current models hot-spots are the regions where energy is input to the extended components on a more or less continuous basis. The energetics, the structure and morphology of the extended components therefore depend mostly on the generation and escape of relativistic electrons from the heads and subsequent confinement by the thermal or ram-pressure of the external medium. It is obviously desirable to study the spectral and structural properties of the hot-spots with high angular resolutions of finer than a second of arc over a range of wavelengths.

Long baseline interferometric and aperture synthesis observations, due to their complexity and cost, have been performed most advantageously at cm wavelengths. At meter wavelengths interferometric observations require baselines of a few thousand kilometers in order to achieve resolutions of the order of 0".1 arc. Observations of interplanetary scintillations of compact radio sources, on the other hand, offer a relatively inexpensive and rapid means of obtaining useful information on the structure of radio sources with angular resolution of ~0".1 arc even at long wavelengths.

1.3 INTERPLANETARY SCINTILLATIONS

Scattering and diffraction of radio waves by plasma density irregularities in the interplanetary medium (IPM) moving radially outwards with the solar wind produce

rapid, faster than about a second, fluctuations in the intensity of radio sources possessing angular diameter less than ~1" arc. These fluctuations or scintillations are referred to as interplanetary scintillations (IPS) in order to distinguish these from analogous phenomena occuring in the ionosphere and the interstellar medium. The phenomenon of IPS, discovered by Hewish and coworkers at Cambridge in 1964, has found a number of applications in studies of the structure of plasma density fluctuations in the interstellar and interplanetary space and of galactic and extragalactic radio sources. A number of reviews covering different aspects of the subject have been published (Cohen 1969, Hewish 1972, Jokipii 1973, Coles et al. 1974, Rickett 1977, Swarup 1978).

The characteristics of the observed scintillations depend on the spatial structure and dynamics of the interplanetary plasma as well as on the angular structure of radio source being observed. The two aspects are not independent, however. Only with a satisfactory knowledge of IPM, IPS data can be interpreted to yield useful information on the structure of sources and vice versa.

In recent years the IPS technique has been established as a useful probe of the solar wind. Numerous single and multi-station observation of IPS of compact radio sources over the last decade have provided valuable new information on the general character of the small scale density fluctuations and the large-scale dynamics of the solar

wind. It is now known that irregularities of electron density responsible for IPS, having a typical scale of ~ 100 km and rms density variations of a few per cent of the background density, are a permanent feature of the interplanetary space out to about 1.5 a.u. from the sun. Measurements of the solar wind velocity have been carried out by cross correlation of the observed scintillation pattern at 3 stations separated by distances of the order of 100 km. Regular observations of a number of strong compact radio sources now provide daily measures of the solar wind velocity over a range of helio-centric distances and latitudes.

Systematic long term monitoring of day to day changes in the IPS activity of a uniform grid of radio sources around the sun have provided valuable ground based method of detecting and studying the structure of corotating high speed streams and flare associated shock waves in the interplanetary medium (Kakinuma and Watanabe 1976 and references therein).

In addition to providing ground based support to in-situ spacecraft observations of IPM, the IPS technique also enables us to probe the solar wind in regions of interplanetary space not yet accessible to space probes i.e. near the sun and outside the ecliptic plane. A number of new results concerning the origin of high speed streams in coronal holes (Watanabe et al. 1974, Rickett et al. 1976) and the increase of solar wind velocity with increasing helio-latitudes (Coles and Rickett 1976) have emerged.

Based on our knowledge of the average characteristics of the structure **of** interplanetary medium, observations of IPS have been extensively used to detect and study the compact sub-arc second structures in a large number of extragalactic radio sources. Comprehensive IPS surveys of radio sources located in the northern sky have been carried out at frequencies ranging from 81.5 MHz to 611 MHz (Cohen et al. 1967b, Little and Hewish 1968, Harris and Hardebeck 1969, Readhead and Hewish 1974). Relatively little attention has been paid to high resolution IPS studies of southern declination radio sources.

1.4 AIMS AND OBJECTIVES OF THE PRESENT WORK

In this thesis therefore our aim is

i) to extend the IPS studies to a large number of radio sources in the declination range of 0° to -30°. To this end the author undertook a large scale IPS survey of about 500 southern Parkes and 4C radio sources at 327 MHz using the Ooty Radio Telescope.

ii) to study the average statistical properties of scintillating components in radio sources of different classes e.g. radio galaxies, QSOs and unidentified radio sources.

iii) to obtain large unbiased samples of radio sources by combining all available IPS studies made at Ooty and elsewhere and study the dependence of scintillation characteristics on distance dependent parameters of radio sources e.g. redshift z, flux density S and

overall angular extent θ.

iv) to investigate the relationship between compact and
extended features of extragalactic radio sources.

In the first part of the thesis (Chapters 2 and 3)
the theory of IPS as applied to the analysis and interpre-
tation of single station of IPS data at 327 MHz is briefly
discussed. The details of the southern sky IPS survey carried
out by the author at Ooty and the results obtained on the
fine structure of first 188 sources are presented in Chapter
4. The correlation of scintillation visibility μ with
spectral index α, redshift z and optical class are also
studied in Chapter 4. In the second part of the thesis
(Chapters 5 and 6) we have examined the statistical corre-
lations between the scintillation visibility μ, the angular
size θ and the flux density S of radio sources. The use
of angular size γ of compact scintillating components derived
from their IPS observations at 81.5 MHz in cosmological
studies is examined. The last chapter summarises the main
conclusion of the present work and comments on some of the
more recent developments in the study of compact components
in extragalactic radio sources.

CHAPTER 2

THEORY OF INTERPLANETARY SCINTILLATIONS

2.1 INTRODUCTION

The phenomenon of interplanetary scintillations (IPS) is caused due to the scattering of radio waves from a distant radio source by the irregularities of plasma density situated in the interplanetary medium (IPM). The general theory of scattering and diffraction effects which occur when electromagnetic radiation traverses a medium containing a large number of randomly distributed inhomogeneities of refractive index, has been discussed extensively in the literature (Ratcliffe 1956, Salpeter 1967, Rumsey 1975 and others).

Most attempts to explain and understand different aspects of scintillation phenomenon are based on the so-called 'thin-screen' approximation. Under this approximation the scattering medium is considered to be equivalent to a thin-transparent phase-modulating screen, located at a certain distance from the observer. In passing through such a screen only the phase of the radio wave is perturbed; the amplitude of the wave remains unchanged. Salpeter (1967) has provided a clear summary of the thin-screen theory of IPS. Little and Hewish (1966, 1968) and Cohen et al. (1967a,b) have discussed the application of the theory of IPS to determine the angular fine structure of scintillating radio sources. Slightly different approaches have been used by the two groups.

Hewish and coworkers base their estimates of the angular size of scintillating components on the variation of the scintillation index of the source with distance from the sun. Cohen and colleagues, on the other hand, determine angular diameters by estimating characteristics of the temporal power spectrum of observed intensity fluctuations.

In this chapter the theory of IPS relevant for determining the fine structure of radio sources from the IPS observations at 327 MHz is briefly reviewed. Theoretical relations between the statistical properties of the random electron density fluctuations in the IPM and the random fluctuations of intensity observed by an observer located on the earth are derived in Section 2.2 for a point source in the thin-screen approximation. Section 2.3 discusses the validity of the thin-screen theory for the present IPS observations at 327 MHz. The effect of the finite angular extent of radio sources on the observed scintillations is investigated in detail in Section 2.4. Expressions for the expected scintillation visibility and angular size of scintillating component are derived for the case of some simplified model brightness distributions representing the observed structure and morphology of extended extragalactic radio sources. A general discussion of the practical limitations of the IPS technique in determining the fine structure of radio sources is provided in the last section.

2.2 THIN-SCREEN THEORY FOR A POINT SOURCE

The geometry of the situation in which the fluctuations in the intensity of a radio source due to IPS are produced and observed by an observer fixed to the earth is sketched in Figures 2.1 (a) and (b). Radiation from an infinitely distant radio source, situated angularly close to the sun in the sky (angular separation ϵ), passes through the IPM. The solar wind plasma containing irregularities of plasma density, flows radially outwards from the sun and fills the interplanetary space. The plane waves from the radio source are scattered in different directions as they encounter the density irregularities. As the unscattered and scattered wave components travel further into the IPM, they interfere with each other to produce a random intensity diffraction pattern. Since the irregularities are convected across the radio path at the solar wind velocity, the spatial intensity pattern is also carried past a stationary observer at the same speed. An observer fixed to the earth, therefore, usually sees irregular temporal intensity fluctuations, which are termed interplanetary scintillations (IPS).

The basic problem in the theory of IPS is to relate the spatial structure of random electron density fluctuations in the IPM to the intensity diffraction pattern at a certain distance z below the scattering region. These relations can, in principle, be obtained by solving the wave equation in a
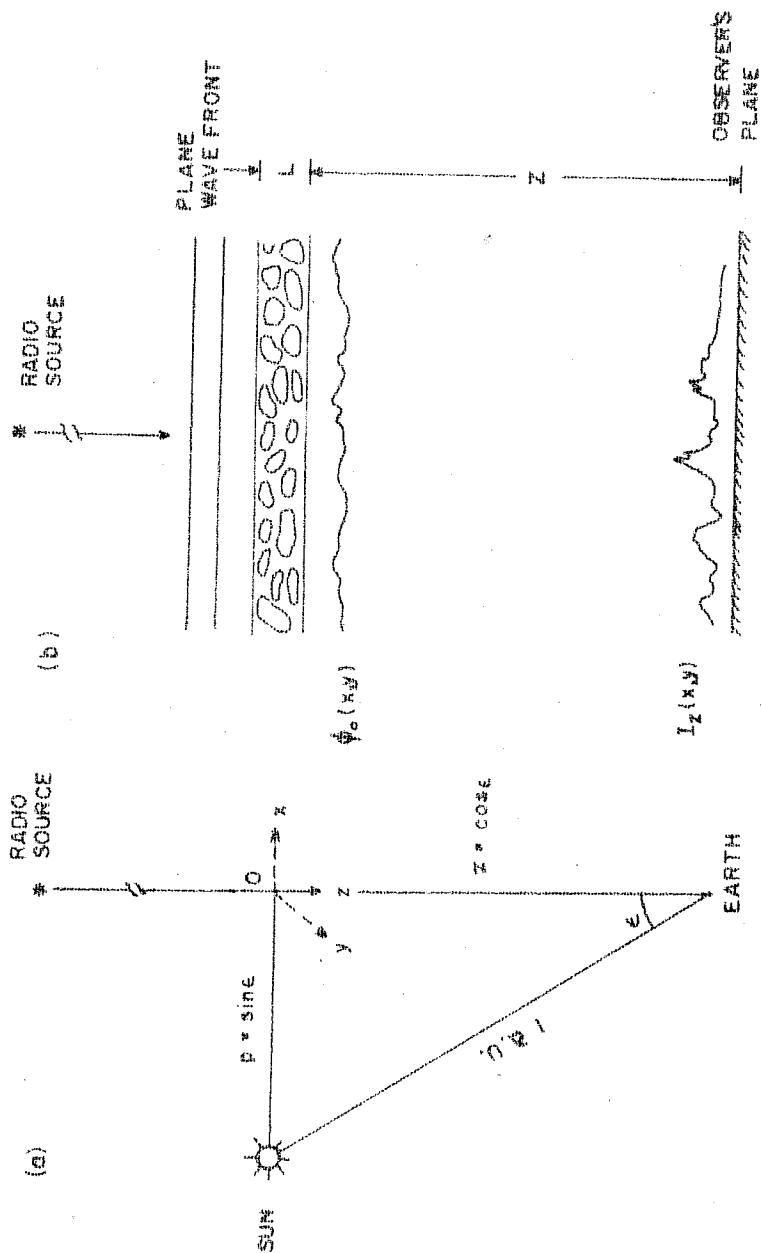
FIG. 2·1 GEOMETRY OF IPS PHENOMENON

randomly inhomogeneous medium. This poses difficult problems and analytical solutions have been obtained after making suitable approximations. These are discussed below.

2.2.1 Thin-Screen Approximation:

Due to the fact that irregularities are present throughout the IPM, radio wave scattering takes place virtually all along the line of sight to the source intercepted by the IPM. However, since both the background electron density N_e as well as the fluctuations in electron density $\triangle N_e$ decrease rapidly with increasing distance R from the sun (approximately as R^{-2}), the scattering power of the medium falls of roughly as R^{-4}. Most of the scattering and phase fluctuations are therefore introduced in a localized region of the IPM in the vicinity of point 0 of the line of sight, which is nearest to the sun. As illustrated in Figure 2.1(b) the extended IPM can be considered to be confined to a layer of equivalent thickness L situated at a distance z from the observer. If L is defined as the distance between those points along the line of sight where the scattering falls to half its maximum value at point 0, then we have

$$L \simeq 1.2\,p \quad \text{in a.u.}$$

$$\cdots (2.1)$$

where $p(=\sin\epsilon)$ is referred to as the solar elongation of the source and is measured in a.u. (see Fig. 2.1). Now if L is small compared to the distance z of the observer from

the scattering layer and if the following inequalities,

$$L \gg a \gg \lambda \qquad \ldots (2.2)$$

where   a is typical size of the electron density irregulari-
ties and λ is the wavelength of the incoming radio waves, are
satisfied then the scattering layer of thickness L can be
replaced by an equivalent thin-screen.   In passing through
such a thin-screen, the phase of the radio wave gets randomly
modulated but the amplitude remains constant.   It is also
assumed that the hypothetical thin-screen imposes the same
amount of phase fluctuations as the actual extended inter-
planetary medium.   Salpeter (1967) has shown that thin-screen
treatment provides a reasonable explanation of the observed
characteristics of IPS. In what follows we derive the theore-
tical relations between the statistical parameters of the
screen and the parameters of the observed intensity fluctuat-
ions based on the thin-screen assumption.

The irregular electron density fluctuations in the
medium are characterized by a stochastic process which is
assumed to be spatially as well as temporally 'stationary'.
The random nature of irregularities suggests that these can
most usefully be described in a statistical manner, in terms
of their correlation functions and power spectra.

Let $\rho(\bar{r})$ represent the spatial auto-correlation
function o(acf) of the electron density fluctuations ΔN_e, then

$$\rho(\bar{r}) = \langle \Delta N_e(\bar{r}_0) . \Delta N_e(\bar{r}_0 + \bar{r}) \rangle / \langle \Delta N_e^2 \rangle \qquad \ldots (2.3)$$

where $\langle \Delta N_e^2 \rangle$ is the mean-square electron density fluctuation, and $\bar{r}$ is the spatial coordinate in the plane perpendicular to the direction of propagation. $\rho(r)$ is normalized such that $\rho(o) = 1$. There is some controversy regarding the form of $\rho(r)$. Jokipii (1973) and many others have argued that both the large scale ($\sim 10^{5-6}$ km) fluctuations in the solar wind parameters as well as the small scale ($\sim 10^2$ km) density fluctuations responsible for IPS could be described by a common power-law wavenumber spectrum. Hewish (1972) and others, on the other hand, support an independent gaussian spectrum for IPS irregularities based on the observed linear dependence of scintillation index on wavelength of observations and flattening of both the spacecraft as well as IPS spectra near wavenumbers corresponding to proton gyro-radius in the IPM. We have assumed here a symmetrical gaussian form for $\rho(r)$ due to its plausibility and analytical simplicity:

$$\rho(r) = \exp(-r^2/2a^2) \qquad \qquad \dots (2.4)$$

The correlation length 'a' can be interpreted as the typical size of the plasma density irregularities. Bramley (1954) has shown that the two-dimensional phase fluctuations $\varphi(x,y)$ imposed on the radio waves traversing the screen along z will also have a gaussian acf with a correlation length equal to that of the density fluctuations. The rms phase fluctuation φ_o at the exit plane of the screen will depend on the wavelength λ of the incoming radiation, the thickness L of the scattering medium, the size a of the irregularities and,

of course, on ΔN_e as

$$\langle \varphi_0^2 \rangle^{\frac{1}{2}} = \varphi_0 = (2\pi)^{\frac{1}{4}} r_e \lambda (aL)^{\frac{1}{2}} \langle \Delta N_e^2 \rangle^{\frac{1}{2}} \qquad \ldots (2.5)$$

where $r_e (= 2.8 \times 10^{-18} \text{ km})$ is the classical electron radius. At this point i.e. when the wave just emerges from the thin-screen, it contains only random phase fluctuations. But as it travels away from the screen, amplitude fluctuations build up progressively until a constant level is reached at large distances.

Once the statistical properties of phase fluctuations at a plane just below the screen are specified, the properties of the intensity pattern $I_z(x,y)$ at certain distance z, can be determined by considering the propagation of the phase-perturbed wavefront in free space beyond z = o to the observer.

Let the statistical properties of the random diffraction pattern $I_z(\bar{r})$ at a distance z below the screen (see Fig. 2.1 (b)) be described by the spatial auto-correlation function $M_z^2(\bar{r})$ and the power spectrum $M_z^2(\bar{q})$ of the intensity. These are given by

$$M_z^2(\bar{r}) = m_z^2 \, \varrho(\bar{r}) = \left[\langle I_z(\bar{r}_0) . I_z(\bar{r}_0 + \bar{r}) \rangle - \bar{I}^2 \right] / \bar{I}^2 \qquad \ldots (2.6)$$

where m_z is the scintillation index and is defined as the root mean square fluctuations in the observed intensity relative

to the total intensity of the incident radiation. If the intensity of the source is taken as $\bar{I} = 1$ then

$$M_z^2(\bar{r}) = \langle I_z(\bar{r}_o) \cdot I_z(\bar{r}_o + \bar{r}) \rangle - 1 \qquad \ldots(2.7)$$

$M_z^2(\bar{q})$ is simply the Fourier transform of the auto-correlation function $M_z^2(\bar{r})$;

$$M_z^2(\bar{q}) = \int_{-\infty}^{+\infty} M_z^2(\bar{r}) \; e^{-i\bar{q} \cdot \bar{r}} dr \qquad \ldots(2.8)$$

The characteristics of the intensity pattern produced at any distance z depends fundamentally on whether the rms phase fluctuation φ_o is substantially smaller or larger than 1 radian. The scintillations in the two regimes, referred to as the weak and the strong scattering conditions respectively, are discussed below.

2.2.2 Weak-Scattering Condition ($\varphi_o^2 \ll 1$):

Salpeter (1967) has shown that in the small φ_o^2 limit the two-dimensional spatial spectrum of intensity fluctuations $M_z^2(\bar{q})$ and the two-dimensional phase spectrum $\phi_o^2(\bar{q})$ at $z = o$ are directly related as

$$M_z^2(\bar{q}) = 4 \phi_o^2(\bar{q}) \; \sin^2(\lambda z q^2 / 4\pi)$$

$$= 4 \phi_o^2(\bar{q}) \; \sin^2(q^2 / q_F^2) \qquad \ldots(2.9)$$

where $q_F = (4\pi/\lambda z)^{\frac{1}{2}}$. The term $\sin^2(q^2/q_F^2)$ is called the Fresnel filter, since it acts as a high pass filter on $\phi_o^2(\bar{q})$; it strongly attenuates small wavenumber $(q < q_F)$ components in the diffraction pattern without appreciably affecting the form of $M_z^2(\bar{q})$ at large wavenumbers. This implies that irregularities of size equal to the diameter of the first Fresnel zone $2\sqrt{\lambda z}$ or smaller are most effective in producing intensity fluctuations at a distance z from the screen. Larger irregularities contribute mainly to phase fluctuations.

The intensity spectra are usually described by two parameters; the total fluctuation power

$$m_z^2 = \int_{-\infty}^{+\infty} M_z^2(\bar{q}) \, d\bar{q} \qquad \qquad \ldots(2.10)$$

where m_z is the scintillation index and the scale q_2 along any direction x perpendicular to the line of sight

$$q_2^2 = \int_{-\infty}^{+\infty} q_x^2 M_z^2(\bar{q}) \, d\bar{q} \Big/ \int_{-\infty}^{+\infty} M_z^2(\bar{q}) \, d\bar{q} \qquad \ldots(2.11)$$

From eqn. (2.4) we have the phase spectrum as

$$\phi_o^2(\bar{q}) = (\phi_o^2 a^2/2\pi) \, e^{-a^2 q^2/2} \qquad \qquad \ldots(2.12)$$

Thus eqn. (2.9) becomes

$$M_z^2(q) = (4\varphi_0^2 a^2/2\pi) \; e^{-a^2 q^2/2} \; \sin^2(\lambda z q^2/4\pi) \qquad \ldots(2.13)$$

Using the definitions provided in (2.10) and (2.11) we obtain

$$m_z^2 = 2\varphi_0^2 \left[1+(z_0/2z)^2\right] \qquad \text{and} \qquad \ldots(2.14a)$$

$$q_2^2 = (1/a^2) \left[1+2/\left\{1+(2z/z_0)^2\right\}\right] \qquad \ldots(2.14b)$$

where $z_0 = 2\pi a^2/\lambda$ is the 'Fresnel distance' of irregularities of size a. In analogy with the diffraction at optical wavelengths the behaviour of scintillation in the near field $(z/z_0 \ll 1$; Fresnel region) and the far field $(z/z_0 \gg 1$; Fraunhofer region) is different as discussed below.

a) $\qquad z/z_0 \ll 1$

In the near-field case we have from eqns. (2.14)

$$m_z^2 = 8(z\varphi_0/z_0)^2 \quad \text{or} \quad m_z = \sqrt{2}\,\varphi_0(2z/z_0) \qquad \text{and} \qquad \ldots(2.15a)$$

$$q_2^2 = 3/a^2 \qquad \text{or} \quad q_2 = \sqrt{3}/a \qquad \ldots(2.15b)$$

This means that, close to the screen the scintillation index is very small since both φ_0 and z/z_0 are less than one. Also the scale of intensity fluctuations ℓ is smaller than a by about $\sqrt{3}$. This is due to the effect of the Fresnel filter

discussed earlier.

b) $z/z_o \gg 1$

In this far-field case, the $\sin^2$ term in eqn. (2.9) oscillates rapidly and can be replaced by its mean value of 1/2. This gives

$$m_z^2 = 2\varphi_o^2 \quad \text{or} \quad m_z = \sqrt{2}\,\varphi_o \quad \text{and} \qquad \text{...(2.16a)}$$

$$q_2^2 = (1/a^2) \quad \text{or} \quad q_2 = 1/a \qquad \text{...(2.16b)}$$

This shows that at distances from the screen larger than z_o, the intensity scintillations are fully developed and m_z is independent of z. Also the Fresnel filtering effects are negligible and the pattern scale ℓ is equal to the scale of phase fluctuations close to the screen. This is the simplest case since, only when $\varphi_o^2 \ll 1$ and $z/z_o \gg 1$, the parameters of the observed diffraction pattern can be directly related to the properties of the scattering medium. As will be shown later, most of the present IPS observations at 327 MHz with $p \gtrsim 0.2$ a.u. satisfy these conditions and therefore can be used directly to estimate ΔN_e and 'a' at different distances from the sun (Cohen et al. 1967a, Rao et al. 1974, Rao 1975).

2.2.3 Strong-Scattering Condition ($\varphi_o^2 \gg 1$):

When $\varphi_o^2 \gg 1$ the analytical solution of the full wave equation poses difficult problems. Until recently no satisfactory theory was available for interpreting observations taken in strong scattering conditions which occur when the line of sight to the source passes through the denser corona close to the sun. Earlier, using numerical methods, Mercier (1962) and Bramley and Young (1967) computed the variation of the index and scale as a function of distance for values of φ_o up to about 3. Recently, numerical evaluation of the appropriate integrals have been extended to arbitrarily large values of φ_o and at all distances z from the screen. Both the rms intensity fluctuations as well as the intensity spectra are evaluated as a function of z for screens with gaussian as well as power-law wavenumber spectra (Buckley 1975, Rumsey 1975, Marians 1975). Close to the screen geometrical optics approximation is valid and irregularities act as individual lenses, randomly focussing and defocussing the intensity at different points. Close to the screen, the scintillation index is small but increases rapidly with increasing distance from the screen. At distances comparable or equal to the focal length of irregularities of size a (given by $2\pi a^2/\lambda\varphi_o$), the scintillation index approaches values close to unity and the scintillations have a 'spiky' appearance. At distances much larger than z_o or z_o/φ_o the index asymptotically settles to unity. The

scale of the diffraction pattern ℓ , however, always remains smaller than the correlation length a of phase fluctuations. When $\varphi_o^2 \gg 1$ and $z/z_o \gg 1$, we have

$$m_z = 1 \qquad \text{and}$$

$$q_2 \simeq \sqrt{2}\, \varphi_o /a \qquad \qquad \ldots (2.17)$$

2.2.4   The Observed Spectra of IPS:

In the sections above we have derived and discussed the relation between $\phi_o^2(\bar{q})$ and $M_z^2(\bar{q})$ in different conditions. Determination of $M_z^2(\bar{q})$ requires sampling of $I_z(\mathbf{x},y)$ over a region much larger than the spatial scale ℓ of the pattern and is therefore extremely difficult. Measurements of the intensity pattern at the plane of the observer is however made possible because the solar wind plasma moves radially outwards from the sun in a fairly ordered way, allowing the observer to sample different portions of the intensity pattern as it drifts past the observer. An observer located at a fixed point on the earth therefore measures, not $I(x,y)$ but $I(t)$ i.e. the intensity as a function of time. Scintillation data therefore yield temporal rather than the spatial spectrum. Nevertheless, if the screen is assumed to drift across the observer without changing or restructuring itself over time periods large compared to the time scales of intensity fluctuations, the observed temporal spectra can be related

to the spatial spectra. If, as indicated in Figure 2.1(a), the screen is assumed to move along the x-axis, with a velocity v, then the two-dimensional spatial spectrum $M_z^2(\bar{q})$ will be observed as a temporal spectrum $P(f)$:

$$P(f) = (2\pi/v) \int_{-\infty}^{+\infty} M_z^2(2\pi f/v, q_y) \, dq_y \qquad \ldots(2.18)$$

where the temporal frequency f is related to spatial frequency by $q = 2\pi f/v$. Thus the observed temporal spectrum $P(f)$ is effectively a one-dimensional strip-scan of the two dimensional spatial intensity spectrum.

The second moment f_2 of the temporal power spectra $P(f)$ can be evaluated using eqns. (2.13), (2.14) and (2.18). For the thin-screen, weak-scattering case

$$f_2^2 = (v/2\pi a)^2 \left[1+2 / \left\{1+(2z/z_0)^2\right\}\right] \qquad \ldots(2.19)$$

(Rao et al. 1974).

Eqn. (2.19) reduces to

$$f_2 = v/2\pi a \qquad \ldots(2.20)$$

for the far field ($z/z_0 \gg 1$) case. It must be noted that the measured width of the one-dimensional temporal power spectrum corresponds to the width of the spatial power spectrum in the x-direction.

2.3 VALIDITY OF THE THIN-SCREEN APPROXIMATION

In deriving the theoretical expressions for the observed intensity pattern produced due to the scattering of radio waves in the extended interplanetary medium, we have replaced the medium by a thin-phase screen. The advantages we had were that the multiple scattering and diffractive effects leading to amplitude fluctuations within the medium could be safely ignored. Salpeter (1967) has shown that the thin-phase screen approximation can be considered valid if the thickness of the medium L satisfies the following conditions.

i) $\qquad L \gg a \gg \lambda$ and

ii) $\qquad L \ll z , \qquad L \ll z_o \qquad$ or $\quad L < (2\pi a^2/\lambda).$

First set of inequalities are a consequence of the requirement that the scale size over which the phase varies must be large compared to wavelength and ensures small angle scattering. $L \gg a$ requires that a large number of irregularities contribute to phase fluctuations. Since L is of the order of 0.1 - 1.0 a.u., $a \simeq 100$ km and $\lambda \simeq 10^{-3}$ km, these inequalities are always satisfied strongly.

The second set of inequalities directly relate to the validity of replacing the extended medium by a thin-screen. The equivalent thickness L of the scattering layer must be smaller than its distance z from the observer. Further, in order that no diffractive intensity fluctuations develop

before the perturbed wavefront emerges from the layer, L must be much smaller than z_o, the Fresnel distance of the irregularities.

Most IPS observations described in this thesis were carried out at 327 MHz for $0.1 \lesssim p \lesssim 0.7$ a.u. Therefore, from Figure 2.1 and eqn. (2.1) we have

$$1.0 > z > 0.7 \text{ a.u.}$$
$$0.1 \lesssim L \lesssim 0.8 \text{ a.u.}$$

and $\quad z_o = 2\pi a^2/\lambda \simeq 0.45 \text{ a.u.} \checkmark$

The condition $L < z_o$ is therefore violated only when $p \gtrsim 0.3$ a.u. and implies that intensity fluctuations may develop within the scattering layer. For observations with $p \gtrsim 0.3$ a.u. the effects of the thickness of the screen must be taken into account. However, as will be shown later, for observations at 327 MHz, $\varphi_o^2 << 1$ for $p \gtrsim 0.2$ a.u. Any intensity fluctuations within the layer therefore, are likely to be negligibly small (Rao et al. 1974). The problem of scintillations produced by an extended medium can still be treated by considering the medium to be made up of a number of independent thin-screens lying on top of each other. The intensity spectrum produced under such conditions is the integral of eqn. (2.9) over the thickness of the medium, and the scintillation index is equal to the rms of indices produced by individual thin screens (Little and Hewish 1968). We must however make sure that the observer is located in the far-field for each of the

individual screens, i.e. $\bar{z} \gg z_0$. This condition is satisfied for $p \lesssim 0.8$ a.u.

Thus for IPS observations at 327 MHz for $0.2 < p < 0.7$ a.u., the thin-screen assumption is fully justified. The theory discussed in Section 2.2 can be directly applied to the IPS data for determination of the properties of the irregular plasma density irregularities in the IPM or the determination of fine structure in scintillating sources.

2.4 EFFECT OF STRUCTURE OF RADIO SOURCES ON IPS

In the theory outlined in Section 2.2 we have considered the radio source to be of negligibly small angular extent i.e. the incident wave is plane. Since the principal aim of the present work is to study the angular structure of radio sources by observing and analysing their scintillation characteristics, we must evaluate how the diffraction pattern produced at the earth gets modified if the source being observed is not a point source.

In the case of radiation from a small extended source incident normally on the thin-screen, different points of the source will produce independent intensity patterns shifted laterally by an amount $z\theta$ where z is the distance of the observer's plane from the screen and θ is some measure of the angular extent of the source. These patterns will overlap each other and will produce general smearing of intensity

pattern over scales of the order of $z\theta$. If $z\theta$ is much smaller than the scale ℓ of the pattern for a point source, the smearing will be negligible and the source will behave as a point source. If, on the other hand, $z\theta$ is comparable or larger than ℓ, the scintillations will be smeared and the pattern scale will be larger than that for a point source. This forms the physical basis for the common knowledge viz. 'stars twinkle and planets do not'. Thus, by comparing the scintillation index and the scale of intensity pattern produced by a point source and an extended source, it should be possible to make measurements of the angular structure of scintillating components in radio sources.

For typical values of 1 a.u. for z and 100 km for pattern scale ℓ in the weak scattering case, significant smearing will occur for $\theta \gtrsim a/z$ or $\gtrsim 0\overset{''}{.}15$ arc. For observations close to sun taken in the strong scattering conditions, however, the pattern scale ℓ is much smaller than a and IPS observations can be used to resolve structures smaller than $\sim 0\overset{''}{.}05$ arc or so (Cohen and Gundermann 1969).

If $I_z(\bar{r})$ is the intensity pattern produced by a point source, then another point source, removed from the first by a small angle θ in the plane of sky, will produce an intensity pattern $I_z(\bar{r} - z\bar{\theta})$. If, instead of individual point sources located close to each other, the radio source has a continuous distribution of brightness $B(\theta)$ extending

over θ, then the intensity pattern produced by it is given by the convolution of the point source pattern with the brightness distribution of the source,

$$I_{ext}(\bar{r}) = \int B(\bar{\theta}).I_z(\bar{r}-z\bar{\theta}) \, d\theta \qquad \qquad ...(2.21)$$

Taking the Fourier transform and using the convolution theorems (Bracewell 1965) we have

$$M^2_{ext}(\bar{q}) = M^2_{pt}(\bar{q}). \left| V(zq/2\pi) \right|^2 \qquad \qquad ...(2.22)$$

where V is the visibility function of the source and is given by

$$V(zq/2\pi) = \int_{-\infty}^{+\infty} e^{-i(z/2\pi)\bar{q}.\bar{\theta}} \, B(\bar{\theta}) \, d\theta \qquad \qquad ...(2.23)$$

For a point source $V = 1$ and for any extended source $V < 1$. From eqn. (2.22) it is clear that the effect of finite size of the source is to filter out high spatial frequencies from the intensity spectrum. This results in a reduction of second moment and the scintillation power. Effectively the situation is similar to an intensity interferometer where one measures $|V|^2$ at a given baseline. The scintillation power spectrum, in principle, has information about $|V|^2$ at all baselines, ranging from zero to a certain cut-off. The observed power at a wave-number q corresponds to $|V|^2$ at an equivalent interferometer baseline $D \simeq zq$ wavelengths. For $z = 1$ a.u. and an observed cut-off in the temporal power spectrum at a few Hz, say 3 Hz,

corresponding to $q \simeq 0.05$ km^{-1}, $D \simeq 7 \times 10^6$ wavelengths.

2.4.1 Characteristics of Observed Scintillations from Extended Extragalactic Radio Sources:

Many extragalactic radio sources show structure on angular scales large compared to that essential for producing strong scintillations. A majority of them show two (or more) peaks in their brightness distribution. High resolution aperture synthesis, lunar occultation and VLBI observations of strong radio sources have revealed multiple compact sub-components within each of the main components. In the following we estimate the expected reduction in the index and the width of the scintillation power spectrum for simplified brightness distribution representing the observed morphological structure of extragalactic radio sources. We will assume that the observations satisfy the weak-scattering and far-field conditions and proceed in steps.

First we consider a double source with two symmetrical gaussian components, having 1σ angular diameters of $2\theta_1$ and $2\theta_2$ with fractional flux densities α_1 and α_2 respectively and separation θ_d. The brightness distribution for such a source can be written as

$$B(\theta_x, \theta_y) = (\alpha_1 / 2\pi\, \theta_1^2) \exp\left[-(1/2\theta_1^2)\left\{(\theta_x+\theta_d /2)^2 + \theta_y^2\right\}\right]$$

$$+ (\alpha_2 / 2\pi\, \theta_2^2) \exp\left[-(1/2\theta_2^2)\left\{(\theta_x-\theta_d /2)^2 + \theta_y^2\right\}\right]$$

$$\dots(2.24)$$

The visibility function

$$V(zq/2\pi) = \alpha_1 \exp\left[-(z^2\theta_1^2/2)(q_u^2+q_v^2)\right] \cdot \exp(-iq_u z\theta_d/2)$$

$$+ \alpha_2 \exp\left[-(z^2\theta_2^2/2)(q_u^2+q_v^2)\right] \cdot \exp(iq_v z\theta_d/2) \quad ..(2.25)$$

and $|V|^2 = V \cdot V^*$, where V^* is the complex conjugate of V.

In order to obtain the power spectrum $M_{ext}^2(\bar{q})$ produced by an extended source, we must first know the exact shape of $M_{pt}^2(\bar{q})$ for a point source. Following Cohen et al. (1967 b) we assume that $M_{pt}^2(\bar{q})$ has a gaussian shape given by

$$M_{pt}^2(q_u,q_v) = 2^2 \pi^2 a^2 m_{pt}^2 <I>^2 \exp\left[-(1/2a^2)(q_u^2+q_v^2)\right] ...(2.26)$$

Substituting eqns. (2.25) and (2.26) in eqn. (2.22) we obtain

$$M_{ext}^2(q_u,q_v) = M_{pt}^2(q_u,q_v) \left[\alpha_1^2 \exp\left\{-z^2\theta_1^2(q_u^2+q_v^2)\right\}\right.$$

$$+ \alpha_2^2 \exp\left\{-z^2\theta_2^2(q_u^2+q_v^2)\right\}$$

$$\left. + 2\alpha_1\alpha_2 \exp\left\{-z^2\left[(\theta_1^2+\theta_2^2)/2\right](q_u^2+q_v^2)\right\}\right]$$

$$...(2.27)$$

The scintillation index m_{ext} for an extended source can be calculated by using the definition

$$m_{ext}^2 = (4\pi^2 <I>^2)^{-1} \iint M_{ext}^2(q_u,q_v)\, dq_u\, dq_v$$

Thus

$$m^2_{ext} = \alpha^2_1 \left[1+2(z\theta_1/a)^2\right]^{-1} + \alpha^2_2 \left[1+2(z\theta_2/a)^2\right]^{-1}$$

$$+ 2\alpha_1\alpha_2 \left[1+2(z^2/2a^2)(\theta^2_1+\theta^2_2)\right]^{-1}.$$

$$\cdot \exp\left[-\tfrac{1}{2}(z\theta_d/a)^2 \left\{1+2(z^2/2a^2)(\theta^2_1+\theta^2_2)\right\}^{-1}\right] \quad \ldots(2.28)$$

which in terms of the half-power diameter Ψ of the gaussian defined in eqn. (2.24) becomes

$$m^2_{ext} = \alpha^2_1 \left[1+0.36(z\Psi_1/a)^2\right]^{-1} + \alpha^2_2 \left[1+0.36(z\Psi_2/a)^2\right]^{-1}$$

$$+ 2\alpha_1\alpha_2 \left[1+0.36(z\Psi_{12}/a)^2\right]^{-1}.$$

$$\cdot \exp\left[-\tfrac{1}{2}(z\theta_d/a)^2 \left\{1+0.36(z\Psi_{12}/a)^2\right\}^{-1}\right] \quad \ldots(2.29)$$

where $\Psi_1 = 2.34\,\theta_1$, $\Psi_2 = 2.34\,\theta_2$ and $\Psi^2_{12} = (\Psi^2_1+\Psi^2_2)/2$

These equations have been obtained with the assumption that

a point source would show $m_{pt} = 1$ since $\alpha_1+\alpha_2 = 1$.

In order to simplify writing of equations, we rewrite eqn. (2.29) as

$$m^2_{ext} = \alpha^2_1 m^2_1 + \alpha^2_2 m^2_2 + 2\alpha_1\alpha_2 m^2_{12}\cdot\exp\left[-\tfrac{1}{2}(z\theta_d/a)^2 m^2_{12}\right] \quad \ldots(2.30)$$

where m has been used to denote expressions of the form $\left[1+0.36(z\Upsilon/a)^2\right]^{-\frac{1}{2}}$ with appropriate subscripts to m and Υ .

Similarly the second moment q_2 of the spatial power spectrum for the extended source along the solar wind direction can be obtained from

$$q^2_{2,ext} = \iint q^2_u \cdot M^2_{ext}(q_u,q_v)dq_u \ dq_v \Big/ \iint M^2_{ext}(q_u,q_v)dq_u \ dq_v$$

Substituting M^2_{ext} from eqn. (2.27) and integrating we get

$$q^2_{2,ext} = (1/a^2)(A/B) \hspace{3cm} \dots(2.31)$$

where $A = \alpha^2_1 \ m^4_1 + \alpha^2_2 \ m^4_2 + 2\alpha_1 \alpha_2 \ m^4_{12} \left[1-(z\theta_d/a)^2 \ m^4_{12}\right]$

and $B = m^2_{ext}$

Since for a point source $q_2 = 1/a$ in the weak-scattering, far-field conditions (Sec. 2.2.2) we have

$$\frac{q^2_{2,ext}}{q^2_{2,pt}} = (A/B)$$

Further the second moment q_2 of the spatial spectra is related to the second moment f_2 of the observed temporal spectra, under the assumption that the screen moves rigidly across the observer with a constant velocity v along the

x-direction, by

$$q_2 = 2\pi f_2/v$$

Then

$$\frac{f_{2,ext}^2}{f_{2,pt}^2} = (A/B) \qquad\qquad \ldots(2.32)$$

where A and B are as above.

In order to proceed further and calculate expected scintillation index when multiple components are present in each of the main components of the source considered above, we now consider the case when the separation θ_d between the two components is zero, i.e. when the two gaussian components of size ψ_1 and ψ_2 are located concentrically. In such a case, putting $\theta_d = 0$ in eqn. (2.30) we obtain the scintillation index

$$m_{ext}^2 = \alpha_1^2 m_1^2 + \alpha_2^2 m_2^2 + 2\alpha_1\alpha_2 m_{12}^2 \qquad \ldots(2.33)$$

This can be easily extended to three or more components. Now if, as is observed in radio sources (see Fig. 5.7), there is a pair of such components containing multiple sub-components within each of them, the observed scintillation index will be reduced by the presence of the exponential term similar to that occuring in eqn. (2.30). If the separation θ_d is much larger than the size of the first Fresnel zone then the resultant effect would be to reduce the index m by $\sqrt{2}$.

These considerations have been used later in Chapter 5 (Sec 5.5.2) for estimating the expected scintillation indices for simplified brightness distribution models representing the well-studied sources 3C 33 and Cygnus A.

2.5 DISCUSSION OF PRACTICAL CONSIDERATIONS

Eqn. (2.22) shows that the two dimensional spatial power spectrum of scintillations produced by any source of finite angular size is simply the product of the spectrum that would be produced by a point source and the spectrum of angular distribution of brightness across the source. The scintillation power spectrum contains information about the structure of the radio source equivalent to that produced by a series of intensity interferometers operating simultaneously over a range of baselines from zero to about 10^6 wavelengths. Thus if we can determine $M^2_{ext}(\bar{q})$ & $M^2_{pt}(\bar{q})$ it should be possible, in principle, to obtain the squared magnitude of the source visibility. In practice, it is not possible to measure the true spatial spectrum. Usually, with a single antenna, IPS is observed and recorded as temporal fluctuations of intensity, which are analysed to yield the temporal power spectra. Although, the temporal and spatial spectra are related to each other, the relation is not straightforward. Firstly, the observed temporal spectrum is one-dimensional projection of the two-dimensional wavenumber spectrum along the solar wind velocity vector. The observed temporal intensity spectrum, therefore, provides information about the

angular structure of the source only along the direction of the solar wind.

Secondly, the conversion from frequency to wave-number spectrum assumes that the screen moves rigidly across the line of sight with a fixed velocity v. However, since the solar wind plasma moves radially outwards from the sun, the transverse components of the velocity of irregularities located at different points along the z axis will show a spread around the maximum near point O (Fig. 2.1). Such a dispersion will lead to smearing of some features of the wavenumber spectrum.

Due to these difficulties, it is not possible to recover the brightness distribution of the scintillating sources from their temporal intensity spectra. Some information on their structure can still be got by computing and comparing their observed temporal spectra with those of a point source under identical circumstances.

In Section 2.4.1 we have computed the ratios (m_{ext}/m_{pt}) and $(f_{2,ext}/f_{2,pt})$ for an ideal two component source. Similar calculations have been made by Little and Hewish (1966) and Cohen et al. (1967b) for several simplified models of brightness distribution. These ratios depend on the parameter $(z\gamma/a)$, where γ represents the angular size of the scintillating components in the source. Since z/a is not a strongly varying function of decreasing elongation (see Chapter 3) different models give similar values under

weak scattering conditions. At sufficiently small elongations where $M_z^2(\vec{q})$ as well as $P(f)$ for a point source become extremely broad due to combined effects of decreasing irregularity size and strong scattering, the observed spectrum of the extended source directly reflects its visibility function and it may be possible to distinguish sources with widely different compact component sizes. The difficulty of discriminating between different models, however, limits the amount of structural details which may be derived. IPS observations, therefore, are usually interpreted in terms of a simple model (Cohen et al. 1967b, Little 1976), having a compact scintillating component with a gaussian half power diameter ψ and an extended component which does not contribute to scintillations. If the fractional flux densities in these components are α_1 and α_2 respectively then equations (2.29) and (2.32) give, after putting $\theta_d = 0$

$$(m_{ext}/m_{pt}) = \left[\alpha_1/(\alpha_1+\alpha_2)\right] \cdot \left[1+0.36(z\psi/a)^2\right]^{-\frac{1}{2}} \text{ and}$$

$$\dots (2.34)$$

$$f_{2,ext}/f_{2,pt} = \left[1+0.36(z\psi/a)^2\right]^{-\frac{1}{2}}.$$

This gives

$$\alpha_1/(\alpha_1+\alpha_2) = (m_{ext}/m_{pt}) \cdot \left[1+0.36(z\psi/a)^2\right]^{\frac{1}{2}} \text{ and}$$

$$\dots (2.35)$$

$$\psi = (v/(1.2\pi f_{2,ext}z)) \cdot \left[1- (f_{2,ext}/f_{2,pt})^2\right]^{\frac{1}{2}}$$

where $f_2 = v/2\pi a$, for the fractional flux density and the angular size of the compact scintillating component respectively.

Hence, by measuring m and f_2 of the observed temporal power spectra of IPS of a point and an extended source under identical interplanetary conditions, and by adopting a model of the plasma density irregularities in the solar wind, it is possible to estimate the scintillation visibility μ (defined as the ratio of the flux density arising from the compact scintillating component to that of the whole source i.e. $\alpha_1/(\alpha_1+\alpha_2)$) and the angular size ψ of the scintillating component in the extended source. In the absence of measured value of $f_{2,pt}$, a useful limit on the angular diameter ψ can be arrived at from equation (2.35) as

$$\psi \leq v/(1.2\,\pi\,f_{2,ext})$$
...(2.36)

In the next chapter we describe extensive IPS observations of several strong point-like radio sources at 327 MHz to determine the average values of m_{pt} and $f_{2,pt}$ in the range of distances $0.1 \lesssim p \leq 1.0$ a.u. from the sun. Based on these observations a self-consistent model of the characteristic scale size and the strength of interplanetary irregularities responsible for IPS has been derived. These have later been used to estimate μ and ψ of compact scintillating structures in a large number of radio sources from their IPS observations at 327 MHz under the assumption that the brightness distribution in radio sources can be represented by a simple core-halo type model.

As discussed in Section 2.4.1, many extragalactic radio sources possess complex structures with two or more spatially distinct components of comparable intensity and size. Usually the source is not resolved by the antenna beamwidth and IPS of all components are observed collectively. It is therefore important to estimate how the complexity of source structure affects the estimated values of μ and ψ. Calculations of these effects on the lines of Section 2.4.2 cannot be made in the absence of a priori knowledge of the fine structure of radio sources. In fact, IPS observations are made to determine the characteristics of compact features in them. Elementary considerations, however, suggest that if a source contains two or more scintillating components separated from each other by more than the angular size of the first Fresnel zone (e.g. in the case of a double radio source), their scintillations will add incoherently and μ will in general be an underestimate of the total flux density originating in the compact components. The estimated angular diameter ψ will also be weighted according to the sizes and strengths of individual scintillating components in the source. Some implications of these biases on the interpretation of IPS data in terms of the overall structure of radio sources are discussed in Chapters 5 and 6.

CHAPTER 3

OBSERVATION AND ANALYSIS OF INTERPLANETARY SCINTILLATIONS AT 327 MHz

3.1 INTRODUCTION

Observation of scintillations of radio sources provides a unique method of probing the irregular plasma which imposes phase and amplitude fluctuations on the radio waves propagating through it. Extensive observations of amplitude scintillations of natural radio sources over the last decade have resulted in important information about the size, strength and velocity of the plasma density irregularities present in the ionosphere, interplanetary and interstellar media (see e.g. Aarons 1975; Cohen et al. 1967a, Hewish and Symonds 1969, Jokipii 1973, Rao et al. 1974, Coles et al. 1974; Guelin 1973, Rickett 1977 for recent reviews).

It was shown in the previous chapter how the observations of interplanetary scintillations (IPS) can be used to derive information on the angular sizes and fractional flux densities of compact scintillating components in radio sources provided the properties of the plasma density irregularities in the interplanetary medium (IPM) are sufficiently well determined. In this chapter we use systematic IPS observations of strong compact point-like radio sources at 327 MHz to derive the characteristics of the small scale irregularities in the IPM.

The observations were carried out at the Radio Astronomy Centre, Ootacamund using the Ooty Radio Telescope. The antenna and the receiver system used for IPS observations are described in Section 3.2. Observations of strong point sources to determine the average response of the IPM at 327 MHz are discussed in Section 3.3. The method of analysis of the scintillation data, obtained by a single antenna, to estimate the scintillation visibility and the angular size of the scintillating compact components in radio sources is outlined in Section 3.4.

3.2 THE OOTY RADIO TELESCOPE

The Ooty Radio Telescope (ORT), shown in Figure 3.1, is the only instrument available in India for extragalactic astronomy in the radio band. It was designed and constructed by the Radio Astronomy team of the Tata Institute of Fundamental Research, Bombay, mainly for studying the high resolution structure of weak radio sources using the method of Lunar Occultation. Consequently, it has the following important features; large collecting area, full E-W steerability and N-S steerability of $\pm 35^O$ around the equator so as to provide full coverage of the moon's changing position in the sky. The above features also make ORT suitable for carrying out observations of interplanetary scintillations of a large number of radio sources located close to the equatorial and
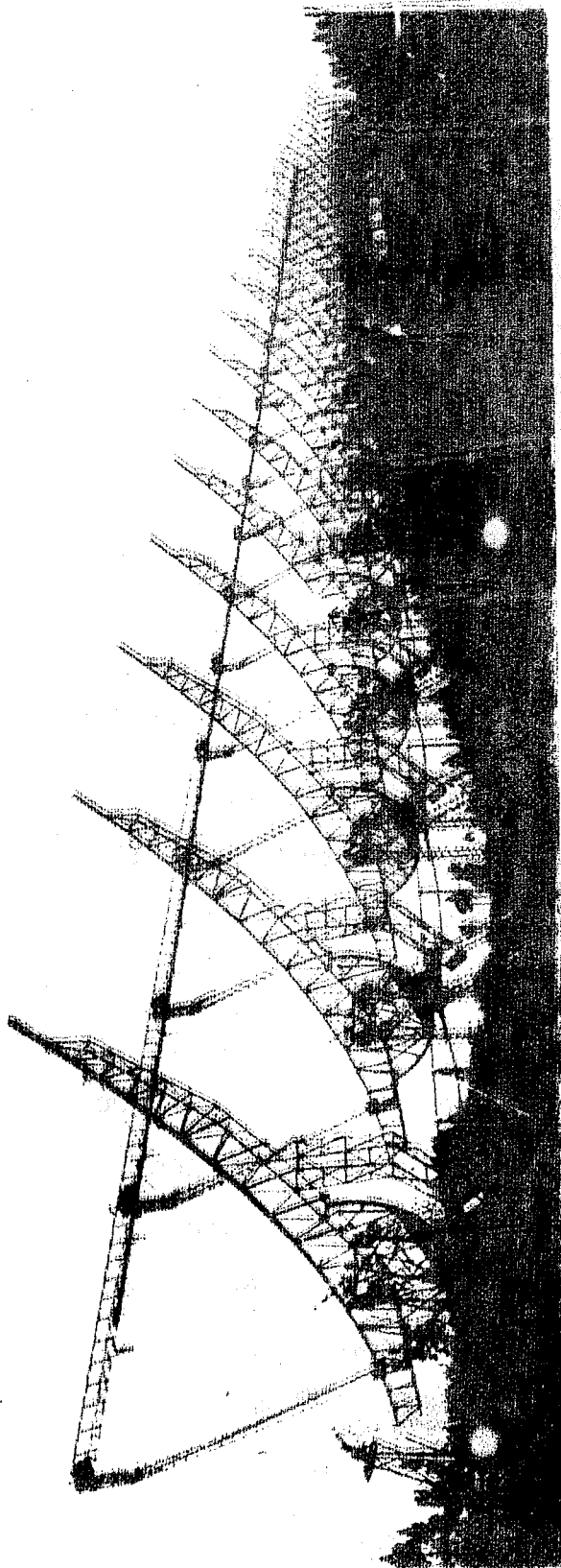
FIG. 3.1 The Ooty Radio Telescope.

the ecliptic plane. The ORT operates at a frequency of 326.5 MHz. The choice of operating frequency, although governed largely by the requirements of the lunar occultation observations, also allows scintillations to be observed over a wide range of distances from the sun. In this section we describe, in brief, the antenna, the receiver system and the mode of operation of ORT employed in the IPS observations. For a detailed description of the ORT the reader is referred to papers by Swarup et al. (1971), Kapahi et al. (1975) and Sarma et al. (1975).

3.2.1 The Antenna and the Receiver:

The antenna consists of an equatorially mounted parabolic cylindrical trough reflector having dimensions of 530 m and 30 m in the N-S and E-W directions respectively. It provides an effective collecting area of about 7500 m^2. By mechanical rotation of the reflector around the polar axis, it is possible to track or scan any region of the sky within an hour angle range of -4.0 to +5.5 hours. A radio source can therefore be tracked continuously, if needed, for about 9.5 hours. The N-S steerability of ± 35° around the equator is achieved by appropriate electrical phasing of the dipole array placed at the focal line of the reflector. The dipole array consists of 968 half-wave dipoles and is divided into 22 sections of 44 dipoles each. On either side of the center of each section, the 22 dipoles are connected in series

through equal but variable lengths of coaxial transmission line (Trombone type RF phase-shifters). The telescope is steered in the N-S direction, in steps of 0.5 arc, by remote control of the length of the variable transmission lines between individual dipoles. The signals from 22 dipoles in each half section are combined and amplified in the RF amplifiers located at the center of each section. The amplified signals are then mixed with the local oscillator signal fed to each section through a X'mas branching system. The 22 IF (Intermediate Frequency = 30 MHz) outputs are brought to the receiver system, and amplified again to compensate for the cable losses. Phases and time delays between one section and another are then introduced at the intermediate frequency. Signals from each of the 11 north and 11 south sections, all in phase at this stage, are divided into 12 equal parts and corresponding parts are combined in two different ways to simultaneously synthesize 12 total-power (TP) and 12 phase-switched (φ) beams. The half-power width of these beams in the E-W direction is about 2° and the N-S separation between adjacent beams is 3' (sec δ) arc, δ being the declination of the direction in which the center of the beam system is pointed in the sky. The half-power widths of the TP and φ -switched beams in the N-S direction are 5.6 (sec δ) arc and 3.9 (secδ) arc respectively.

After the beams are formed, the signals from each of the beams pass through a final stage of amplification where the signal bandwidth is limited to ~ 4 MHz. This is followed by a square-law detector and an integrator (low-pass filter) circuit. Outputs with different RC time constants are available for digital and analogue recording. Figure 3.2 shows the block diagram of the phase-switched system from the final amplification stage onwards.

In addition to the above, the receiver system provides a facility to independently shift (flip) the position of any of the beams by 36' arc north or south of its original position, instantaneously. This feature, designed for tracking the moon in declination in a step mode, has also proved useful in the IPS observations. Also several IF amplifiers with narrow bandwidths (~ 800 and 300 kHz) are available and can be plugged in place of broad-band (~ 4MHz) amplifiers whenever desired.

3.2.2 Sensitivity of the Phase-Switched System:

Although the total power system provides $\sqrt{2}$ times higher sensitivity than the phase-switched system, we used the latter because of its better stability. In the φ-switched mode the signals from the two halves of the antenna are multiplied and correlated (Blum 1959). This eliminates the slow drift due to the broad background sky fluctuations and makes
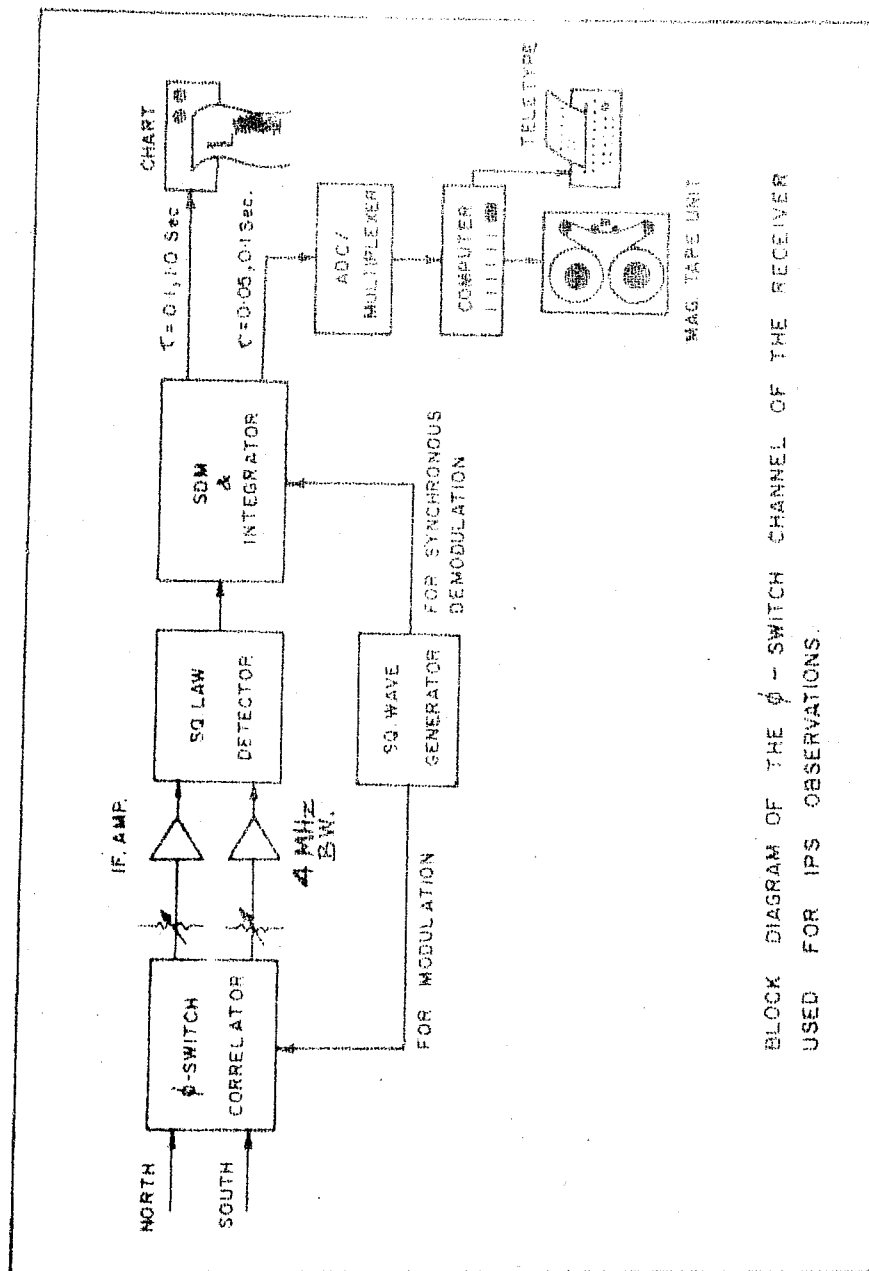
BLOCK DIAGRAM OF THE φ - SWITCH CHANNEL OF THE RECEIVER
USED FOR IPS OBSERVATIONS.

Fig. 2.2 Details of the phase-switch channel and the analogue and digital recording system.

Table 3.1 - Parameters of the ORT in the Phase-Switched Mode

Beam Width (Half-Power)	2^O arc E-W
	$3.9'$ arc N-S
Effective Collecting Area A_e	7500 m2
System Temperature T_s^*	400^OK
Pre-Detection Bandwidth $\Delta\nu$	~ 4 MHz
Post-Detection Time Constant τ	1.0 sec Analogue recording
	0.1, 0.05 sec Digital recording for IPS

----

*Sum of the contributions from sky background, antenna spillover, RF amplifier noise, cable losses and receiver noise.

Table 3.1 - Parameters of the ORT in the Phase-Switched Mode

Beam Width (Half-Power) 2° arc   E-W

                                 3.9 arc   N-S

Effective Collecting Area A_e 7500 m2

System Temperature T_s^* 400°K

Pre-Detection Bandwidth $\Delta\nu$ ~ 4 MHz

Post-Detection Time Constant τ 1.0 sec   Analogue
                                                   recording

                                      0.1, 0.05   Digital
                                          sec   recording
                                                   for IPS

----

*Sum of the contributions from sky background, antenna

spillover, RF amplifier noise, cable losses and receiver

noise.

the φ-switched records more stable than the TP records, where the two signals are simply added in phase. Further, the phase-switching technique also helps in rejecting the local interference which is likely to be uncorrelated in the two halves of the antenna. The parameters of the φ-switched system used for IPS observations are summarized in Table 3.1.

With these parameters, a source having a flux density of ~0.5 Jy produces a signal to noise ratio of 5 when $\tau = 1.0$ sec. This is the sensitivity limit of the telescope. However, because of the broad EW beam, the observations are affected by confusion below about 1.5 Jy.

3.3 RESPONSE OF THE INTERPLANETARY MEDIUM

As discussed in Chapter 2, the interplanetary medium casts a diffraction pattern on the earth which is a convolution of the brightness distribution of the radio source with the response function of the interplanetary medium (the screen) for a point source. In principle, therefore, if the point source response of the interplanetary medium can be determined, it should be possible to obtain the brightness distribution of any extended radio source by measuring the diffraction pattern produced by it. In practice there are two difficulties. Firstly, by observation at one or a few points on the earth, it is not possible to sample the diffraction pattern completely and secondly, even if it is possible to sample the pattern at many

different points, the occurrence of random changes in the response of the medium and hence the diffraction pattern with time pose a severe limitation. The best one can hope to do is to determine the average statistical response of the interplanetary medium for point sources and use this to derive information about the fine structure of extended sources. In the following we describe observations of IPS of a few strong point sources and determine the average properties of the interplanetary medium.

3.3.1 Observation of Point Sources:

During 1971 we carried out systematic IPS observations of nine compact extragalactic radio sources in order to calibrate the effect of the irregular interplanetary medium (IPM) on the incoming plane waves at 327 MHz. Sources selected for observations were sufficiently strong and were known to be extremely compact from earlier IPS (Harris and Hardebeck 1969) and VLBI observations (Broten et al. 1967, Clark et al. 1968, Kellermann et al. 1968). These sources, namely 3C2, 0115-01, 0116+08, 3C49, 0202+14, CTA 21, 3C138, 2203-18 and 3C446, were also chosen to be close to the ecliptic plane so as to allow us to probe the IPM at all distances from the sun upto about 1 a.u.

The 6 central beams (Beams 4 to 9) of the phase switched system of the ORT were used to observe the source and monitor the signals from the neighbouring background.

The declination was set in such a way that the main response due to the source appeared in beam 7. The positioning of the beams in the sky is such that the adjacent beams (Beams 6 and 8) produce a null response for the source and the next adjacent beams (Beams 5 and 9) produce a reduced negative response for the source. This multibeam response pattern is very useful in locating the sources as well as in distinguishing between genuine scintillation spikes and spikes due to local interference. The analogue outputs from these beams are displayed on paper chart recorders running at speeds of 1 inch/min. The time constant used for recording the analogue signals is 1 sec. The signal from beam 7, on which the source is observed, is also displayed on charts with a time constant of 0.1 sec for the purpose of observing IPS. Another output of beam 7 with $\tau = 0.1$ sec (later changed to 0.05 sec) is digitized and sampled every 20msec using a 12 bit analogue to digital converter (ADC). Sampling and recording of data on magnetic tapes for off-line analysis were carried out using the Varian 620/i on-line computer.

After setting the antenna at the declination of the source and taking an E-W scan over the source region, the antenna was made to track the source and the ON-source scintillations were recorded. Computer is programmed to take 2750 samples of the signal at the rate of 50 samples/sec ., put the samples in the form of a record on the magnetic tape,

calculate mean and variance of data points and print them on
the teletype for quick-look analysis. Normally 6 to 10 minutes
of scintillations are recorded using this procedure. The in-
formation concerning the name of the source, position of the
antenna, time of observations etc. was included as a legend
record on the magnetic tape. The antenna is then moved to a
nearby cold region of the sky and 3 to 5 minutes of OFF-source
data were recorded in the above manner while the antenna is
tracking the OFF-source region. Occasionally when it was not
possible to arrive at a nearby clean OFF-source region by E-W
movement of the antenna, it was made to look 36' arc north or
south using the beam flipping facility described earlier. The
records were mostly disturbance free but whenever disturbance
occurred, it was noted down and the affected records were not
utilised in the analysis of scintillations. Typically an
observing session consisted of observations of 4 to 5 point
sources as described above. A flux calibrator was also observed,
although the IPS analysis in itself does not need any flux cali-
bration. Observations of point sources were carried out as fre-
quently as possible so as to provide maximum coverage of the
range of elongations between 0.1 and 1.0 a.u. Analogue chart
recording of the data were mainly used for the purpose of dis-
play during the observations. All quantitative analyses were
performed with the digital data using the CDC 3600 computer
system at TIFR, Bombay.

3.3.2 Reduction and Analysis of Data:

The random intensity fluctuations are characterized
by their statistical moments e.g. mean, variance and the auto-
correlation function (acf) and its Fourier transform, the power
spectrum.

In the following we estimate the variance and the
power spectrum of the observed intensity fluctuations using the
Fast Fourier Transform (FFT) algorithm (Cooley and Tukey 1965).
With the availability of FFT algorithm it is faster to calculate
the power spectrum of the data directly by squaring the Fourier
coefficients rather than calculate the acf and transform it to
obtain the power spectrum. Also the power spectrum facilitates
a simpler and more direct interpretation of scintillations.The
raw power spectrum of observed fluctuations however does not
represent the actual spectrum of interplanetary scintillations
since instrumental effects modify the frequency characteristics
of the incoming signal. The observed variance and the power
spectrum must therefore be suitably corrected for the effects
of finite antenna size, receiver bandwidth and the time con-
stant used at the receiver output.

On-line Analysis:

The mean and variance of each of the 55 sec data
record were computed on-line and printed on the teletype during

the 5 sec duration in which the data were also transferred to magnetic tape. After the ON and OFF source data were acquired the scintillation index was calculated using the definition

$$m = (\text{Var. ON} - \text{Var. OFF})^{\frac{1}{2}}/\text{Intensity}$$
$$= (\text{Var. ON} - \text{Var. OFF})^{\frac{1}{2}}/(\text{Mean ON} - \text{Mean OFF})$$

The on-line analysis provided an on-the-spot idea of the strength of scintillations and was useful in planning further observations of the source.

Time-constant smoothing:

The scintillation index computed above is an under-estimate of the actual index since the low pass filter used at the output of the receiver attenuates the high frequency power present in the scintillations. It is possible to correct the scintillation index for this attenuation if both the power transfer characteristics of the filter L(f) and the true spectrum of IPS are known. The low pass filter used was a simple RC circuit with $\tau = 0.1$ sec. Its characteristics were easily determined by measuring the power spectrum of the receiver for OFF source white noise. The power spectrum of IPS, $P_I(f)$, is determined by observations of point sources described below. The variance of true and observed scintillations are then related by

$$\alpha^2 = \int_0^\infty P_I(f)df \Big/ \int_0^\infty P_I(f) \, L(f) \, df$$

The corrected scintillation index is obtained by multi-plying the on-line index by α. The multiplication factor α can be estimated only after $P_I(f)$ is determined off-line.

Off-line Analysis:

The scintillation data in digital form were recorded on magnetic tapes in the following manner. First the parameters of the observations are put as a label record. Then 2750 samples of data, acquired at the rate of 50 samples/sec for 55 sec are put as a data record. Successive minutes of data, acquired with a 5 sec gap in between, are put as individual records. At the end a file mark is written. This procedure is followed for recording ON and OFF source data for every source. Power spectrum of each data record was estimated separately and power spectra of all data records in a file were added cumulatively to obtain a stable ON or OFF power spectra. After correcting the power spectra for the instrumental effects, the OFF source power spectrum was subtracted from the ON source spectrum to obtain the final spectrum of scintillations produced by the source. Power spectrum calculations were performed using the FFT algorithm and only the important steps in the analysis are described below.

Estimation of Power Spectra:

In order to remove slow drifts and possible contribution from ionospheric scintillations, a running mean over 512 data points (i.e. over 10.24 sec) was subtracted from each data record giving rise to a time series of length about 45 sec, and having zero mean. The variance of the record at

this stage was printed out for calculation of scintillation index. The effect of the subtraction of the running mean in the frequency domain is to multiply the power spectrum by the function

$$H(f) = \left[1 - \left\{ \sin(\pi f \cdot 10.24)/(\pi f \cdot 10.24) \right\} \right]^2$$

While effectively removing the power below ~ 0.1 Hz it affects the higher frequency components also. The calculated power spectrum must therefore by corrected for the effect of $H(f)$. The high pass filter also removes some genuine low frequency power due to IPS but this effect is very small and was neglected.

Since the FFT algorithm requires 2^n data points, where n is an integer, only first 2^n (=2048) data points were retained. In order to avoid sharp discontinuities at the ends, the data (200 points on either side) were tapered using a cosine bell weightage. The Fourier transform was then computed and the Fourier coefficients were squared to give the power spectrum. Since the spacing between the data points was 20 msec, the Fourier transform consisted of 2048 points equally spread over -25 to +25 Hz. Power spectrum values at intervals of $(50/2048) \simeq 0.025$ Hz were thus generated by the program.

In order to correct for the effects of running mean high pass filter $H(f)$, these raw power spectral estimates

were divided by H(f), except in the case of zero frequency
(dc) value, which is zero due to removal of mean from the
data. The statistical uncertainty in the power spectrum esti-
mates P so computed is given by (Cooley et al. 1970)

$$Var.(P) = P^2$$

i.e. the rms uncertainty in P is equal to 100% of P itself.
The raw power spectrum is therefore a highly unreliable esti-
mate. In order to obtain more reliable spectral estimates
four adjacent values of P were averaged. This led to an
improvement in the stability of estimates by a factor of 2 at
the cost of poorer resolution of 0.1 Hz, which is sufficient
for our purpose.

The power spectrum with a resolution of 0.1 Hz was
corrected for the high frequency attenuation due to RC time
constant by dividing it by the frequency response L(f) of the
filter. L(f) was determined by calculating the power spectrum
of a long strech of broad band receiver noise. The ON source
spectrum $P_S(f)$ at this stage is the sum of the true spectrum
of IPS $P_I(f)$, the OFF source spectrum $P_N(f)$ which is a con-
stant (independent of frequency) and another constant due to
increased system noise because of the presence of the source
in the beam. Since there is negligible scintillation power
beyond about 15 Hz the sum of constants due to receiver noise
constitute the constant power beyond about 15 Hz in $P_S(f)$.
The value of this constant, determined from the high frequency

plateau of the ON source spectrum itself, was subtracted from $P_S(f)$ to arrive at the final spectrum of the scintillation produced by the source.

The final rms error of $P_I(f)$ values is given by

$$\triangle P_I(f) = \left(P_I(f) / \sqrt{(N_P \cdot N_{rec})} \right) \cdot \left[1 + \left\{ P_N(f) / P_S(f) \right\} \right]$$

where

N_P = no. of spectral estimates (usually four) over which averaging is done to obtain stable spectra with a lower resolution,

N_{rec} = no. of data records whose power spectra were cumulatively added,

$P_S(f)$ = spectrum of ON source scintillations and

$P_N(f)$ = spectrum of OFF source noise

The term within brackets arises due to subtraction of OFF spectra from the ON spectra and contributes more and more to the error at high frequencies, where noise power becomes comparable to scintillation power. For the normal observations with N_{rec} = 6 and N_P = 4 the term outside the brackets is 0.2 $P_I(f)$. The second moment f_2 and the correction $\propto$ to the scintillation index m were estimated for each power spectrum using the relations

$$f_2^2 = \sum_0^{f_c} f^2 P_I(f) / \sum_0^{f_c} P_I(f)$$

and

$$\alpha^2 = \sum_0^{f_c} P_I(f) \Big/ \sum_0^{f_c} P_I(f) L(f)$$

where f_c is the cut-off frequency beyond which the ON source spectrum settled to the constant OFF source value. The correction factor α was found to be generally less than 10% for observations at $p > 0.2$ a.u. Closer to sun where scintillation spectra broaden considerably, α increased steeply with decreasing p as expected.

Effects of Anntenna Aperture and Receiver Bandwidth:

In the above analysis we have not considered the effects of finite antenna aperture and receiver bandwidth on the observed scintillations. Following discussion shows that both these effects are negligible over the range of elongation where most IPS observations were carried out.

Aperture Smoothing - The intensity pattern is observed with an antenna of large dimensions. Consequently any intensity fluctuations which have spatial scale comparable to or smaller than the antenna aperture are likely to get smeared. For IPS observations at $p > 0.2$ a.u. in the weak scattering region at 327 MHz, the spatial scale of intensity pattern over the ground is ~ 100 km (Rao et al. 1974). The largest dimension of the antenna (ORT) used is only ~ 0.5 km and this does not lead to any smearing. Closer to sun than ~ 0.2 a.u., the pattern scale decreases due to decreasing irregularity size in the solar wind and due to

strong scattering effects at 327 MHz. For values of p as small as 0.05 a.u. the pattern scale is still ~5 km or more (Rao 1975). No correction for aperture smoothing is required for present IPS observations with ORT.

Bandwidth smearing - Little (1968) has shown that the scintillations are strongly correlated over a limited bandwidth and significant smearing takes place when

$$\Delta\nu \gtrsim 8\pi^2 l^2 \nu/zc \times \qquad \Delta\nu \gtrsim 8\pi^2 l^2 c/z\lambda^2$$

where ν is the frequency of observations and $\Delta\nu$ is the pre-detection bandwidth. For the present observations with ν =327 MHz and $\Delta\nu$ =4 MHz, the bandwidth smearing can be serious only when the pattern scale $l \lesssim 5$ km which, as noted above, occurs for $p \lesssim 0.05$ a.u. The calculated scintillation parameters for $p > 0.1$ a.u. are therefore not affected by the finite bandwidth of the receiver employed for IPS observations at 327 MHz.

3.3.3 Results - Average m-p and f_2-p Curves for Point Sources:

For each of the nine compact sources selected, we have made about 20 to 30 IPS observations covering the range of elongations $0.1 < p < 1.0$ more or less uniformly. For each observation, the scintillation power spectrum was calculated and values of m and f_2 were derived using the procedure described above. Before utilizing these

observations to define the characteristics of the inter-planetary plasma relevant to IPS, we must first make sure whether the sources observed approximate to the 'point source' description. For a point source we expect m to increase with decreasing p till at a certain p where scattering becomes sufficiently strong, m satu-rates to a value of unity. Scintillation power spectra should also widen close to sun unless the presence of finite structure in the source cuts off high frequency components.

We have therefore studied the variation of observed m and f_2 as a function of decreasing elongation. It is found that all sources observed show a similar variation of m with p, although at any given elongation their m values differ considerably. First, with decre-asing p from 1.0 to ~0.2 a.u. m increases and then for p upto ~0.1 a.u. remains near the peak value. Closer to sun than 0.1au. the trend is reversed; m decreases with decreasing p. The peak value of m observed for the strongest scintillating source is only about 0.6 in com-parison with the theoretically expected value of 1. This observed behaviour of m-p curve indicates that either all the 9 sources observed are broader in angular extent than anticipated or they contain appreciable extended (non-scintillating) components. The first possibility can be

checked from their f_2 measurements. It is seen that 3 sources viz. 0202 + 14, 3C 138 and 3C 446 show values of f_2 which are significantly lower than the remaining sources over certain ranges of elongations, indicating that measured f_2 values are affected by finite source size. These sources were therefore excluded from further analysis on point sources. Interesting structures for the scintillating components in these sources have been deduced from the present IPS observations (Rao et al. 1974).

The remaining 6 sources show equally high values of f_2 and their strong-scattering spectra widen rapidly with decreasing p, as expected for an as yet unresolved source. We can derive an upper limit on the angular diameter ψ of scintillating components in these sources from the observed values of f_2 from eqn.(2.36). Using the maximum observed value of f_2 of about 2 Hz at $p \approx$ 0.1 a.u. and assuming z = 1 a.u. and v = 300 km s^{-1} for IPS observations at p $\sim$ 0.1 a.u., we obtain $\psi \lesssim$ 0".06 arc. The sintillating components in these sources can thus be regarded as point sources for IPS observations in the weak-scattering condition. The effect of source structure on the observed values of f_2 appears in the form $\left[1 + 0.36 \left(z \psi / a \right)^2 \right]^{\frac{1}{2}}$. Hence for p $\gtrsim$ 0.2 a.u. it can be seen that the above assumption will introduce < 5% error, taking the scale size a to be about 100 km (see next section). However,

even these sources show peak values of m much less than the theoretically expected value. The origin of this discrepancy is not entirely clear. The simplest explanation is that all the observed sources have extended halo components containing appreciable ($\sim$30% or so) fraction of total flux density. Since these components do not contribute to observed scintillations, their angular sizes should be $\gtrsim 0\overset{''}{.}5$ arc.

Similar observations on the behaviour of m-p and f_2-p curves for compact sources e.g. CTA 21 etc. have been made earlier (Cohen et al. 1967a, Cohen and Gundermann 1969). Usually, without regard to the above discrepancy, in past CTA 21 has been used to represent an ideal point source and its observed m and f_2 have been used to interpret structure in other radio sources (Harris and Hardebeck 1969). Although CTA 21 is known to be very compact from interferometric studies at 408 and 610 MHz, the possibility of double or complex structure on angular scale of $\sim 0\overset{''}{.}1$ arc or the presence of weak ($\sim$20%) extended meter wavelength component can not be ruled out (Clarke et al. 1969, Purcell 1973, Broderick and Condon 1975, Armstrong 1977). However, in order to be consistent with the existing large scale IPS survey of radio sources at a nearby frequency of 430 MHz (Harris and Hardebeck 1969) we also assume that the observed values of m and f_2 for CTA 21 represent m_{pt} and $f_{2,pt}$. It

must however be kept in mind that the estimated values of (m/m_{pt}) for any source using m_{pt} for CTA 21 could thus be overestimated by as much as a factor of 2 since the peak value of m observed for CTA 21 is about 0.53.

Presently, therefore, we normalize the observed m values for the remaining 5 sources to those of CTA21 and combine them to study the average m_{pt}-p variation. Since all sources observed showed similar shape of m-p curve for $p \geqslant 0.25$ a.u. normalization was achieved by multiplying their m values by a constant scaling factor, such that their m-p curves for $p \geqslant 0.25$ a.u. coincide with that of CTA 21. The scaling factors used for this normalization and the limits on the angular size of scintillating components in these sources derived from their f_2 values close to sun, are listed in Table 3.2. 3C 2 being a relatively weak scintillator has been omitted. It is interesting to note that in one source, PKS 0115-01, values of m consistently higher than those of CTA 21 by about 10% were observed. However, in view of the above discussion we have multiplied its m values by 0.9.

Thus by ensuring that the scintillating components in the 5 compact sources namely 0115-01, 0116+08, 3C 49, CTA 21 and 2203-18 behave as unresolved point sources, we can use the observed values of m and f_2 to derive the

Table 3.2 IPS Observation of Point Sources at 327 MHz

Source	Scaling factor used to normalize* m to CTA 21 values	Scintillation visibility μ	Angular diameter of scintillating component γ ($''_{arc}$)
0115-01	0.9	1.0	$\lesssim 0.1$
0116+08	1.3	0.75	$\lesssim 0.08$
0138+13 (3C49)	1.3	0.75	$\lesssim 0.06$
0316+16 (CTA 21)*	1.0	1.0	$\lesssim 0.08$
2203-18	1.0	1.0	$\lesssim 0.1$

* CTA 21 has been used as a calibrating point source for determination of structure in other sources.

average variation of m_{pt} and $f_{2,pt}$ as a function of elongation. In Figures 3.3 and 3.4 we have plotted the normalized scintillation index m_{pt} and the square root second moment f_2 respectively, for the five sources mentioned above. Each point is typically a result of 6 min of ON source and 4 min of OFF source data. Often longer (15-20 min) streches of data were recorded and used. The smooth curves drawn in these figures represent the average variation of m_{pt} and $f_{2,pt}$ for point sources at 327 MHz as a function of elongation. The substantial scatter around the mean values is mostly due to genuine changes is the activity of the IPM. The statistical uncertainties in the estimation of m and f_2 are comparatively small, being $\sim 10\%$.

3.3.4   Model of the Interplanetary Meidum:

As discussed in Section 2.2.2, the parameters of the observed intensity pattern for point sources can be directly related to the properties of the electron density irregularities in the IPM when the weak-scattering and far-field conditions are satisfied. At 327 MHz, these conditions are satisfied for IPS observations with elongations between ~ 0.25 and 0.7 a.u. Observations of point sources described in the earlier section show that
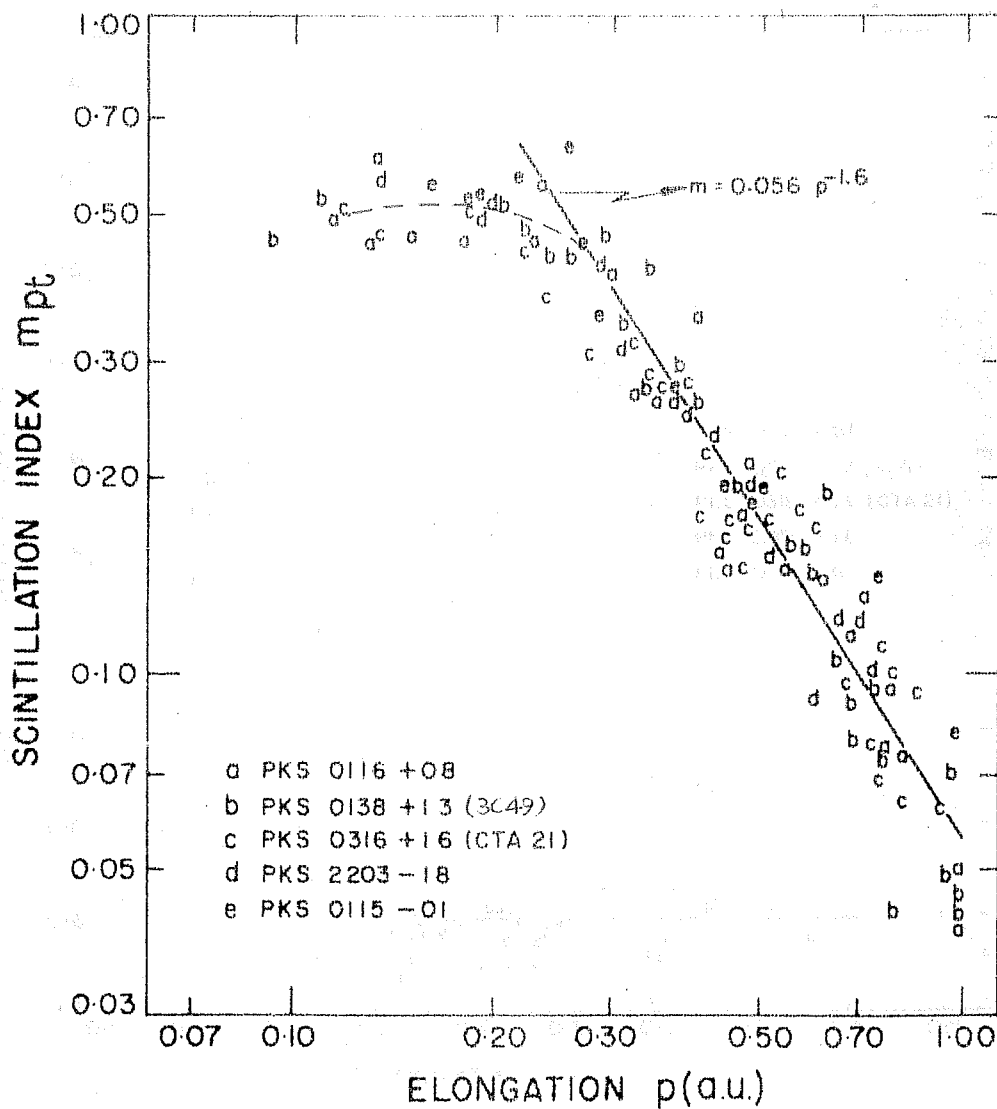
FIG. 3.3   Variation of the normalized scintillat-
ion index m_{pt} for point sources as a
function of elongation p. The solid
line through the data points represents
average variation in the weak scatter-
ing regime.
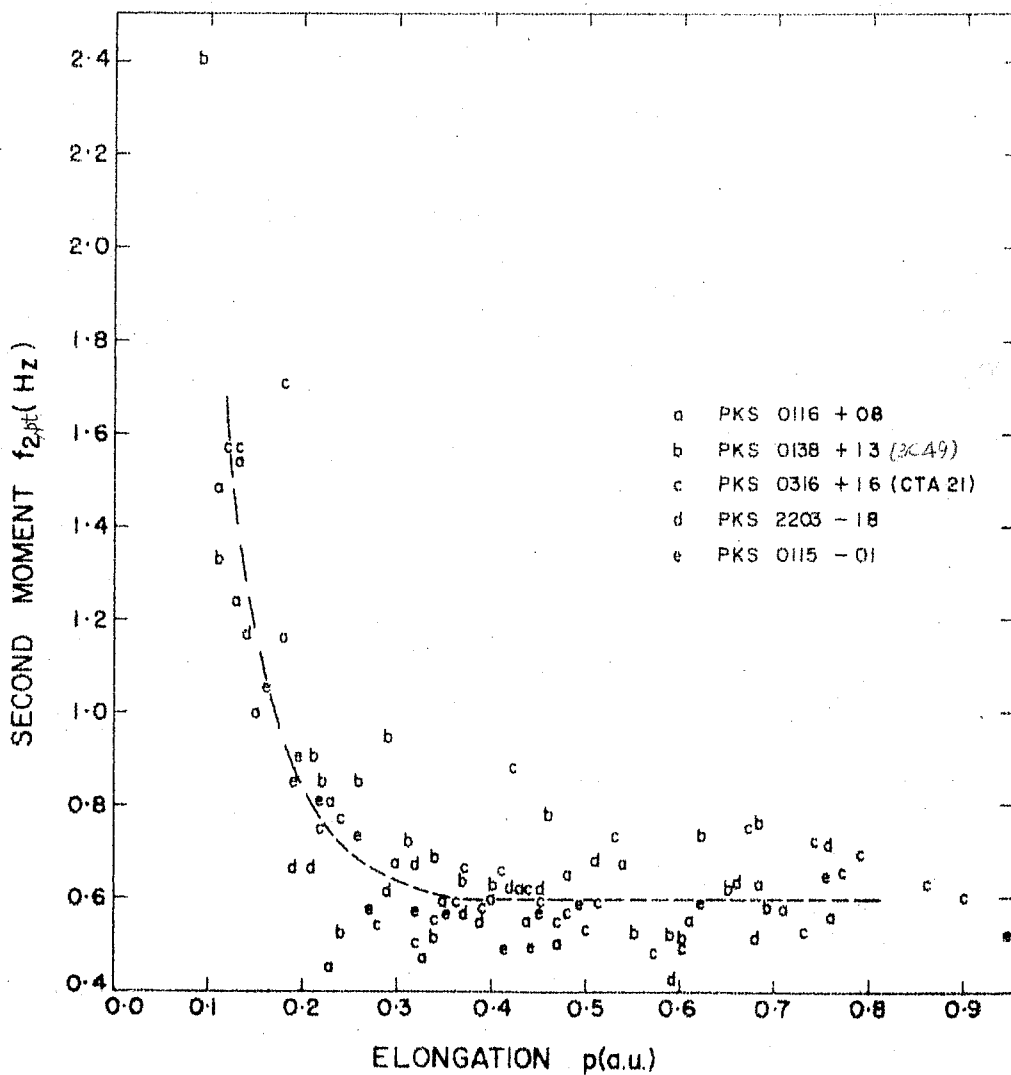
FIG. 3.4 Variation of the square-root second moment $f_{2,pt}$ of the scintillation power spectra for point sources as a function of elongation p. Broken line shows the average variation.

for $p \gtrsim 0.25$ a.u., m_{pt} and $f_{2,pt}$ vary with p as

$$m_{pt}(p) = 0.056 \, p^{-1.6} \quad \text{and}$$

$$f_{2,pt}(p) = \text{constant} \simeq 0.6 \text{ Hz.}$$

The observed scintillation index and second moment for point sources depend on the rms phase fluctuation φ_o and the scale size a of the irregularities and from eqns. (2.16a) and (2.20), we have

$$\varphi_o = m_{pt}/\sqrt{2} \quad \text{and}$$
$$a = v/(2\pi f_{2,pt}).$$

It is known from systematic multi-station IPS observations of a number of compact radio sources as well as from in-situ spacecraft measurements that, in agreement with theoretical models, the solar wind flows radially outwards from the sun with an average velocity of ~ 400 km s^{-1} which is roughly constant between $0.3 < p < 1.0$ a.u. (Coles et al. 1974). Due to integration along the line of sight the resultant transverse component of solar wind velocity i.e. the effective velocity with which the pattern moves across the observer, is less by about 10% (Jokipii and Lee 1973). We therefore use $v = 350$ km s^{-1} for converting temporal frequencies to

spatial scales and obtain

$$\varphi_o(p) = 0.04 \; p^{-1.6} \quad \text{and}$$
$$a(p) = 100 \text{ km.}$$

In order to derive a model of variation of ΔN_e and a as
a function of radial coordinate R from the sun, numerical
calculations were made incorporating a more realistic
multiple-thin screen model for the extended IPM. Power law
dependence on R was assumed for both the quantities and
best-fit exponents were determined by comparison with
observed m and f_2 variation. The results for $R > 0.25$ a.u.
are

$$\Delta N_e(R) = 0.08 \; R^{-2.05} \quad \text{electrons cm}^{-3} \quad \text{and}$$
$$a(R) = 100 \; R^{0.15} \quad \text{km,}$$

where R is in units of a.u. (Rao et al. 1974, Rao 1975).

Since $\Delta N_e \propto R^{-2.05}$, the scattering power of the
medium falls of as $R^{-4.1}$. Most of the scattering and scin-
tillations therefore arise due to that region of the line
of sight which is closest to sun. From the geometry of
Fig. 2.1, the distance z to the scattering layer is
$z = (1-p^2)^{\frac{1}{2}}$. Most IPS observations pertinent to measure-
ments of the structure of radio sources at 327 MHz were
made when $p \lesssim 0.4$ a.u. and hence z can be taken as 1 a.u.
without much error.

3.4 PROCEDURE FOR ESTIMATION OF THE STRUCTURE OF SCINTILLATING SOURCES

Once the average characteristics of the electron density irregularities in the IPM have been determined from the observed variation of m_{pt} and $f_{2,pt}$ with elongation for point sources, the structure of any scintillating source can be derived from a comparison of its observed m and f_2 values with the corresponding point source values at the same elongation. For this purpose, IPS observations must be carried out near the sun where scintillations are sufficiently strong and the effect of finite size of the source can be easily recognized. At 327 MHz, the scintillations are appreciably reduced outside the region $0.1 \leqslant p \leqslant 0.4$ a.u. In Section 3.3.3 we have shown that our measurements of m_{pt} and $f_{2,pt}$ for the 5 compact sources observed, represent true point source response of the IPM only for $p \gtrsim 0.25$ a.u. Thus for observations made in the region $p \gtrsim 0.25$ a.u. eqns.(2.35) can be directly used to estimate μ and ψ of the scintillating component in radio sources. For observations closer to sun, the measured $f_{2,pt}$ values themselves could be a result of cut off due to finite size of the sources studied. Values of ψ derived using eqns. (2.35) will therefore be underestimates of the angular size of the scintillating component. Eqn. (2.36) however provides a stronger upper limit on ψ for observations with $p < 0.25$, since in this region $\phi_o > 1$

and the point source spectrum is very broad. We have adopted the following procedure for estimation of μ and ψ of radio sources from their IPS observations.

Observations of IPS of radio sources were made at 327 MHz when the elongation was within the range 0.1-0.5 a.u. For each observation the power spectrum of scintillations was calculated and values of m and f_2 were derived. The methods of observations and analysis were the same as those described above **for** point sources. A source was considered to be scintillating if the power spectrum showed the characteristic excess towards low fluctuation frequencies (zero to a few Hz) and the observed index at different elongations roughly followed the expected behaviour.

For the scintillating sources if the ratio $(f_{2,ext}/f_{2,pt})$ was found to be less than 0.8, the source was considered to be resolved and the angular diameter ψ of the scintillating component was estimated using eqn. (2.35);

$$\psi = (v/(1.2 \, \pi \, f_{2,ext} \, z)) . \left[1 - (f_{2,ext}/f_{2,pt})^2 \right]^{\frac{1}{2}}$$

with $v = 350$ km s^{-1} and $z = 1.5 \times 10^8$ km. Once ψ is determined the scintillation visibility μ was estimated from eqn. (2.35) as

$$\mu = (m_{ext}/m_{pt}) . \left[1 + 0.36 \, (z \, \psi /a)^2 \right]^{\frac{1}{2}}$$

where the irregularity size a was taken to be 100 km.

If the ratio $(f_{2,ext}/f_{2,pt})$ was $\geqslant 0.8$, the scintillating component was considered point-like and an upper limit to its angular size was obtained from eqn. (2.36) as

$$\psi \leqslant v/(1.2\,\pi\,f_{2,ext}\,z)$$

For observations near $p \sim 0.25$ a.u. this limit turns out to be $\sim 0\rlap{.}''15$ arc. Often it was possible to make observations closer to sun and obtain an improved upper limit on ψ. We have however set a uniform limit of $0\rlap{.}''15$ arc for unresolved scintillating components in our IPS observations. For such sources with $\psi < 0\rlap{.}''15$ arc, the correction to observed m due to source size is negligible and μ was estimated from

$$\mu = m_{ext}/m_{pt}.$$

The division at $(f_{2,ext}/f_{2,pt}) = 0.8$ was decided arbitrarily in view of the day to day changes ($\sim 15\%$ rms) in the observed values for point sources.

Some sources did not display any scintillations above the receiver noise fluctuations either because of small flux of the scintillating component or due to the fact that observations could be made only at large p where scintillations become very weak. These source were called non-scintillating. No estimate of ψ is possible in such

cases. An upper limit on the flux of any compact scintil-
lating component in the sources, if present, can however
be obtained from a consideration of the system noise. As
a simple criterion we have assumed that any contribution
due to scintillations does not exceed half the observed ON
source variance. This provided a rough upper limit on
index m given by

$$m_{ext} < \left[(Var.\ ON)/2 \right]^{\frac{1}{2}} / \text{Intensity}.$$

Upper limit on μ for these sources was then derived by
dividing this value of m_{ext} by the observed m_{pt} value at
the elongation of the observations.

3.5 CONCLUSIONS

In this chapter we have described the methods of
observation and analysis of IPS at 327 MHz. The observ-
able in IPS is the random temporal fluctuations in the
intensity of a radio source. Information about the elec-
tron density irregularities in the IPM as well as the
fine structure of the scintillating source is contained
in this fluctuating signal and can be extracted by
examining its various statistical properties. In most
IPS work, statistical properties of order 2 i.e. the
variance and its Fourier decomposition, the power
spectrum, have been studied for this purpose. Some

attempts to use the third and fourth moments of the probability histogram of IPS intensities have also been made (Bourgois and Cheynet 1972, Milne 1975, Armstrong 1977).

In Sections 3.3 and 3.4 we have discussed the procedures for determining the characteristics of the interplanetary irregularities and the structure of radio sources from measurements of the scintillation index m and the width f_2 of the temporal power spectrum of IPS. The present method, based on the power spectrum analysis of intensity fluctuations, was developed and used by the Arecibo IPS group in interpreting the fine structure of radio sources in the IPS survey at 430 MHz (Cohen et al. 1967b, Harris and Hardebeck 1969). In low frequency IPS surveys undertaken at Cambridge, on the other hand, an alternative procedure based on measurements of m alone has been employed (Little and Hewish 1968, Readhead 1971, Readhead and Hewish 1974). In this method both μ and γ of the source are estimated by comparing the observed shape of the m vs. p variation (its slope, defined by the ratio $m(35^{\circ})/m(90^{\circ})$, and its peak value) with that computed theoretically for different source diameters. In these computations, the IPM is specified by gaussian irregularities whose scale is taken to vary roughly as $R^{1.5}$ with distance R from the sun (Readhead 1971). Our observations of a constant value of f_2 for $p \gtrsim 0.25$ a.u.

and a sharp increase in f_2 below 0.2 a.u. for compact point sources observed at 327 MHz do not support any variation in scale size faster than $\sim R^{0.25}$. A detailed discussion of the origin of this discrepancy, which may arise due to the correction to the observed scale sizes applied by the Cambridge workers for the finite size of the observed source 3C 48, has been given by Rao (1975) and will not be repeated here. As discussed in Section 3.3.3 our measured values of $f_{2,pt}$ for $p \gtrsim 0.25$ a.u., presented in Fig. 3.4, represent true point source parameter of the IPM and do not require any correction. We have therefore taken a $\simeq 100$ km for $0.25 < p < 0.7$ a.u. in all our calculations.

The power spectrum method is suitable for carrying out rapid surveys of the fine structure in radio sources by IPS technique as only one or a few observations under suitable circumstances allow reliable estimates of μ and γ to be obtained. The m-p curve method, on the other hand, requires a large number of IPS observations over an extended period of a few months. Also the angular diameter γ obtained from f_2 measurements near the sun is less dependent on the adopted model for the IPM than those determined using m. This is so because f_2 is more sensitive to high frequency tail of the scintillation power spectrum which is determined

mainly by the cut-off due to source structure. Furthermore, f_2 is also sensitive to source structure along the position angle (p.a.) of the solar wind scan whereas m, being the integral under the power spectrum, is invariant. By making IPS observations of a source on different days as the sun-source orientation changes, it is possible to combine f_2 measurements along various p.a. and study its two-dimensional structure. In this manner elongated components have been found in a number of radio sources from their IPS observations at 327 MHz (Rao et al. 1974, Ananthakrishnan 1976). The diameter estimates used in the present work are average gaussian half-power diameters of the scintillating components which are assumed to be circularly symmetrical.

Using the power spectrum method we have undertaken an IPS survey of known radio sources in the southern sky accessible with ORT. At the observing frequency of 327 MHz, the IPS technique is sensitive to components with angular sizes $\lesssim 0\overset{''}{.}5$ arc which is the angular size of the first Fresnel zone at z = 1 a.u. Since most of the sources observed during the survey were weaker (a few Jy at 327 MHz) than strong compact sources observed for calibrating the response of the IPM, the statistical uncertainties in the derived estimates of μ and ψ from a single IPS observation were large and comparable to the errors due

CHAPTER 4

THE IPS SURVEY OF SOUTHERN SKY SOURCES AT 327 MHz

In this chapter we present the results on the angular sizes and flux densities of the scintillating components found in the southern radio sources studied during the IPS survey at Ooty at 327 MHz. In Section 4.1 the criteria for selection of sources for IPS observations are given and a sample of stronger sources is defined for the purpose of statistical studies. A comparison of the IPS results with other high resolution studies of radio sources in the survey is made in Section 4.2. The dependence of scintillation properties on optical class, spectral index and redshift is investigated in Section 4.3. Finally, in Section 4.4 a detailed discussion of the radio and optical structure of one of the interesting sources in the IPS survey, namely PKS 1514-24, is presented.

4.1 THE IPS SURVEY AT OOTY

The phenomenon of IPS has been used extensively to study the fine structure in radio sources. Soon after the discovery of IPS at Cambridge (Hewish et al. 1964), the Cambridge as well as Arecibo groups have been actively engaged in studying the nature of compact components in radio sources by observing their IPS at meter wavelengths. A number of IPS surveys have been carried out. The most extensive ones are i) the IPS survey of about 500 northern ecliptic sources stronger than about 2 Jy at 430 MHz made by Harris and Hardebeck (1969) using the giant

Arecibo telescope and (ii) the Cambridge IPS survey by Readhead and Hewish (1974) in which more than 1500 radio sources covering entire northern sky are studied at 81.5 MHz. In contrast, no systematic IPS studies of radio sources in the southern sky have been made so far. There have been references to the IPS observations of southern sources at Parkes (Ekers 1967, Ekers 1969, Gardner et al. 1969) and Molonglo (Milne 1975). However, no quantitative estimates of the compact components in southern radio sources have been published. In 1970, we therefore decided to undertake an IPS survey of southern sky sources at 327 MHz using the Ooty Radio Telescope.

For selecting the radio sources for observations, two comprehensive catalogues of known radio sources in the southern sky were available at nearby frequencies of 178 and 408 MHz. The 4C catalogue at 178 MHz (Gower et al. 1967) covers a declination strip of 0° to -7° and the Parkes catalogue (Ekers 1969) covers the whole of the southern sky excluding the galactic plane region. Sources were selected for IPS observations from these two catalogues according to the following criteria:

i) $\left| b^{II} \right| > 10^o$,

ii) Declination (δ) between 0° and -30°,

iii) Expected flux density S at 327 MHz greater than or roughly equal to 1.5 Jy and

iv) Right Ascension (R.A.) between 09^h and 03^h.

The region of the sky to be surveyed was limited to the above R.A. range for the following reason. At 327 MHz, a

given source is observed to exhibit appreciable scintillations when the sun-source elongation is in the range of about $10^{\circ}-30^{\circ}$. Outside this range the scintillations are considerably reduced. In the region of the sky between 0° and -30° declinations, only sources in the above specified R.A. range (i.e. between 09^h and 03^h) attain solar elongations of less than about 30°, at some time of the year or other. Further when the sun was passing the region of sky between the R.A. of 17^h to 22^h only some selected strong point sources were observed due to the limitations of telescope time. The IPS survey of sources was therefore initially restricted to regions between 09^h and 16^h and between 22^h and 03^h of R.A.

Out of a list of more than 600 radio sources prepared for IPS studies we were able to make IPS observations of about 500 of them during the southern declination passage of the sun in 1970-71 and 1973-74. For most of the sources more than 2 observations were carried out while the elongation of the source was within the range $10^{\circ} - 30^{\circ}$. For the purpose of calibration of scintillation data several strong point sources were observed regularly so as to cover a wide range of elongations. In the following we present the IPS results on the 188 sources which were observed during 1970-71.

4.1.1   The Ooty IPS Sample;

Since the ORT is also used for a number of other programmes, IPS observations could not be carried out daily so as to observe each and every source in a given area of the sky. Rather,

we attempted to observe sources whose IPS could be observed most favourably during a given observing session. The 188 sources studied therefore do not constitute a complete sample in the usual sense of including all sources above a given flux density within a specified area of the sky. For the purpose of statistical studies concerning the average properties of scintillating radio sources we have therefore selected a sample of 149 sources according to the following criteria:-

(i) $S_{327} \geq 2.5$ Jy - We included sources with expected S_{327} greater than or equal to 2.5 Jy for the following reasons.

(a) For sources with $S_{327} < 2.5$ Jy there is no finding survey which provided a homogeneous list of known radio sources. Sources weaker than 2.5 Jy were in fact those for which either the Parkes catalogue listed flux densities only at 1415 MHz or only 4C fluxes at 178 MHz were available. Observations of these weaker sources at 327 MHz may therefore be biased against flat or steep spectrum sources respectively.

(b) In deriving the scintillation index m deflection produced by the source on the observed records is used to represent the total intensity. Due to the broad E-W beam of the telescope the observations are confusion limited below about 1.5 Jy. Therefore, depending upon the background near the source, the observed deflection will be affected, making the calculated value of μ less reliable for weaker sources.

(ii) $\left|b^{II}\right| \geq 20°$ - All sources having galactic latitude less than 20° were excluded since

(a) For sources close to the galactic plane the observed angular size might be affected by interstellar scattering (Readhead and Hewish 1972), specially since the present, southern sky observations correspond to longitudes towards the galactic center.

(b) To keep the sample free of any galactic radio sources.

With the above criteria i.e. with $S_{327} \geq 2.5$ Jy and $|b^{II}| \geq 20^{\circ}$, we are left with a sample of 149 extragalactic radio sources. Since sources were observed independent of their scintillation behaviour, we consider this sample to be reasonably random and unbiased for the purpose of statistical studies. In Table 4.1 the values of μ and Ψ alongwith other parameters for these 149 sources are listed. The entries are arranged in increasing order of right ascension. The information given in various columns is as follows:

Col. 1 — Name of the source in Parkes notation.

Col. 2 — 3C/4C name; whenever source is not listed in the Parkes catalogue, the 4C name is underlined.

Col. 3 — Optical identification from one of the following references: Parkes catalogue (Ekers 1969), Munro (1971a,b) and Veron and Veron (1974). Usual designations for galaxies (G) unidentified (−) and QSOs (Q) have been used.

Col. 4 and 5 — Expected flux density of the source at 327 MHz on the KPW scale and the spectral index α at 327 MHz defined as $S \propto \nu^{-\alpha}$ respectively. The values of S_{327} and α were determined by compiling the spectra of

Table 4.1 The Ooty IPS Sample of 149 Radio Sources with

$S_{327} \geq 2.5$ Jy and $|b^{II}| \geq 20^\circ$

Source name	3C/4C name	Optical Identification	Expected S_{327} Jy	α_{327}	Visibility μ	Angular size ψ''_{arc}
(1)	(2)	(3)	(4)	(5)	(6)	(7)
0003-00	3C2	Q	10.5	0.7	0.6	≤ 0.15
0005-06	3C3	G	4.5	1.0	0.8	~ 0.25
0016-12	-	-	6.4	0.7	< 0.2	-
0018-09	-	-	2.5	1.1	< 0.3	-
0018-01	-01.01	-	3.5	0.5	0.7	≤ 0.15
0019-00	+00.02	-	3.6	0.2	1.0	≤ 0.15
0020-08	-	-	3.5	0.7	< 0.3	-
0023-13	-	-	4.5	0.4	0.3	≤ 0.15
0027-12	-	-	4.1	0.4	< 0.4	-
0029-01	-01.02	G	2.7	0.9	< 0.5	-
0031-07	-	-	3.2	1.2	0.3	~ 0.20
0034-01	3C15	G	11.5	0.7	< 0.1	-
0035-02	3C17	G	18.0	0.8	< 0.1	-
0047-02	-03.02	Q	4.0	1.0	< 0.2	-
0051-03	3C26	G	6.6	0.8	0.5	≤ 0.15
0056-00	-00.06	Q	4.3	0.3	1.0	≤ 0.15
0115-01	-01.07	G	4.0	0.0	1.0	≤ 0.15
0117-15	3C38	Q	14.0	0.6	< 0.2	-
0119-04	-04.04	Q	3.4	0.6	0.8	≤ 0.15
0123-01	3C40	G	15.0	1.0	< 0.1	-

(1)	(2)	(3)	(4)	(5)	(6)	(7)
0129-07	–	G	4.2	0.9	1.0	≤ 0.15
0144-05	– 05.07	Q	3.5	1.0	0.4	≤ 0.15
0144-02	– 02.08	–	2.5	0.8	0.6	≤ 0.15
0148-09	–	–	3.4	0.9	0.4	~ 0.15
0150-03	3C53	–	4.8	0.9	0.7	≤ 0.15
0155-10	–	Q	5.6	0.5	0.3	≤ 0.15
0218-02	3C63	G	13.0	0.7	< 0.1	–
0222-00	– 00.12	G	2.8	0.9	0.5	≤ 0.15
0232-04	– 04.06	Q	4.8	0.4	0.6	≤ 0.5
0240-00	3C71	G	13.0	0.6	0.3	≤ 0.5
0919-14	–	–	4.6	(0.6)	< 0.5	–
0934-04	– 04.31	–	2.6	0.9	< 0.2	–
0939-11	3C224	–	4.3	(1.4)	< 0.3	–
0941-08	–	G	4.0	0.4	1.0	≤ 0.15
0944-13	–	–	3.5	(1.3)	< 0.7	–
0958-00	– 00.37	–	5.1	0.9	< 0.2	–
1005-09	–	Q	3.7	1.0	< 0.4	–
1006-11	–	–	2.8	1.1	0.5	≤ 0.15
1007-07	–	–	2.8	0.9	< 0.4	–
1008-01	– 01.21	G	2.5	0.7	< 0.3	–
1025-07	–	–	2.5	0.8	< 0.5	–
1026-05	– 05.42	–	2.6	0.6	0.4	≤ 0.15
1028-09	–	–	3.6	0.6	< 0.4	–
1031-11	–	–	3.9	0.4	0.7	~ 0.15
1036-04	– 04.36	Q	3.8	0.2	1.0	≤ 0.15

(1)	(2)	(3)	(4)	(5)	(6)	(7)
1046-02	-02.43	-	3.1	0.8	<0.3	-
1049-09	3C246	Q	4.7	1.1	0.2	~0.3
1059-01	3C249	-	9.2	0.9	0.1	≤0.15
1103-00	-00.43	Q	3.2	0.6	<0.3	-
1103-24	-	G	3.5	1.3	<0.6	-
1103-20	-	G	5.2	1.1	<0.2	-
1104-05	(-05.46)	-	3.4	0.6	<0.4	-
1110-01	3C253	-	4.7	0.8	<0.3	-
1116-05	(-05.47)	-	3.3	0.5	<0.6	-
1116-02	3C255	-	8.8	0.6	1.0	≤0.15
1127-14	-	Q	4.4	-0.3	1.0	≤0.15
1131-19	-	-	5.1	1.0	<0.4	-
1132-00	-00.45	Q	2.8	0.0	1.0	≤0.15
1136-13	-	Q	12.0	0.8	<0.2	-
1142-00	-00.46	-	2.9	0.9	<0.7	-
1148-00	-00.47	Q	3.1	-0.1	1.0	≤0.15
1212-00	-00.48	-	3.1	0.8	<0.5	-
1229-02	-02.55	Q	4.1	1.0	<0.7	-
1239-04	3C275	-	10.5	0.5	0.3	≤0.15
1244-11	-	-	4.3	1.0	<0.6	-
1245-19	-	-	7.0	-0.4	1.0	≤0.15
1247-19	-	G	4.1	0.8	<0.5	-
1252-12	3C278	G	17.0	0.7	<0.2	-
1253-05	3C279	Q	14.2	0.7	0.5	≤0.15
1306-09	-	G	9.0	1.2	0.7	~0.3

(1)	(2)	(3)	(4)	(5)	(6)	(7)
1309-22	(3C283)	G	22.0	0.9	0.8	≤ 0.15
1312-18	-	-	5.5	0.9	0.7	~ 0.15
1316-06	-06.33	-	2.5	0.6	0.7	~ 0.2
1317-00	-00.50	Q	3.5	0.4	< 0.4	-
1325-01	-01.29	G	3.5	1.0	< 0.3	-
1327-21	-	Q	6.0	1.0	< 0.3	-
1330-14	-	Q	3.0	0.6	< 0.6	-
1331-09	-	-	5.9	0.2	< 0.2	-
1334-29	-	G	5.5	-0.4	< 0.6	-
1334-17	-	G	4.5	0.4	1.0	~ 0.15
1335-06	-06.35	Q	10.0	1.0	< 0.3	-
1339-12	-	-	3.1	(0.9)	1.0	≤ 0.15
1342-00	-00.51	-	2.8	0.5	< 0.4	-
1344-07	-	-	6.3	0.9	0.3	~ 0.25
1348-12	-	Q	3.7	0.6	1.0	≤ 0.15
1358-11	-	G	4.6	0.5	< 0.3	-
1401-05	(-04.48)	-	3.0	0.4	< 0.6	-
1401-04	(-04.48)	-	2.8	1.0	0.4	~ 0.35
1403-02	-02.59	-	3.3	1.2	0.4	~ 0.20
1404-01	-01.31	Q	3.7	0.8	< 0.3	-
1411-05	-05.60	-	6.0	0.7	< 0.3	-
1412-10	-	-	2.9	0.7	0.8	≤ 0.15
1412-14	-	-	2.5	0.7	1.0	~ 0.2
1414-21	-	G	4.0	0.3	< 0.5	-
1414-03	3C297	-	4.8	0.9	1.0	~ 0.4

(1)	(2)	(3)	(4)	(5)	(6)	(7)
1416-15	-	G	4.5	0.5	<0.6	-
1417-19	-	G	5.0	0.9	<0.5	-
1420-27	-	Q	7.2	1.1	0.3	~0.25
1422-29	-	Q	7.6	0.9	<0.7	-
1424-11	-	Q	4.7	1.2	<0.3	-
1425-01	3C300.1	G	8.2	0.7	0.2	~0.25
1428-03	-03.52	-	3.5	0.8	1.0	~0.15
1436-16	-	G	5.4	0.5	0.7	~0.15
1445-16	-	-	2.7	0.4	1.0	≤0.15
1449-13	-	G	9.3	0.8	<0.2	-
1452-04	3C306.1	G	5.2	1.0	<0.2	-
1453-10	-	Q	9.0	1.0	0.5	~0.35
1500-02	-02.62	-	2.6	0.3	1.0	<0.5
1509-12	-	-	2.6	0.9	<0.5	-
1510-08	-	Q	4.7	0.3	1.0	~0.15
1512-05	-05.65	-	3.7	0.8	<0.5	-
1514-16	-	-	3.3	1.0	<0.4	-
1518-29	-	-	3.1	0.9	<0.4	-
1520-04	-04.55	-	4.3	0.7	<0.5	-
1524-13	-	Q	5.4	0.2	1.0	≤0.15
1528-29	-	Q	3.6	1.0	<0.2	-
1534-12	-	-	3.0	0.4	0.6	~0.15
1537-14	-	-	4.1	0.0	<0.5	-
1537-05	-05.68	-	3.1	1.0	0.9	~0.20
1539-09	-	-	2.5	1.0	1.0	~0.25

(1)	(2)	(3)	(4)	(5)	(6)	(7)
1553-06	-06.43	-	2.7	0.0	0.7	≤ 0.15
1556-21	-	-	6.8	0.5	< 0.3	-
1602-28	-	G	6.8	1.0	< 0.2	-
1602-17	-	-	5.9	0.8	< 0.2	-
1602-09	-	-	8.4	0.8	< 0.2	-
1635-14	-	-	3.6	0.0	< 0.5	-
2234-17	-	-	5.0	0.8	0.8	≤ 0.15
2235-12	-	-	3.8	1.0	< 0.2	-
2235-14	-	-	3.0	1.0	0.5	≤ 0.15
2236-17	-	G	4.3	0.8	< 0.3	-
2237-04	-04.85	-	4.6	1.2	< 0.2	-
2243-19	-	-	2.6	1.1	0.4	≤ 0.15
2243-03	-03.81	G	4.1	0.8	0.5	~ 0.15
2308-10	-	Q	3.0	0.2	1.0	≤ 0.15
2313-18	-	G	4.1	0.2	0.5	≤ 0.15
2313-16	-	-	3.2	1.2	0.4	≤ 0.15
2318-16	-	-	9.0	0.7	0.7	~ 0.2
2322-12	-	G	7.9	0.8	< 0.3	-
2325-15	-	G	5.7	0.7	0.3	~ 0.45
2329-16	-	-	3.8	0.2	0.9	≤ 0.15
2329-10	-	-	4.1	0.6	0.5	~ 0.2
2335-18	-	Q	2.5	0.4	0.3	≤ 0.15
2337-06	-06.76	-	2.9	0.1	1.0	~ 0.15
2338-16	-	-	5.2	0.8	0.2	≤ 0.15
2347-02	-02.90	-	6.2	0.1	0.9	≤ 0.15

(1)	(2)	(3)	(4)	(5)	(6)	(7)
2348-16	–	G	2.9	1.2	<0.3	–
2349-01	-00.61	G	4.0	0.7	0.2	~0.4
2354-18	–	–	5.2	(1.7)	<0.7	–
2354-11	–	Q	2.8	0.7	0.8	≤0.15

all the sources in the survey using all available
flux measurements. Values of α derived by extra-
polation from only one measurement at a higher or
lower frequency are enclosed within brackets, indi-
cating that these values are less reliable.

Col. 6 - The derived scintillation visibility μ of the
and 7   source and the half power angular diameter Ψ of the
scintillating component respectively.

The IPS results on sources which fail to satisfy the
criteria for inclusion in Table 4.1 are listed in Table 4.2,
which is arranged in the same fashion.

4.2 COMPARISON OF IPS MEASUREMENTS WITH OTHER HIGH RESOLUTION STUDIES AT METER WAVELENGTHS

Before attempting to study the characteristics of
compact features in radio sources found by the IPS method it is
important to establish the reliability of the scintillation
measurements. For this purpose we compare the visibility esti-
mates derived by independent methods of observations and ana-
lysis. There are 65 sources in the Ooty IPS survey for which
either IPS observations are available at more than one freq-
uency or high resolution long baseline interferometric (LBI)
or lunar occultation (LO) observations are available at meter
wavelengths with resolution better than ~ 5' arc.

Table 4.3 summarises the fine structure information
on these 65 sources. Column 1 gives the source name. Column
2 gives the values of μ and Ψ derived from IPS observations
at various frequencies. Long baseline interferometric obser-

Table 4.2 Sources in the Ooty IPS Survey with

$$S_{327} < 2.5 \text{ Jy} \quad \text{or} \quad |b^{II}| < 20°$$

Source name	3C/4C name	Optical Identification	Expected S_{327} Jy	α_{327}	Visibility μ	Angular size $\psi_{\text{"arc}}$
(1)	(2)	(3)	(4)	(5)	(6)	(7)
0013-00	-	Q	1.4	1.4	0.7	~0.2
0016-10	-	-	2.4	1.3	<0.2	-
0044-05	-05.03	-	1.6	0.9	0.6	≤0.15
0046-06	-06.04	-	1.1	1.0	<0.4	-
0047-10	-	Q	1.3	0.4	1.0	≤0.15
0122-00	-	Q	1.1	-0.2	0.6	≤0.15
0131-00	(-00.11)	G	1.1	1.2	0.8	≤0.15
0140-07	-	-	1.7	(0.8)	<0.6	-
0140-01	-01.09	-	2.2	0.9	<0.1	-
0153-05	-05.08	-	1.6	0.6	0.9	≤0.15
0232-02	-02.12	Q	1.9	1.0	0.4	≤0.5
0300-00	-00.14	Q	2.1	1.0	<0.4	-
0902-04	-04.30	-	1.6	1.2	<0.3	-
0955-01	-01.20	-	2.1	0.4	0.5	≤0.15
1007-03	-03.40	G	1.7	1.5	<0.4	-
1017-02	-	-	1.8	0.2	<0.6	-
1044-00	-00.39	-	2.0	1.5	<0.4	-
1052-00	-00.41	Q	1.9	0.7	<0.7	-
1101-04	-04.37	-	1.8	0.6	<0.4	-
1105-02	-02.45	Q	1.8	0.6	<0.4	-

(1)	(2)	(3)	(4)	(5)	(6)	(7)
1115-02	-02.46	-	2.4	1.0	0.3	≤0.15
1158-05	-	-	2.0	0.6	1.0	~0.3
1257-00	-00.49	-	1.8	0.7	<0.5	-
1322-01	-01.28	-	1.8	0.8	<0.6	-
1333-05	-05.58	-	2.3	0.6	<0.5	-
1404-06	-06.37	-	2.2	0.6	<0.5	-
1408-03	-03.49	G	1.3	1.6	<0.3	-
1410-06	-	G	2.3	1.0	1.0	~0.3
1433-05	-04.51	-	2.2	0.5	1.0	≤0.15
1503-00	-00.58	-	2.3	0.6	<0.5	-
1514-24	-	G	1.5	0.0	0.8	≤0.15
1524-04	-04.56	-	2.0	1.2	<0.7	-
1542-05	-05.69	-	2.2	0.3	1.0	≤0.15
1609-14	-	-	2.1	0.4	1.0	≤0.15
1622-29	-	-	4.5	-0.2	1.0	≤0.15
1640-15	-	-	5.9	(1.1)	<0.3	-
2239-10	-	-	2.2	0.4	1.0	≤0.15
2300-18	-	G	2.4	1.0	<0.4	-
2345-16	-	Q	2.4	0.6	0.5	≤0.15

vations of fringe visibility γ and angular size ψ are given in Column 3 and similar information derived from lunar occultation observations is listed in Column 4 of the table. References to IPS, LBI and LO observations at various frequencies are listed in the 'Notes' following Table 4.3.

There are 34 sources for which the IPS observations are available at two or more frequencies. The values of scintillation visibility derived from IPS observations at 327 MHz are in good agreement with those of Harris and Hardebeck (1969) at 430 MHz. Comparison between 81.5 and 327 MHz indicates that in some cases (e.g. PKS 2243-03) the 81.5 MHz visibilities are slightly higher. This could be due to the fact that a comparatively larger component produces coherent scintillations at lower frequencies. There is however a possibility that larger values of μ arise due to the method by which scintillation data is analyzed to obtain μ at 81.5 MHz (see Chap. 6, and Ananthakrishnan 1976).

The LBI observations are available for 28 of the survey sources at frequencies ranging from 111 MHz to 610 MHz. Most of these are strongly scintillating ($\mu = 1.0$) sources. Whenever the LBI studies have resolutions comparable to IPS, the agreement is good. In other cases where LBI studies have resolutions considerably poorer than IPS studies, it is only possible to check whether LBI and IPS results are consistent with each other. In all the cases where broad or complex structure is indicated by LBI observations, little or no

scintillations were observed. No inconsistencies are found except in the case of PKS 2329-16, which is known to be a widely separated double (separation ~ 3' arc) with compact components. The high value of μ observed for this source implies component sizes $\lesssim 0''.15$ arc.

Furthermore, 11 sources in Tables 4.1 and 4.2 have been studied by LO and except for PKS 1453-10, results for all other sources agree well with the IPS results. In the case of PKS 1453-10, both IPS and LO observations find the source to be resolved. The different resolutions of IPS ($0''.35$ arc) and LO (~ $0''.8$ arc) observations at 327 and 410 MHz might explain the observed discrepancy in μ .

Thus it is seen that the fractional flux densities of compact components in radio sources obtained by IPS measurements at 327 MHz are quite consistent with independent measurements of compact components using different techniques. There are three 3CR sources which appear to show a systematic change of μ with frequency, implying frequency dependent compact structures. These are discussed below:

(1) 0003-00 (3C2)

The IPS observations at 178, 318, 327 and 430 MHz as well as the lunar occultation observations of Lyne (1972) at 408 MHz show that about 60% of the total flux of this source originates in a compact component of size $\lesssim 0''.1$ arc. The IPS observations of Readhead and Hewish (1974) at 81.5 MHz, however, give $\mu = 0.9$. In addition to the compact component, the

Table 4.3   Comparison of IPS/LBI/LO Measurements of Fine
Structure of Sources in the Ooty IPS Survey

Source Name	IPS			LBI (Freq.)		LO (Freq.)	
	Freq. MHz	μ	ψ''_{arc}	γ	ψ''_{arc}	γ	ψ''_{arc}
(1)	(2)			(3)		(4)	
0003-00	53	~0.7	-	(430) 0.07	≤0.05	(408) 0.6	<0.7
	81.5	0.9	0.5				
	111	~0.7	-				
	151.5	1.0	0.4				
	178	0.5	≤0.07				
	195	0.6	~0.1				
	318	~0.6	-				
	327	0.6	≤0.06				
	408	~0.4	≤0.06				
	430	0.6	≤0.06				
0005-06	81.5	>0.55	<0.4				
	327	0.8	~0.25				
0013-00*	318	>0.5	-				
	327	0.7	0.2				
0018-01	81.5	1.0	~0.15				
	327	0.7	≤0.15				
	430	1.0	≤0.15				
0019-00	327	1.0	≤0.15	(430) 0.66	≤0.05		
				(610) ~1.0	~0.015		
0029-01	81.5	>0.65	<0.3				
	318	<0.3	-				
	327	<0.5	-				

(1)	(2)		(3)	(4)
0034-01	81.5	$>$ 0.15 $<$ 1.4		(408)
	178	$<$ 0.2 —		Complex
	327	$<$ 0.1 —		3 comps.,
	430	$<$ 0.1 —		each $\sim$2"arc
0035-02	81.5	$<$ 0.2 —		
	178	$<$ 0.2 —		
	327	$<$ 0.1 —		
0051-03	81.5	$>$ 0.45 $<$0.6		
	327	0.5 $\leq$ 0.15		
0056-00	327	1.0 $\leq$ 0.15	(430)	
	430	1.0 $\leq$ 0.08	$\sim$0.60 $\leq$ 0.05	
0115-01	81.5	$>$ 0.8 $<$ 1.2		
	327	1.0 $\leq$ 0.1		
0122-00*	327	0.6 $\leq$ 0.15	(610)	
	430	1.0 $\leq$ 0.2	— $\sim$ 0.015	
0123-01	81.5	$<$ 0.15 —	Complex	
	178	$<$ 0.2 —		
	195	$<$ 0.05 —		
	327	$<$ 0.1 —		
0129-07	81.5	0.2-0.9 $<$1.0		
	327	1.0 $\leq$ 0.15		
0144-02	81.5	$>$ 0.7 $<$ 0.3		
	327	0.6 $\leq$ 0.15		
0150-03	81.5	1.0 $\sim$ 0.4		
	327	0.7 $\leq$ 0.15		

(1)	(2)		(3)	(4)
0218-02	81.5	<0.2 —		
	178	<0.2 —		
	327	<0.1 —		
0232-04	81.5	$>0.35 < 0.7$		
	327	0.6 <0.5		
0240-00	81.5	0.3 <0.6	(430)	
	178	<0.3 —	<0.01 ≤ 0.05	
	195	<0.1 <0.3		
	327	0.3 <0.5		
0919-14	327	<0.5 —	(408) Double comp. ~ 3" arc	
0934-04	81.5	$>0.35 < 0.7$		
	327	<0.2 —		
0944-13	327	<0.7 —	(408) Single ~4" arc	
0958-00	81.5	<0.35 —		
	327	<0.2 —		
1008-01	318	~ 0.15 —		
	327	<0.3 —		
1059-01	81.5	<0.2 —		
	178	<0.2 —	(408) Double	
	195	0.3 ≤ 0.3		
	327	0.1 ≤ 0.15		
1110-01	195	<0.3 —		
	327	<0.3 —		

(1)	(2)			(3)	(4)
1116-02	81.5	0.45	<0.2		
	178	0.7-1.0	~0.15		
	327	1.0	≤0.15		
1127-14	327	1.0	≤0.15	(408) 1.0 ≤0.01	
1132-00	327	1.0	≤0.15		(327) 1.0 <1.4
1136-13	327	<0.2	-	(408) Double comp. ~3" arc	
1148-00	327	1.0	≤0.15	(111) 1.0 <0.2	
	430	1.0	-	(196) ~0.8 <0.1 (408) 1.0 ~0.03	
1212-00	81.5	>0.5	<0.5		
	327	<0.5	-		
1229-02	318	0.2	-		
	327	<0.7	-		
1239-04	81.5	1.0	~0.5	(151) 1.0 ≤3.5	
	151.5	1.0	~0.6		
	178	0.5-1.0	0.15		
	327	0.3	≤0.15	(408) ~0.45 ≤0.3	
1253-05	81.5	0.3-0.8	<0.7	(408) ~0.3 ~0.02	(81.5) ~0.4 < 2.5
	151.5	0.6	~0.5		
	327	0.5	≤0.15		(240) ~0.4 <0.5
	408	~0.4	-		(408) ~0.5 <0.5 complex

(1)	(2)			(3)	(4)
1306-09	81.5	0.3-0.6	<0.5		
	327	0.7	~0.3		
1309-22	327	0.8	≤0.15	(408) some struc-ture of ~0".4 arc	
1330-14	327	<0.6	-	(408) double, comps. <4".0 arc	
1335-06	81.5	>0.15	<1.5		(240) double or ex-tended
	327	<0.3	-		
1344-07	327	0.3	~0.25		(408) 0.7 <1x ≤5 double
1411-05	81.5	>0.45	<0.6		
	327	<0.3	-		
1412-14	327	1.0	~0.2	(408) 1.0 <3	
1414-03	81.5	>0.3	<1.0	(408) 1.0 ~2x <1	
	327	1.0	~0.4		
1416-15	327	<0.6	-	(408) <0.4 <3	
1425-01	81.5	>0.4	<0.65		
	178	<0.3	-		
	195	0.1	<0.3		
	327	0.2	~0.25		
1433-05*	81.5	1.0	~0.15		
	327	1.0	≤0.15		

(1)	(2)		(3)	(4)
1436-16 327	0.7	~0.15		(408) — ∠1x <5
1449-13 327	<0.2	–	(408) double comp. 4"arc	
1453-10 327	0.5	~0.35		(410) ~0.8 <0.8 double
1510-08 327	1.0	~0.15	(408) <0.8 ~0.03	
1514-24* 327	0.8	≤0.15		(327) 1.0 <0.8
1524-13 327	1.0	≤0.15	(408) 1.0 ≤3.0	
1537-14 327	<0.5	–	(408) <0.4 ≤4.0	
1609-14 327	1.0	≤0.15	(408) 1.0 ~2.5	
1635-14 327	<0.5	–	(408) double, comp. <4"arc	
1640-15 327	<0.3	–	(408) double, comp. ~6"arc	
2235-14 327	0.5	≤0.15	(408) double, comp. ~2"arc	
2237-04 81.5	<0.4	–		
327	<0.2	–		
2243-03 81.5	1.0	~0.45		
327	0.5	~0.15		

(1)	(2)	(3)	(4)
2318-16 327	0.7 $\sim$0.2	(408) $\sim$1.0 $\sim$2.5	
2325-15 327	0.3 $\sim$0.45	(408) double, comp. $\sim$4" arc	
2329-16 327	0.9 $\lesssim$0.15	(408) double, comp. $\lesssim$3" arc	
2345-16 327	0.5 $\leq$0.15	(408) $\sim$0.5 $\lesssim$5	
2347-02 81.5 327	$>$0.6 $\leq$0.35 0.9 $\lesssim$0.15		
2348-16 327	$<$0.3 –	(408) double, comp. $\sim$2" arc	

* Sources from Table 4.2

Notes to Table 4.3 (References)

IPS Studies

FREQ. (MHz)	Ref.
53, 111, 318	Harris (1974)
81.5	Readhead and Hewish (1974)
151.5	Duffett-Smith and Readhead (1976)
178	Little and Hewish (1968)
195	Cohen et al. (1967a)
318	Harris (1973)
408	Milne (1975)
430	Harris and Hardebeck (1969)

LBI Studies

FREQ. (MHz)	Ref.
111, 196	Clark and Erickson (1973)
151, 408	Wraith (1972)
408	Critchley, Palmer and Rowson (1972)
408, 448	Broten et al. (1969) and Clarke et al. (1969)
430	Broderic and Condon (1975)
610	Jauncey et al. (1970)

LO Studies

FREQ. (MHz)	Ref.
81.5	Collins and Scott (1969)
327	Kapahi (1975b)
408	Lyne (1972)
410	Hazard and Sutton (1971)

lunar occultation observations at 408 MHz show that, the source has an elongated (jet) component which is about $5'' \times < 0''.5$ arc in p.a. $240°$. This component is inferred to have a steep spectrum (Lyne 1972), contributing about 60 % of the total flux at 80 MHz. Increase in scintillation visibility below 178 MHz, also noted by Harris (1974) at 53 and 111 MHz, indicates the presence of fine structure in the elongated jet component known to have its transverse dimension $< 0''.5$ arc.

(2) 1116-02 (3C 255)

The decreasing value of μ with decreasing frequency observed for this source can be explained in terms of a core-halo structure. The core being compact scintillates, has a self-absorbed spectrum and contributes to most of the flux of the source above 200 MHz. Below 200 MHz the non-scintillating halo dominates resulting in the decrease in the value of μ. The total spectrum of the source shows a break which is indicative of the presence of a compact and an extended component.

(3) 1239-04 (3C 275)

Both IPS and LBI observations show that μ increases with decreasing frequency. Interferometric observations of Wraith (1972) at 151 and 408 MHz are in agreement with all the IPS observations. Wraith has fitted a core-halo model to the interferometric observations at 408 MHz. The increase of visibility with the decreasing frequency of observation seen in Table 4.3 is difficult to explain, however, in terms of the

core-halo model unless one assumes that the spectrum of the extended halo is flatter than the core.

4.3 FINE STRUCTURE IN RADIO SOURCES AT 327 MHz

About half of the radio sources observed exhibited detectable interplanetary scintillations at 327 MHz indicating the presence of small scale components with angular size $\lesssim 0\overset{''}{.}5$ arc in them. For the remaining sources which did not show scintillations we have been able to put upper limits on their scintillation visibility. As seen from Tables 4.1 and 4.2, in some cases these upper limits are poorly determined (0.4 or more). Some of these sources may indeed be moderate or weak scintillators. Thus the actual percentage of sources which scintillate may be considerably higher than 50 %.

In Figure 4.1 we show the distribution of μ for the 149 sources in the Ooty Sample. Sources with adjacent values of μ (e.g. 0.1 and 0.2, 0.3 and 0.4 etc.) have been grouped and the upper limits are plotted as blank areas with arrows. In Table 4.4, we give the percentages of sources having $\mu \geq 0.3$, $\mu \geq 0.5$ and $\mu = 1.0$. It is seen that at least 48 % of all sources have $\mu \geq 0.3$. We must, however, note that the scintillation visibility is derived on the assumption that radio sources have a simple core-halo structure in which only the compact core contributes to scintillation and the halo has a non-scintillating, broad structure. However, since a majority of radio sources are known to be double or complex, the derived visibility will almost always be an underestimate of the
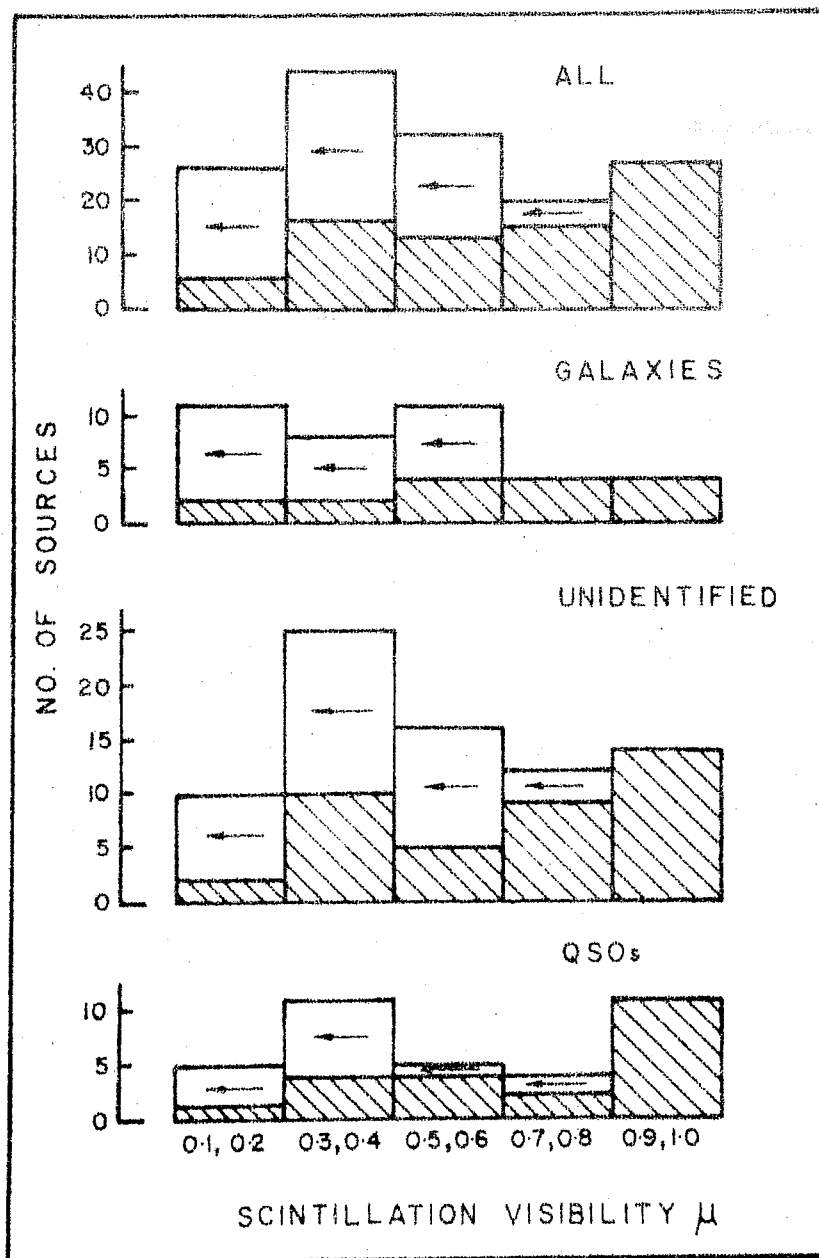
FIG. 4.1 Distribution of scintillation visibility for different classes of sources in the Ooty IPS sample.

Table 4.4 Occurrence of Scintillating Fine Structure
in Radio Sources in the Ooty Sample

Source type	Total No. of sources	Percentage of sources with		
		$\mu \gtrsim 0.3$	$\mu \gtrsim 0.5$	$\mu = 1.0$
All	149	> 48	~ 37	16
Galaxies	38	> 37	~ 32	10
Unidentified sources	77	> 49	~ 36	14
QSOs	34	> 56	~ 44	26

fractional flux density originating in compact components. For example, in the case of a double source with point components with separation exceeding the size of the first Fresnel zone, we would observe $\mu = 0.7$ instead of 1.0. Thus, we see that in more than half the sources 30 to 50 % or more of their flux density may arise from compact components. Further, in about 15 % of all the sources, there does not seem to be any structure with angular scales ≥ 0.5 arc. All these results show that compact components are an important feature of all extragalactic radio sources. Their relationship with the over-all structure and morphology of the sources is discussed in the next chapter.

For studying the occurrence of fine structure in different classes of radio sources, we have divided the sample into three categories; galaxies, unidentified sources and QSOs. There are 38 galaxies, 77 unidentified sources and 34 QSOs in the Ooty sample of 149 sources. The histograms showing the distribution of μ for these three classes are shown in the lower part of Figure 4.1.

4.3.1 Identified Radio Galaxies and QSOs:

From Figure 4.1 and Table 4.4 it is seen that the frequency of occurrence of scintillation as well as the average scintillation visibility of QSOs is higher than that of galaxies. Also percentages given in Table 4.5 indicate that the scintillating components in QSOs are more often unresolved than in the case of galaxies. Although these results are based

Table 4.5   Percentage of Scintillating Sources with
            Resolved and Unresolved Components in the
            Ooty Sample

Source type	No. of Scint. sources	Resolved	Unresolved
All	76	28%	72%
Galaxies	16	37	63
Unidentified sources	40	31	69
QSOs	20	15	85

on small number of QSOs and galaxies in the sample, high average value of μ together with higher percentage of unresolved scintillating components in QSOs suggest that QSOs have more compact angular structures than galaxies. Studies of structure of radio galaxies and QSOs with angular resolutions ranging from < 1" arc to a few tens of seconds of arc (Miley 1971 etc.) have also indicated that as far as their overall radio dimensions are concerned, QSOs are scaled down versions of radio galaxies.

4.3.2 Unidentified Sources;

In all radio source catalogues there is a large fraction of sources for which no obvious optical counterpart can be located on the Palomar Sky Survey plates. The fraction of such unidentified radio sources increases with decreasing flux density limit of the radio survey. Typically at meter wavelengths, in surveys complete down to about 2 Jy, about half of the sources remain unidentified to apparent magnitude of ~ 21. The μ distribution for the 77 unidentified sources in the Ooty sample of 149 sources with $S_{327} \geq 2.5$ Jy is shown in Figure 4.1 alongwith that for radio galaxies and QSOs.

Since unidentified sources represent a large fraction of all radio sources, it is important, in the study of extragalactic radio sources, to investigate whether these are similar to identified galaxies or QSOs or they represent a new class of objects. Various authors have tried to study the nature of unidentified sources by comparing their observed properties with those of galaxies and QSOs. Bolton (1966) and many others

(Braccessi et al. 1970, Munro 1971c, Wall 1972) compared the distribution of spectral indices of identified and unidentified sources at various frequencies and reached the conclusion that unidentified sources should mostly be galaxies fainter than the limiting magnitude of the Sky Survey plates. Bolton also showed that among other things, e.g. comparison of the slope of log N-log S relation, polarization and distribution of optical magnitudes of identified galaxies and QSOs, the angular structure data provided by IPS can also be used to infer the nature of unidentified sources. Since, qualitatively, the radio properties of these sources are similar to the identified sources, we will assume that they consist of some mixture of galaxies and QSOs only. On the basis of this assumption, a quantitative estimate of the proportion of galaxies and QSOs in the unidentified sources can be made by comparing the scintillation characteristics of the three classes of sources.

First, we compare the relative frequencies of occurrence of scintillation in the three classes. For this purpose we use only the percentage of sources with $\mu \geq 0.5$, since below $\mu = 0.5$ the presence of a large number of upper limits on μ make a quantitative estimate unreliable. We find from Table 4.4 that about 32 % of galaxies, 36 % of unidentified sources and 44 % of QSOs have $\mu \geq 0.5$. If the unidentified sources are a mixture of galaxies and QSOs, this would require the composition of unidentified sources to be such that for every QSO there are two galaxies. Again a comparison of percentage of fully scintil-

lating sources with $\mu = 1.0$ (from the last column of Table 4.4), indicates that about 75 % of the unidentified sources should be galaxies. Independent support to the above conclusion is provided by the statistics of angular sizes of scintillating components. From Table 4.5, we find that about 69 % of unidentified sources have unresolved components whereas 63 % of galaxies and 85 % of QSOs have unresolved components. Now, if indeed unidentified sources are mainly galaxies located relatively farther away so as to appear fainter than the sky survey limit, then we would expect them to be generally more compact than the sources already identified with galaxies. On the other hand, if they are similar to QSOs they should appear even more compact than sources already identified with QSOs. The percentages mentioned above support the former hypothesis that unidentified sources are predominantly galaxies having similar absolute magnitudes as the identified galaxies but are located farther away so as to appear fainter than ~ 20 to 21 mag.

4.3.3 Correlation of Scintillation Visibility with Spectral Index:

It is known from the earlier studies of IPS of radio sources that the flat spectrum radio sources are generally more compact than the steep spectrum sources (Harris and Hardebeck 1969). In Figure 4.2 we have plotted scintillation visibility μ against spectral index α around 327 MHz for galaxies, unidentified sources and QSOs separately for the Ooty IPS sample.
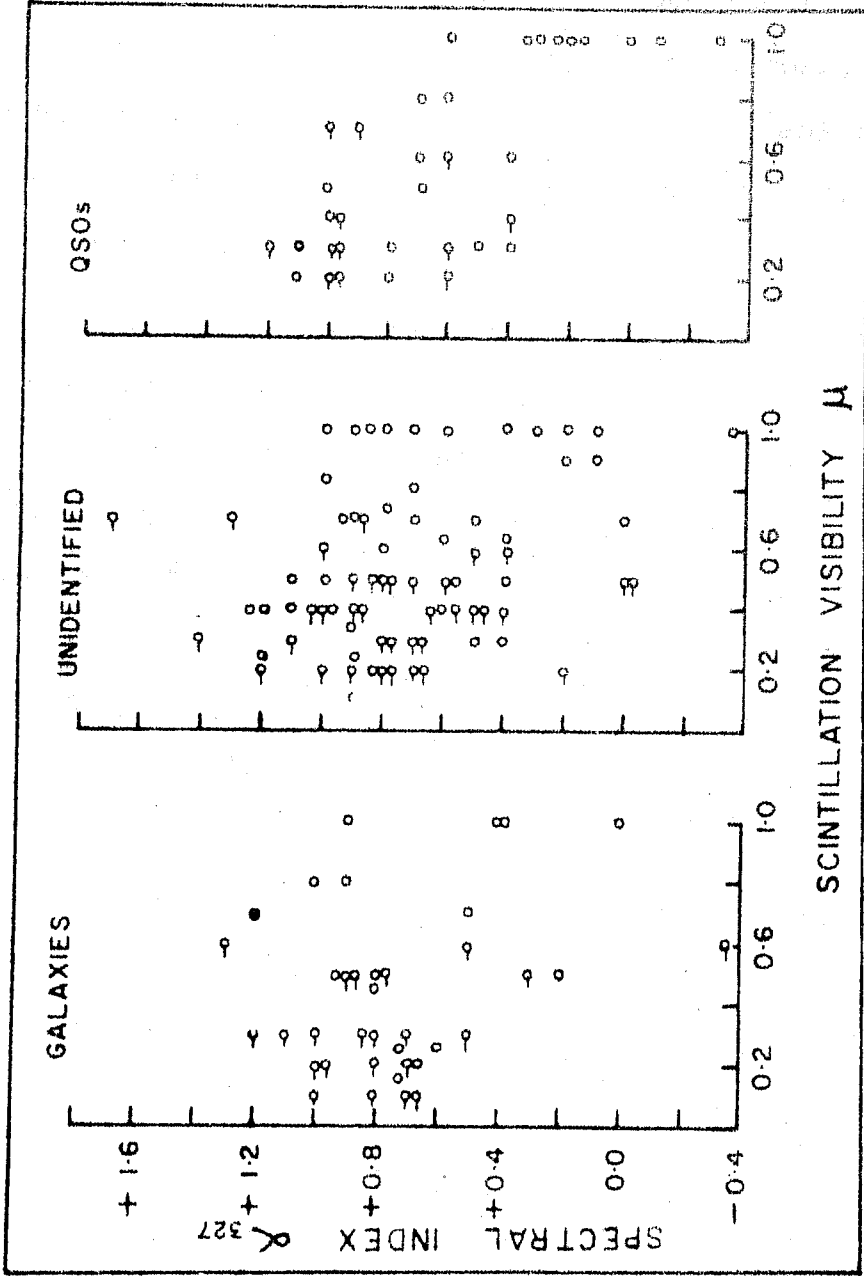
FIG. 4.2 Scatter plot of spectral index against scintillation visibility for galaxies, unidentified sources and QSOs in the Ooty sample.

The upper limits on μ for non-scintillating sources are plotted with a horizontal bar attached to the points. It is seen that, in general, all the flat spectrum sources ($\alpha < 0.4$) have high scintillation visibility. For normal, steep spectrum sources, however, there does not seem to be any significant correlation between μ and α ; at any α sources are distributed over a large range of μ .

Flat spectrum sources in general are characterised by their high scintillation visibility and extremely small angular size ($\lesssim 0''.15$ arc). This stands out more clearly for QSOs; all QSOs with $\alpha < 0.4$ in the Ooty sample have $\mu = 1.0$ and angular size $\Psi \lesssim 0''.15$ arc. Similar conclusion is reached by Wills (1974) who, using the largest angular size θ of QSOs, at 2700 MHz, showed that most QSOs with $\alpha \lesssim 0.5$ remain unresolved with $\theta \lesssim 2''$ arc while QSOs with $\alpha > 0.5$ (steep) have angular sizes uniformly distributed in the range $\sim 2''$ to $40''$ arc. That QSOs may be separated into two classes by their radio spectrum is also brought out by the observation that only flat spectrum QSOs show radio and optical variability, high polarization and extremely compact structures (Kraus and Gearhart 1975 and references therein). On the other hand, steep spectrum QSOs have radio structures and other radio properties similar to radio galaxies.

4.3.4 Correlation of Scintillation Visibility with Redshift:

Redshifts of radio galaxies are believed to be due to the cosmological expansion of the Universe and therefore can be

used to determine their distances. The cosmological interpretation of redshifts for QSOs, although generally accepted, has been questioned by many workers. A study of the variation of the properties of radio sources with redshift may therefore be important in exploring whether both radio galaxies and QSOs are located at distances indicated by their redshifts. Miley (1971) was the first to establish a correlation of the largest angular size Θ of QSOs with redshift z. Also a redshift-magnitude correlation, similar to that seen for radio galaxies was shown to exist for QSOs (Setti and Woltzer 1973), indicating that the redshift of these objects should also be largely cosmological. In such a case we would expect a correlation between μ and z for radio galaxies and QSOs in the sense that μ increases with increasing z. This is because with increasing redshift, a larger and larger fraction of the source would subtend an angle small enough to produce IPS.

Using IPS data on 22 QSOs with known z Cohen et al. (1967b) studied the correlation between μ and z. No correlation was seen; high values of μ for some of the QSOs were found to be due to their flat radio spectra and not due to high redshifts. Later Harris and Hardebeck (1969) and Harris (1973) from the same group, studied the dependence of μ on apparent magnitude of 67 radio galaxies and on redshift of 95 QSOs respectively. The effect of the correlation between μ and α (Cohen et al. 1967b, Sec.4.3.3) was however not considered. In the following therefore we study the dependence of scintillation visibility on redshift for a large number of

radio galaxies and QSOs having steep radio spectra. Since in the Ooty sample, the identified sources for which redshift measurements are available, are not large in number, all published IPS observations have been utilized for studying the $\mu-z$ correlation. Redshift values for radio galaxies were taken from a list kindly supplied by Prof. A.T. Moffet and values of redshifts of QSOs were taken from various compilations available in the literature (e.g. Burbidge and O'Dell 1972, Bell and Fort 1973). There are 131 QSOs and 107 galaxies for which both μ and z are available. Using spectral information provided in Table 4.1 and 4.2 and by Kraus and Gearhart (1975) we have excluded all QSOs which show flat and centimeter excess spectra from the analysis. In case of galaxies no extensive compilation of their radio spectral data exists and depending on the availability of spectral information, flat spectra sources have been rejected. In Figure 4.3, we show the histograms of distribution of μ in 6 different ranges of redshift for 104 galaxies and 88 QSOs with normal spectra. The redshift ranges for QSOs were chosen in such a way as to have approximately equal number of sources in each range, so that the histograms represent comparable statistics. It is evident from the figure that the μ distribution shifts to higher and higher values of μ with increasing redshift. The distribution of μ in the redshift range $0.1 < z \lesssim 0.5$ is plotted separately for radio galaxies and QSOs and the two distributions are seen to be very much alike. A small tail in the μ distribution of galaxies is almost certainly due to
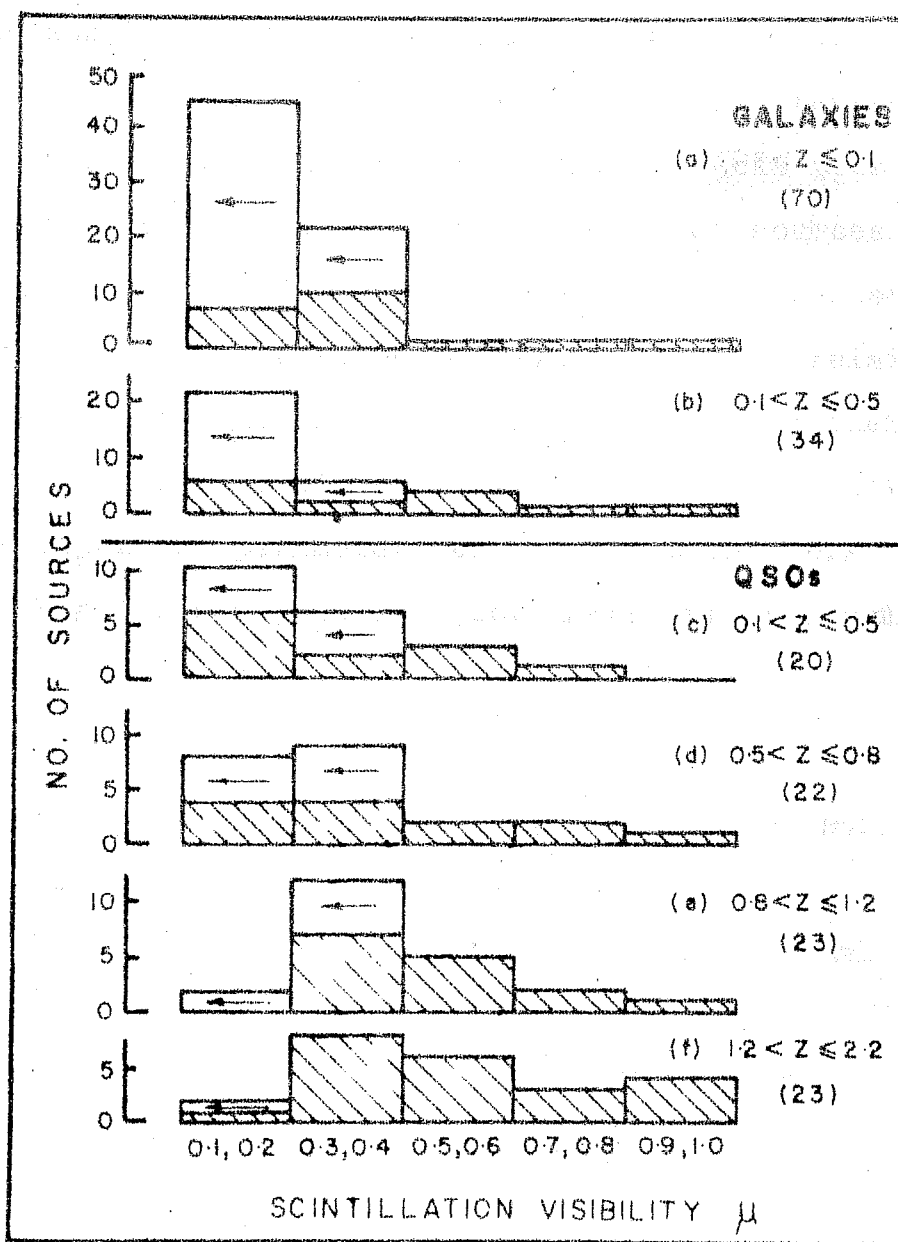
FIG. 4.3 Histograms of scintillation visibility μ in different ranges of redshift z for 104 radio galaxies and 88 QSOs.

the presence of flat spectrum sources which could not be removed from the sample due to lack of spectral information. It must however be noted that the observed correlation between μ and z may not be free of complex selection effects present in the determination of redshifts of the identified sources. For example, in the case of radio galaxies, it has been shown that redshifts have been measured preferentially for relatively bright and nearby galaxies. In the next chapter therefore we study the correlation of scintillation visibility with other distance dependent parameters of radio sources e.g. flux density and angular size, which allow large unbiased samples to be obtained.

Since only a few galaxies and QSOs have resolved scintillating components in them, we do not have sufficient data to study the dependence of Ψ on z . This has, however, been done by Hewish et al. (1974) by choosing a small sample of 23 strongly scintillating 3CR sources from the 81.5 MHz IPS survey of Readhead and Hewish (1974). The selection effects present in their restricted sample as well as the overall validity of cosmological results derived by them is discussed in Chapter 6.

4.4 OBSERVATIONS OF PKS 1514-24 (AP Lib)

During the last few years a number of radio sources have been identified with variable stellar objects, called 'Lacertids' - after BL Lacertae, which is the prototype of the objects in this class. The nature of their radio emission

and the determination of a redshift of 0.07 for BL Lac by Oke and Gunn (1974) indicate that these objects may be extragalactic (Altshuler and Wardle 1975). One of the radio sources in the southern sky IPS survey carried out by us, namely PKS 1514-24, is identified with an interesting optical object AP Librae, having optical properties similar to BL Lac. In this section we present the observations of its interplanetary scintillations at 327 MHz and discuss its known optical and radio structure.

Optical Properties:

The radio source PKS 1514-24 has an interesting optical history. Earlier, on the basis of its photographic appearance and UBV color, Westerlund and Wall (1969) classified it as an N galaxy. Later, Bond (1971) and Biraud (1971) almost simultaneously pointed out that PKS 1514-24 coincides in position with the known optical variable AP Lib. The identification of PKS 1514-24 with AP Lib has been confirmed by Hunstead (1971) and Kapahi (1971) who determined its accurate optical and radio positions. Hunstead also noted that the optical object has a non-stellar appearance. The stellar image is surrounded by irregular nebulosity ($\sim$ 10 "arc) having jets and raylike structures. Many workers have studied its color and intensity variations (e.g. Andrews et al. 1974, Miller et al. 1974). It is known to vary over time scales ranging from fraction of an hour to years, sometimes brightening by as much as 0.5 mag within a period of about half an hour. The intensity variations are also accompanied by color changes; the object becomes redder as it gets fainter.

Both BL Lac and AP Lib are similar in appearance to N galaxies and are shown to have a composite light distribution, made up of a diffused E galaxy and an unresolved bright QSO-like core (Oke and Gunn 1974, Disney et al. 1974). Disney et al. (1974) carried out spectroscopic observations of AP Lib, using different apertures to study the spectrum of the two components separately. Absorption lines characteristic of elliptical galaxies were observed from the diffused underlying galaxy component leading to a redshift $z = 0.0486$. Emission lines were, however, seen only on one occasion, when the object as a whole was brighter in blue and UV. The observed occurrence of emission lines when the object is bluer, alongwith the fact that the object becomes redder when it is fainter (Andrews et al. 1974), suggests that only the QSO component in AP Lib is variable. The situation is similar to that of the well studied N galaxy 3C 371 (Miller 1975).

Radio Structure and IPS Studies:

The radio source PKS 1514-24 is located very close to the ecliptic plane and is therefore suitable for observations of its interplanetary scintillations. We carried out its IPS observations at 327 MHz on a number of days in November 1971 when the elongation was in the range about 6° to 25°. Longer stretches of data, than the usual 6 minutes, were taken on many days since the source had a flux density of only ~ 1.5 Jy at 327 MHz. Strong scintillations, similar in appearance to a point source were observed. Figure 4.4 shows a typical
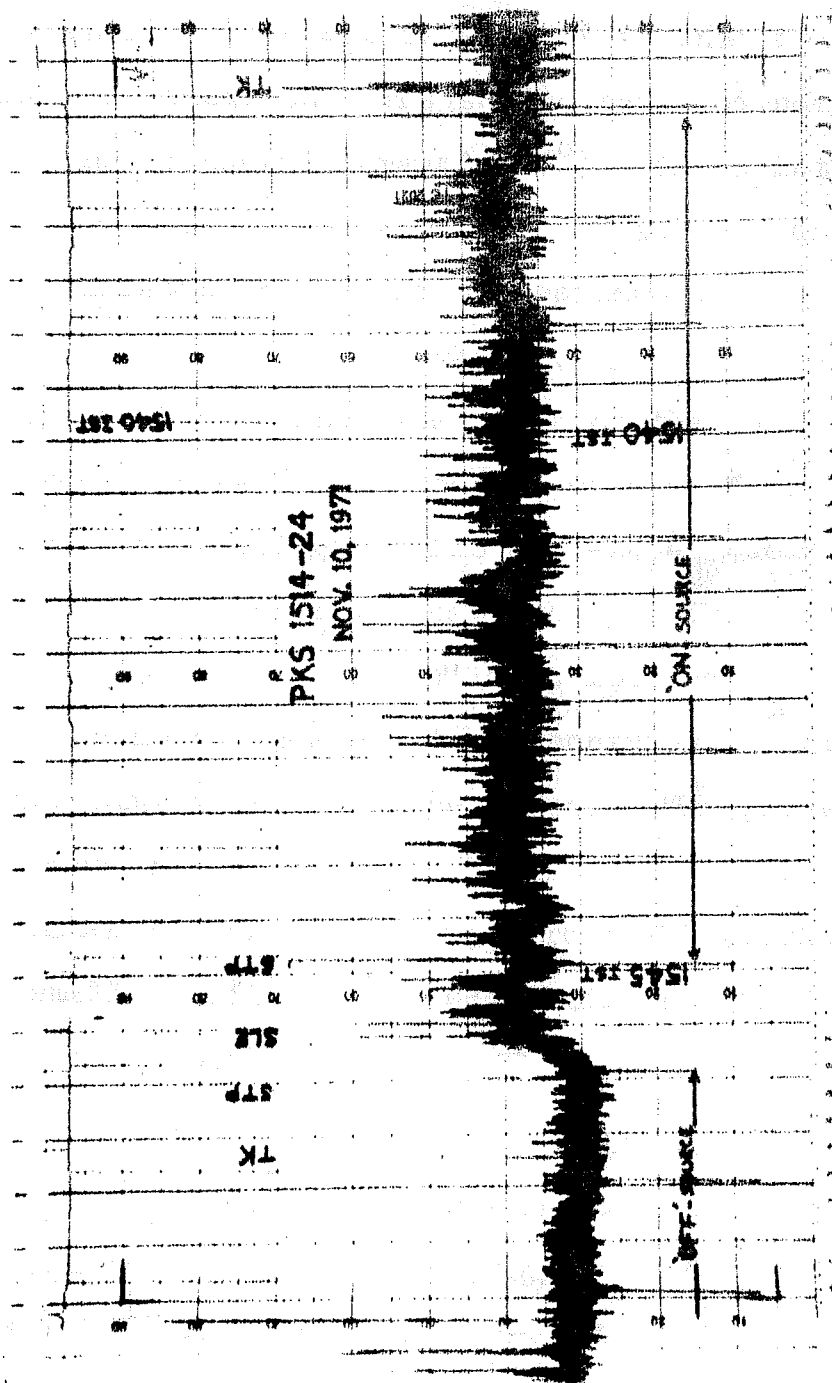
FIG. 4.4   Record of intensity fluctuations observed from the source
PKS 1514-24 (AP Lib) on Nov. 10, 1971.

record of scintillations observed on November 10, 1971 when
the elongation was about 8°. The power spectrum of scintilla-
tions, shown in Figure 4.5, is similar to that for a point source.
The analysis shows that the source remained unresolved at all
elongations (minimum elongation 6°). The scintillation visi-
bility was estimated to be 0.8 ± 0.2 and the angular size of
the scintillating component was estimated to be less than
about 0.035 arc. Lunar occultation observations, also at 327
MHz (Kapahi 1975b), show that most of the radio emission from
the source originates in a region of size < 0.8 arc. Inter-
ferometric observations of PKS 1514-24 at 408 MHz (Conway and
Stannard 1972) however indicate the possible presence of a
component with a size of $\sim 4''$ arc, located $\sim 20''$ arc east of
the main (compact) component and contributing about 25% of
the total flux density of the source. The presence of a weak
broad component is consistent with $\mu = 0.8 \pm 0.2$ derived above
and, as noted by Conway and Stannard (1972), perhaps is the cause
of the small discrepancy between radio positions given by
Hunstead and Kapahi.

Figure 4.6 shows the overall radio, IR and optical
spectrum of the source. We have also included the flux den-
sity measurements by Slee and Higgins (1973) at 80 MHz. The
radio spectrum is flat in the range 0.3 GHz to about 10 GHz.
Using the flux density of the compact component at 327 and 408
MHz we have fitted a synchrotron self-absorbed (SSA) component
to the total spectra as shown by broken lines in the figure.
The residual flux density values at lower frequencies define a

record of scintillations observed on November 10, 1971 when the elongation was about 8°. The power spectrum of scintillations, shown in Figure 4.5, is similar to that for a point source. The analysis shows that the source remained unresolved at all elongations (minimum elongation 6°). The scintillation visibility was estimated to be 0.8 ± 0.2 and the angular size of the scintillating component was estimated to be less than about 0.035 arc. Lunar occultation observations, also at 327 MHz (Kapahi 1975b), show that most of the radio emission from the source originates in a region of size < 0.8 arc. Interferometric observations of PKS 1514-24 at 408 MHz (Conway and Stannard 1972) however indicate the possible presence of a component with a size of $\sim 4"$ arc, located $\sim 20"$ arc east of the main (compact) component and contributing about 25% of the total flux density of the source. The presence of a weak broad component is consistent with $\mu = 0.8 \pm 0.2$ derived above and, as noted by Conway and Stannard (1972), perhaps is the cause of the small discrepancy between radio positions given by Hunstead and Kapahi.

Figure 4.6 shows the overall radio, IR and optical spectrum of the source. We have also included the flux density measurements by Slee and Higgins (1973) at 80 MHz. The radio spectrum is flat in the range 0.3 GHz to about 10 GHz. Using the flux density of the compact component at 327 and 408 MHz we have fitted a synchrotron self-absorbed (SSA) component to the total spectra as shown by broken lines in the figure. The residual flux density values at lower frequencies define a

FIG. 4.5   Power spectrum of scintillations recorded from
the source PKS 1514-24 on Nov. 10, 1971.

steep spectrum component with $\alpha \approx 1.4$, which may be identified with the weak extended component found at 408 MHz. For the SSA component having peak flux density of 2.5 Jy at around 700 MHz, angular size of about 0".0015 arc could be derived assuming a magnetic field of $\sim 10^{-4}$ Gauss. This is consistent with the upper limit on angular size set by the present IPS observations. It should be possible to confirm the existence of the broad component with a steep spectrum by IPS observations at low frequencies; no scintillations should be seen at frequencies below about 200 MHz. As expected the extended steep spectrum component is not observed at 11 and 3.7 cm (Prof. T.K. Menon, Private communication).

No significant variations in the radio emission from PKS 1514-24 were observed by Hunstead (1971), Nicolson (1971) and Altschuler and Wardle (1975). Recent interferometric measurements at cm wavelengths show some changes in its flux density (Prof. T.K. Menon, Private communication). A variable γ-ray sources is thought to be associated with it (Frye et al. 1971).

Thus AP Lib, although similar to BL Lac and other lacertids in its optical properties, seems to show some differences in its radio behaviour. It probably has an extended radio component and does not show large and rapid radio variability characteristic of other lacertids. It has been suggested therefore that it may represent an evolutionary link between BL Lac objects and radio galaxies.
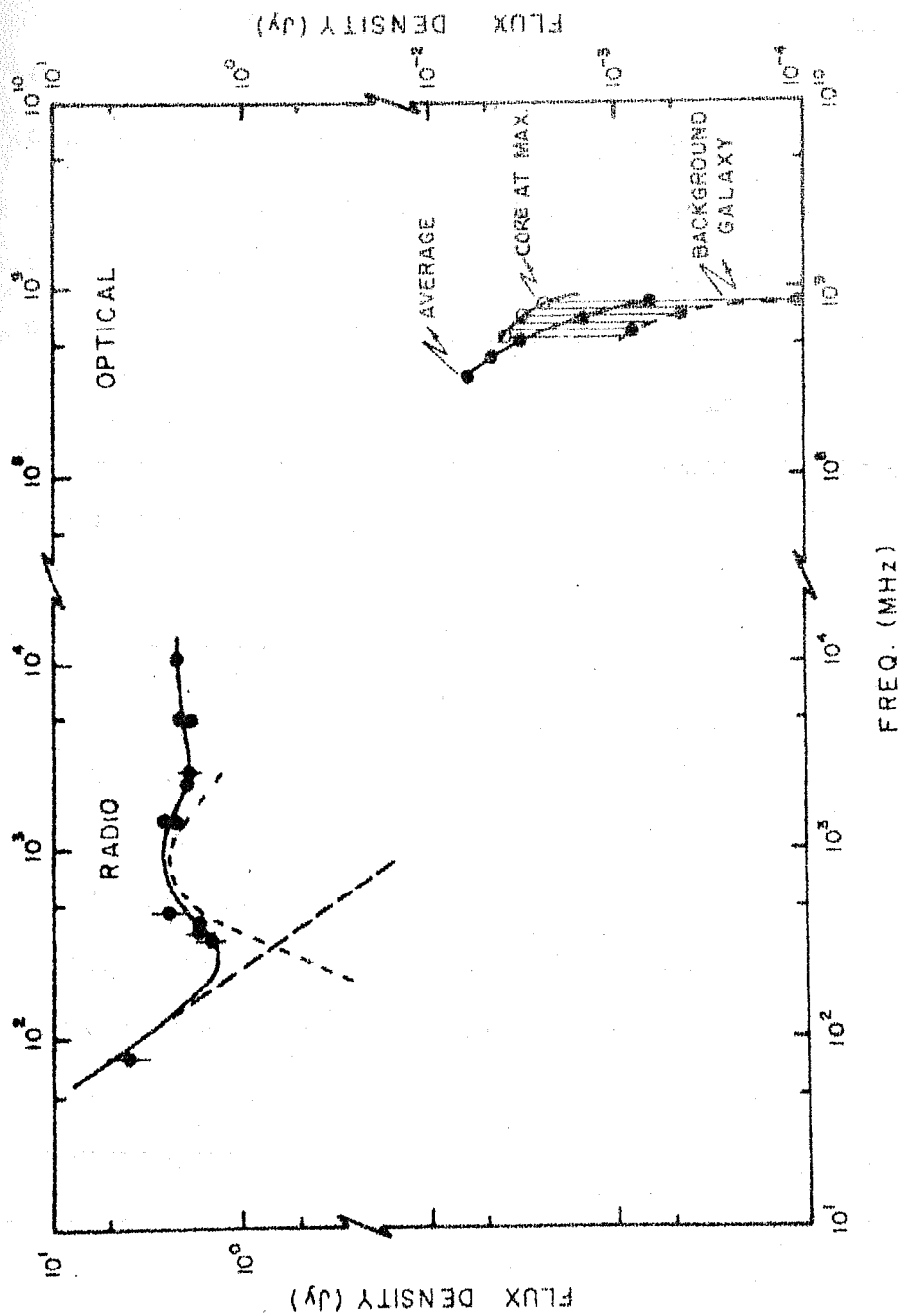
FIG.4.6 The overall spectrum (solid line) of PKS 1514-24. Optical and infrared fluxes are taken from Strittmatter et al. (1972) and Disney et al. (1974). Broken lines show different components in radio and optical bands. Hatched area shows the range of optical variability observed in the QSO component.

In view of the association of such radio sources with composite optical objects discussed by Sandage (1973), it would be worthwhile to carry out low frequency, high resolution IPS and VLBI observations of a large number of such objects recently discovered, to detect and study the compact and extended components. Such observations may lead to an improved understanding of the evolutionary behaviour of these objects. Spectroscopic studies, on the other hand, using techniques similar to those used by Disney et al. (1974), are important to separate the contribution to observed optical emission from thermal and non-thermal processes.

4.5   CONCLUSIONS

The interplanetary scintillation observations of a new sample of about 200 southern declination radio sources have allowed us to estimate the angular size and flux density of the scintillating components in them. These observations provide useful data for further VLBI observations to study the low frequency spectra and structures of compact components in these southern sources. The fine structure data on a sample of 149 stronger sources, obtained by the IPS method, has shown that at meter wavelengths:-

1.   About 50 % of all extragalactic radio sources with $S \geq 2.5$ Jy at 327 MHz show appreciable scintillation i.e. they contain more than 30 % of their total flux density in components with sizes < 0".5 arc. These results confirm the

findings of Harris and Hardebeck (1969) and Readhead and Hewish (1974) who studied IPS of a larger number of northern sky sources at 430 and 81.5 MHz respectively.

2. The average scintillation properties show a progression from galaxies to unidentified sources to QSOs. While galaxies scintillate weakly, most QSOs have strong compact scintillating components in them. The unidentified sources have intermediate properties. The relative frequency of occurrence of scintillation as well as the relative fraction of resolved and unresolved scintillating components for the three classes of radio sources have been used to estimate the proportion of QSOs and radio galaxies among the unidentified sources. Present conclusions support Bolton's inference that a majority of unidentified sources should be galaxies fainter than the plate limit of the Palomar Sky Survey. Recently, deep sky photographs of the optical fields of many unidentified 3CR sources to fainter (21 to ~ 24 mag.) limiting magnitudes by Kristian et al. (1974) and Longair and Gunn (1975) have shown that almost all the new identifications appear to be with galaxies.

3. A study of the correlation between spectral index and scintillation visibility shows that flat spectrum sources represent a separate class. Most of these have high scintillation visibility and a large percentage of them have unresolved scintillating components. This is more pronounced in the case of QSOs.

4.   Combinig the present data with all other IPS data, we have investigated the dependence of μ on redshift z for a larger number of galaxies and QSOs. Since flat spectrum QSOs do not show a smooth variation of their properties with redshift and since they behave differently on the μ-α plot (Fig. 4.2) it is meaningful to study the μ-z relation only for steep spectrum sources. Using μ and z data for 88 QSOs and 104 radio galaxies with steep spectra, we find that μ increases statistically with increasing z. Further, in the region of overlap of redshifts of galaxies and QSOs, the scintillation properties of the two classes are very much similar. This smooth and continuous increase of μ with increasing redshift, from galaxies to QSOs, tends to support the cosmological interpretation of redshifts for steep spectrum QSOs.

5.   Our discussion of the radio spectrum and structure of the radio source PKS 1514-24, associated with the BL Lac object AP Lib, suggests the presence of an extended radio component having a steep low frequency spectrum and accounting for most of the flux of the source below about 200 MHz. Recently, Gopal-Krishna(1977) has detected such extended ($>1"$ arc) radio haloes around compact cores in two more BL Lac sources, AO 0235+164 and 4C 03.59, from their LO and IPS studies at 327 MHz.

CORRELATION OF SCINTILLATION VISIBILITY WITH FLUX DENSITY AND ANGULAR SIZE OF RADIO SOURCES

5.1 INTRODUCTION

Radio source surveys with increased sensitivity and resolution are made with a two-fold aim: i) to measure the physical dimensions of the radio emitting regions and study their morphology to enable us to understand the mechanism which produces and replenishes the large amount of energy emitted by the radio sources and ii) to study the variation of the properties of radio sources as a function of distance to allow us to choose the correct cosmological model. Some progress has been made in the case of the former and many aspects of the dynamics and confinement of extragalactic radio sources by the ambient intergalactic medium are beginning to be understood. A major drawback which has prevented the full use of radio sources in cosmological studies, however, is the fact that radio sources display an extremely wide range of intrinsic properties. It has not been possible as yet to find any class of sources which can serve as a 'standard candle' or a 'rigid rod'. Any approach to use radio sources for cosmological studies must therefore essentially be based on statistical studies by comparing the average properties of statistically complete samples of radio sources at different distances and hence at different epochs. Several authors have carried out such statistical studies involving correlations between radio source parameters which depend on distance e.g. the flux density, the angular size etc.

The most familiar source count or log N-log S analysis, the V/V_m test and the $\Theta - z$ correlation for QSOs have indicated that the observational data do not agree with the predictions of any reasonable non-evolutionary model of the Universe. These studies point out the presence of a strong secular dependence of space density, luminosity and size of radio sources (see review by Longair 1971). Recently, the determination of the angular structure of much weaker radio sources at Ooty has provided independent support to the evolutionary picture of the Universe (Kapahi 1975a,b).

As discussed in the last two chapters, IPS observations provide a convenient means of obtaining high resolution information on a large number of radio sources in relatively short time. Existing IPS surveys provide fine structure data on about 2000 radio sources covering a wide range of flux density. In this chapter, we present a detailed study of the correlations of scintillation visibility (μ) with flux density (S) and angular size (Θ) of radio sources. The observed correlation between scintillation visibility and angular size is used to investigate the relationship between the small scale structure studied by IPS and the known overall morphology of extragalactic radio sources. This relationship is valuable in understanding the physical processes in radio sources as well as in properly defining the use of angular size of compact scintillating sources for studying the geometry of the Universe.

In Section 5.2 a brief summary of important statistical tests and correlations involving S and Θ is given. Sections 5.3 and 5.4 describe the present work on the μ-S and μ-Θ correlations. Discussion and interpretation of these statistical correlations in terms of the observed multicomponent structure of radio sources is provided in the last section.

5.2 SUMMARY OF CORRELATION STUDIES INVOLVING FLUX DENSITY AND ANGULAR SIZE OF RADIO SOURCES

(a)   The earliest and most popular approach to the cosmological problem using radio observations has been to count and compare the relative number of radio sources at different flux density levels. The most extensive of these source count studies have been carried out at Cambridge and source counts at 408 MHz now span a flux density range of about 5000:1 (Pooley and Ryle 1968). A comparison of the observed source counts with the predictions of all reasonable world models indicates that there is an excess of weak radio sources. This means that the sources at earlier epochs were either more numerous or more luminous than now. Longair (1966) has shown that the observed excess of faint sources ($S_{408} \sim 2$ Jy) could be explained by a strong evolution, of the form $(1 + z)^5$, in space density of radio sources with epoch.

It is also possible to test the uniformity in the distribution of radio sources in space by carrying out the luminosity-volume or the so called V/V_m test devised by

Schmidt (1968). This, however, requires redshift measurements of all sources in a radio as well as optically complete sample. Assuming QSO redshifts to be cosmological, Schmidt (1972, 1974) carried out V/V_m test on complete samples of QSOs from 3C and 4C catalogues and concluded that QSOs are non-uniformly distributed. Their space density increases with increasing distance. To account for the higher value of $< V/V_m >$ observed, Schmidt (1974) found that an evolution in the space density of QSOs, at least as strong as found for all radio sources by Longair from the source count analysis, is required.

These tests have indicated that radio source population evolves with time. This is in conflict with the predictions of the strict Steady State theory, in which any change in radio source properties with cosmic epoch is not allowed.

(b)   An alternative approach to cosmology lies in studying the variation of the angular structure of radio sources with redshift or with flux density, since both angular size and flux density vary with redshift in a way which depends on the specific world model.

The correlation between angular size of radio galaxies and QSOs with z has been studied by Legg (1970) and Miley (1971). The plot of the largest angular size (LAS) θ of radio galaxies and QSOs having symmetrical double structure and steep radio spectra, against redshift, shows some scatter but has a well defined upper envelope. The upper envelope of data points shows that θ decreases monotonically with increasing z and

this trend continues up to $z = 2$ and beyond (Wardle and Miley 1974). There is no evidence for a minimum or a reverse trend in $\Theta(z)$ even at values of $z > 1$. A similar correlation is also present if one uses the angular sizes of individual components in double radio sources (Swarup 1975b) in place of Θ. This is in contrast to the expectations of all relativistic world models and indicates that the linear size of QSOs were smaller at the earlier epochs. The observed linear decrease in the linear sizes with z may be expected if the radio sources are confined by the ram pressure of the intergalactic medium since its density varies as $(1 + z)^3$ in all Friedmann models (Wardle and Miley 1974).

Longair and Pooley (1969) and Fanaroff and Longair (1972) have used a combination of log N-log S and the $\Theta(z)$ test described above. They compared the relative number of large diameter radio sources ($\gtrsim 60''$ arc) at different flux density levels using data from 3C and 5C surveys which cover a wide range of flux density. They concluded that a moderately strong $(1 + z)^3$ evolution in space density of radio sources is necessary to explain the observed excess of large diameter radio sources at the low flux density levels.

Recently, high angular resolution information on a large number of weak sources have been obtained through the observation of lunar occultations at Ooty. Swarup (1975a) has made a comparison of largest angular sizes Θ of the weak sources studied at Ooty with those of the strong 3CR sources.

Over a flux density range of about 300:1 he showed that the median value of Θ decreases with decreasing flux approximately as $\Theta_m \propto S^{\frac{1}{2}}$ as expected in Euclidean Universe. Below $S_{408} \sim 1$ Jy, there is some indication that Θ_m does not decrease as fast as given by $\Theta_m \propto S^{\frac{1}{2}}$ relation but reaches asymptotically to a value of $\sim 8''$ arc. Kapahi (1975a) has used the observed $\Theta_m(S)$ relation together with the angular size counts of radio sources to show that the angular size data are in conflict with non-evolutionary cosmological models and density and/or luminosity and size evolution of the form inferred earlier is necessary to explain the observed Θ-S correlation.

With the availability of large scale IPS surveys which provide angular resolution of $\sim 0''.1$ arc, it has now become possible to choose large unbiased samples of radio sources and study the variation of scintillation parameters over a large range of flux densities and angular sizes. Recently, Readhead and Longair (1975) have applied the V/V_m test to the scintillating radio sources in the 3CR catalogue and have concluded that strong evolution is necessary to bring $< V/V_m >$ to 0.5 for strongly scintillating radio sources. For weakly scintillating sources, however, the evolution needed is relatively much weaker. The above results are also supported by observed counts of scintillating sources at different flux density levels, reaching up to about 6 Jy at 81.5 MHz (Readhead and Longair 1975).

In the following sections we present the analysis and results of our study on the correlations of scintillation visibility μ with flux density S and overall angular size θ of radio sources.

5.3 SCINTILLATION VISIBILITY-FLUX DENSITY($\mu - S$) CORRELATION

5.3.1 Earlier Studies:

As soon as IPS observations were available for a substantial number of sources, Cohen et al. (1967b) and Harris and Hardebeck (1969) studied the relation between source intensity and the distribution of μ . No large and significant differences between the μ-distributions at three flux density levels over a 2-20 Jy range were found. A small increase in the relative percentage of sources that scintillate strongly was present at the lowest flux density levels but this could be explained as due to the poor S/N ratio when observing weak sources (Harris and Hardebeck 1969). Hunstead and Jauncey (1970) compared the average scintillation visibility of an arbitrarily defined sample of 27 weak sources at 430 MHz with those of stronger sources. No difference in the occurrence of scintillating sources was found.

In the following we analyse scintillation data using large and statistically unbiased samples of sources which cover a much larger range of flux density and show that there exists a correlation between scintillation visibility and source intensity.

5.3.2 Observational Data used for the Present Study:

In the analysis of the correlation between μ and S we have made use of scintillation data available from the following IPS surveys.

(a) The Cambridge 81.5 MHz IPS Survey:

The IPS survey carried out at Cambridge by Readhead and Hewish (1974) provides scintillation observations of about 1500 radio sources in the declination range -12° to $+90^{\circ}$. Estimates of μ and Υ are given. In cases where it was not possible to obtain a detailed m-p curve only upper or lower limits to μ are given. In the case of sources where a range of values of μ are given, we have taken the mean value of the range.

The catalogue of Readhead and Hewish (1974) also lists 81.5 MHz flux densities for all the above sources. These flux density values are derived from extrapolations from lower or higher frequency observations and are referred to the SS (Scott and Shakeshaft 1971) scale. This scale of flux density is about 20 % higher than the KPW (Kellermann, Pauliny-Toth and Williams 1969) scale at 81.5 MHz. The survey lists IPS observations of sources as weak as 4.4 Jy. However, since the sensitivity of the survey is not uniform over the area of the sky surveyed, it is not complete above the minimum flux density listed. We have therefore restricted the analysis to complete samples as defined below:

Sample 1 -

We have selected all sources with $S_{81.5} \geq 12.0$ Jy

which lie in the area of the sky defined by $-7^{\circ} < \delta < +90^{\circ}$ and $\left| b^{II} \right| > 10^{\circ}$. Within an area of approximately 6.9 sterad of the sky included, there are 685 sources which satisfy the above criteria. A number-flux density analysis shows that this sample is nearly complete above about 12.0 Jy. Out of these 685 sources we have rejected 30 sources, IPS observations of which were contaminated by the presence of another scintillating source in the beam (these sources are marked with an asterisk in the last column of the catalogue of Readhead and Hewish). Thus we are left with a sample of 655 sources. This will be referred to as Sample 1.

Sample 2 -

As mentioned above, the 81.5 MHz survey has nonuniform sensitivity and it is possible to identify some regions of the sky where the sensitivity is sufficiently high to detect sources much weaker than 12 Jy. These high sensitivity regions have been defined and used in the study of weak sources by Readhead and Longair (1975). In order to extend the μ-S relation to weaker sources, we consider a sample of all sources with $S_{81.5} \geq 7.1$ Jy selected from these regions. There are 60 sources in this sample which we shall refer to as Sample 2.

(b) The Ooty 327 MHz IPS Survey:

Sample 3 -

The IPS survey of southern sky radio sources carried out at Ooty has been fully described in Chapter 4 of this thesis. Table 4.1 lists a random sample of 149 sources with

$S_{327} \geq 2.5$ Jy, $|b^{II}| \geq 20^\circ$ and $-30^\circ < \delta < 0^\circ$ alongwith their μ and S at 327 MHz on the KPW scale. These 149 sources constitute the Sample 3.

(c) The Arecibo 430 MHz IPS Survey:

Sample 4 –

Harris and Hardebeck (1969) have published IPS observations of about 500 radio sources at 430 MHz. These sources were selected from Parkes and 4C catalogues in the area of the sky defined by $0^\circ < \delta < +38^\circ$, $|b^{II}| > 10^\circ$ and ecliptic latitude $\beta \leqslant 20^\circ$. Different criteria, regarding the flux density of the sources, were employed while selecting sources from the two catalogues; sources were included from Parkes catalogue if $S_{408} \gtrsim 2.0$ Jy and from 4C catalogue if $S_{178} \gtrsim 4.0$ Jy.

As noted by Harris and Hardebeck, such a selection process produces some biases regarding the spectral characteristics of radio sources, especially at the lowest flux density levels and the survey may not be complete down to 2.0 Jy at 408 MHz. From Table I of Harris and Hardebeck, we have therefore selected a sample of 173 sources (Sample 4) with $S_{408} \geq$ 4.0 Jy. Flux densities for all the sources in the survey were derived from interpolation or extrapolation of measurements at various frequencies available in the literature (Slee and Higgins 1973, Gower et al. 1967, Ekers 1969, Munro 1972). The flux density values at 408 MHz are referred to the KPW scale.

5.3.3 Analysis:

The samples 1 to 4 described above cover a flux density range of about 7 Jy to 1850 Jy at 81.5 MHz. We have divided sources in each of the four samples into a number of flux density ranges. Figure 5.1 shows the histograms of scintillation visibility μ for sources in Samples 1 and 2, and Figure 5.2 shows the same for Samples 3 and 4. Shaded areas represent definite values of μ and unshaded areas with arrows indicate lower or upper limits on μ . It is seen from these figures that for higher flux density ranges, the distribution of μ shifts more and more towards left, i.e. towards lower values of μ . As flux density decreases a larger fraction of sources tend to be strong scintillators, compared to the situation at the high flux density end, where most of the sources are either weak or non-scintillators.

In order to investigate the relationship between μ and S quantitatively we must define some characteristic of the μ distribution in each flux density range and then study its variation with flux density. Due to the presence of upper and lower limits to μ at all flux density levels it is not possible to estimate the mean value of the distributions. The parameter which can be estimated with reasonable accuracy in the presence of limits is the median value. The estimates of the median values of μ and S were made by plotting the cumulative number distributions of μ for sources in each flux density range. Figures 5.3 and 5.4 show these cumulative distributions. Crosses show the lower limits and open circles show
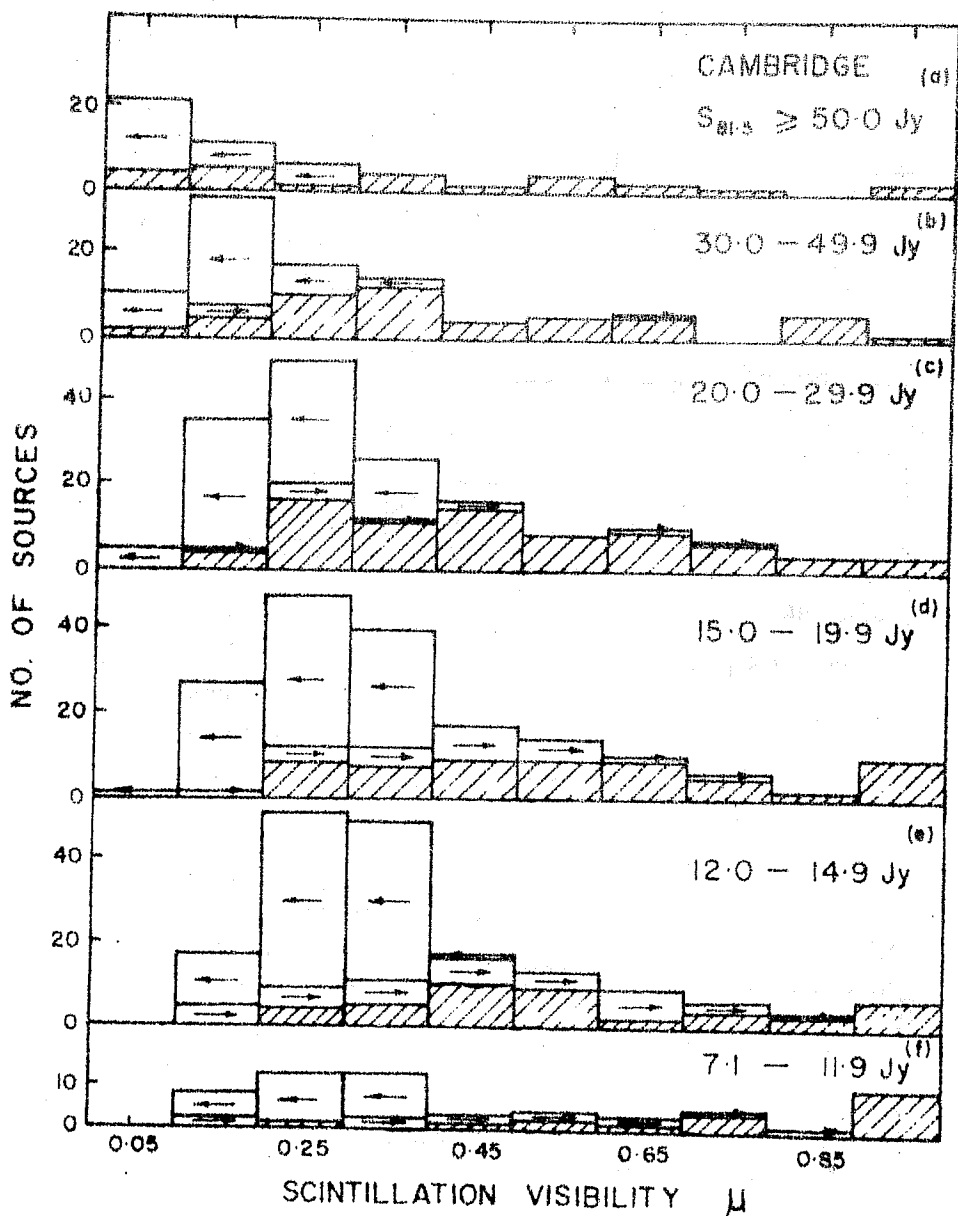
FIG. 5.1 Histograms of scintillation visibility μ in 6 consecutive ranges of flux density $S_{81\cdot5}$ from the IPS survey of Readhead and Hewish (1974). Ranges (a) to (e) are from sample 1 and (f) from sample 2. Shaded areas represent definite values of μ and unshaded areas with arrows represent upper or lower limits on μ.
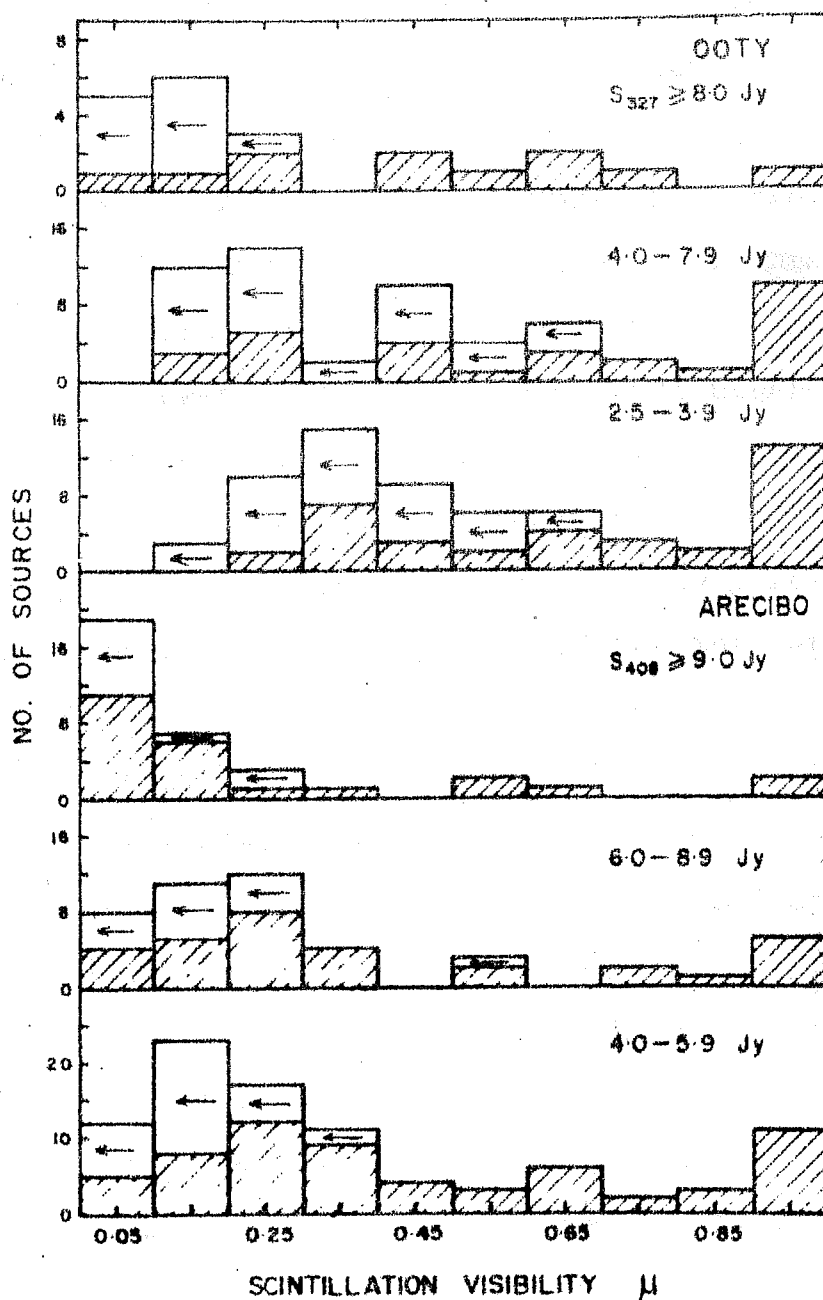
FIG. 5.2 Histograms of μ for samples 3 and 4 in three flux density ranges each. Other details as in Fig. 5.1.

the upper limits on μ . A smooth curve was fitted to the
points in each of these cumulative distributions and the median
value of μ was estimated. The value of μ at which the cumu-
lative number reaches half the total number is marked with a
+ sign on the fitted curves. While doing this it has been
assumed that the sources with lower limits to μ (shown by
crosses) have μ = lower limit and sources with upper limits
(open circles) have $\mu = 0$. Since upper limits are present only
in the case of Samples 3 and 4 these have been assumed to be at
$\mu = 0$. From Figure 5.1 it can be seen that significant number
of lower limits occur only for sources weaker than about 20 Jy
at 81.5 MHz and in these cases the assumptions made above will
lead to an underestimate of the median value of μ . For
stronger sources very few lower limits are present. Further,
since most of the upper limits occur below the median value, the
error due to the assumption that they are at $\mu = 0$, is small.
It is however possible to make a rough estimate of any syste-
matic error that is introduced in curve fitting owing to such
an assumption as follows. Using Figures 5.3 and 5.4 we esti-
mate an upper and a lower limit to the median value from cumu-
lative μ distributions by fitting the curves through the
upper and lower limit points respectively. As a conservative
estimate, we have taken half the difference between these and
the previously estimated median value as the rms value of the
systematic error.

In addition to the systematic error, the estimated
median values have a statistical error associated with them due
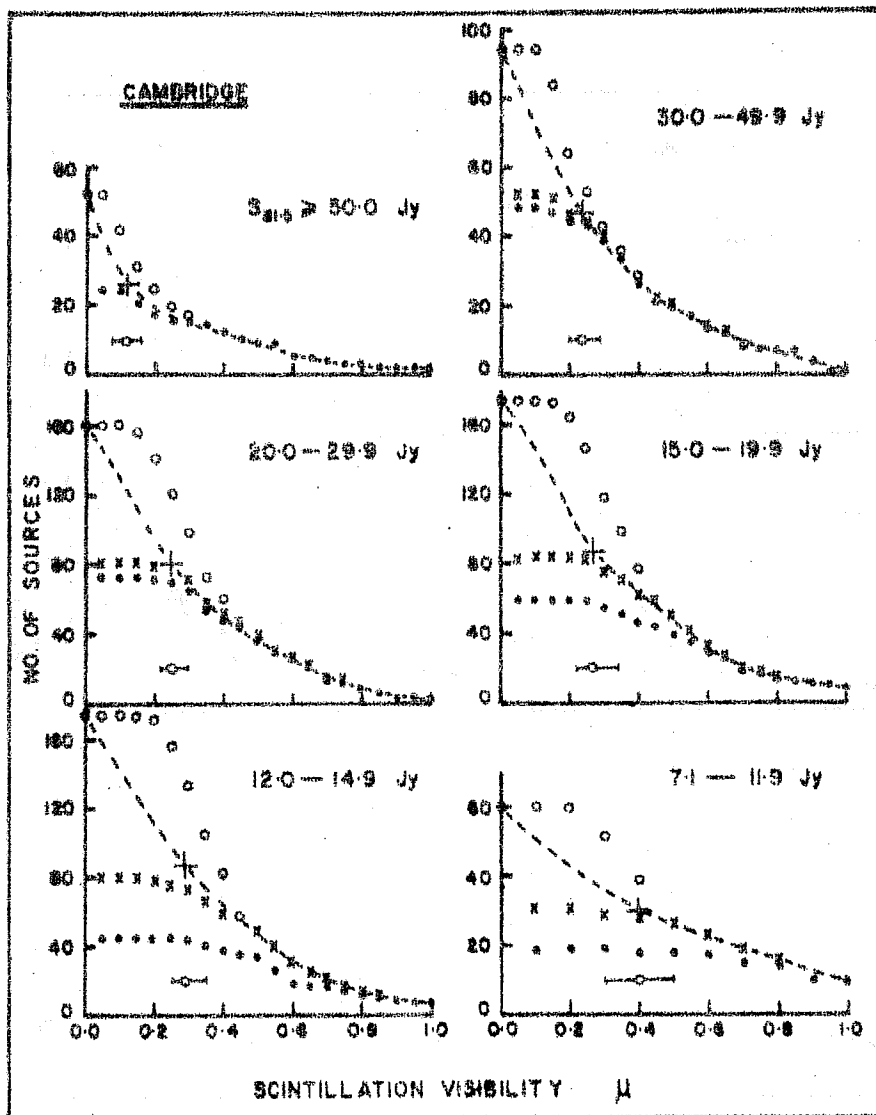
FIG. 5.3   Cumulative distributions for samples
1 and 2 for corresponding histograms
of Fig. 5.1. Dots, crosses and cir-
cles represent difinite values, lower
and upper limits respectively on μ. Bro-
ken line shows the smooth curve fitted
to the distributions. The $+$ sign on
the curve indicates estimated median
value of μ. The circle with hori-
zontal bars above the μ scale gives
median value with the final rms error.
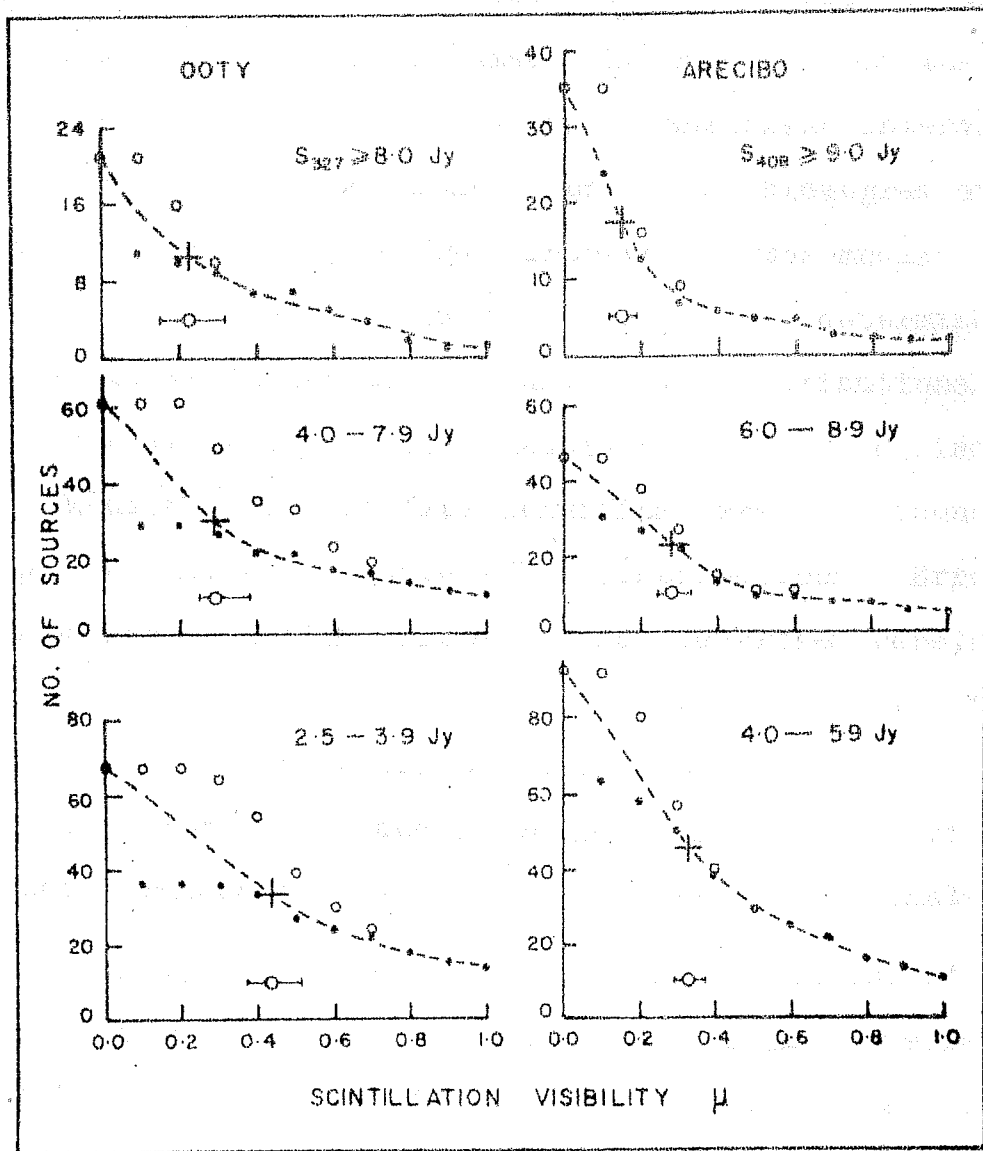
FIG. 5.4 Cumulative μ distributions for samples 3 and 4 corresponding to histograms shown in Fig. 5.2. Other symbols have same meaning as in Fig. 5.3.

to finite number of sources present in finite size of the class intervals used in the histograms. The rms error of the median values is equal to $\sqrt{n}/(2f)$ in units of the class interval, where n is the total number of sources under the histogram and f is the number of sources per class interval at the median value (Yule and Kendall 1950). The value of f was determined from the smooth curve fitted to the cumulative distributions. Variances of the two errors were added to calculate the final rms errors. Median values of flux densities were also found by plotting the cumulative number-flux distributions. Errors in the estimation of median values of flux densities were, however, negligible. In Tables 5.1, 5.2 and 5.3 we have listed the number of sources, the estimated median values of μ_m and S and the rms error of the median value $\Delta\mu_m$, in each of the flux density ranges for samples 1 to 4 used in the analysis.

Figure 5.5 is a plot of the median values of μ against S at 81.5 MHz. The flux densities are referred to the scale of Scott and Shakeshaft. Flux densities at 327 and 408 MHz for Samples 3 and 4 respectively were converted to those at 81.5 MHz by assuming a spectral index of 0.75. The 81.5 MHz flux densities so derived were increased by 20 % to correct for the difference between KPW and SS scale. The increase in the median value of μ with decreasing flux density is clearly evident in the figure where results from all the samples are superposed. The interpretation of the observed μ-S correlation is provided in Section 5.5.

Table 5.1   Median values of μ and $S_{81.5}$ for Samples 1 and 2

Flux Density Range $S_{81.5}(Jy)$	No. of sources n	Median $S_{81.5}(Jy)$	Median μ_m	f	Final rms error of the median $\Delta\mu_m$
7.1-11.9*	60	9.4	0.40	4	+0.1 -0.1
12.0-14.9	173	13.3	0.29	24	+0.06 -0.04
15.0-19.9	175	16.5	0.27	24	+0.07 -0.05
20.0-29.9	161	23.2	0.25	28	+0.05 -0.03
30.0-49.9	94	36.0	0.24	13	+0.05 -0.04
≥ 50.0	53	75.0	0.12	13	+0.04 -0.04

* Sample 2

Table 5.2 Median Values of μ and S_{327} for Sample 3

Flux Density Range $S_{327}(Jy)$	No. of sources n	Median $S_{327}(Jy)$	Median μ_m	f	Final rms error of the median $\Delta\mu_m$
2.5-3.9	67	3.1	0.43	7	+0.08 -0.06
4.0-7.9	61	4.8	0.29	9	+0.09 -0.04
≥ 8.0	21	11.5	0.23	3	+0.09 -0.08

Table 5.3 Median Values of μ and S_{408} for Sample 4

Flux Density Range S_{408}(Jy)	No. of sources n	Median S_{408}(Jy)	Median μ_m	f	Final rms error of the median $\Delta\mu_m$
4.0-5.9	92	4.8	0.33	12	+0.04 −0.04
6.0-8.9	46	7.1	0.28	8	+0.05 −0.04
$\geq$ 9.0	35	13.1	0.15	11	+0.04 −0.03
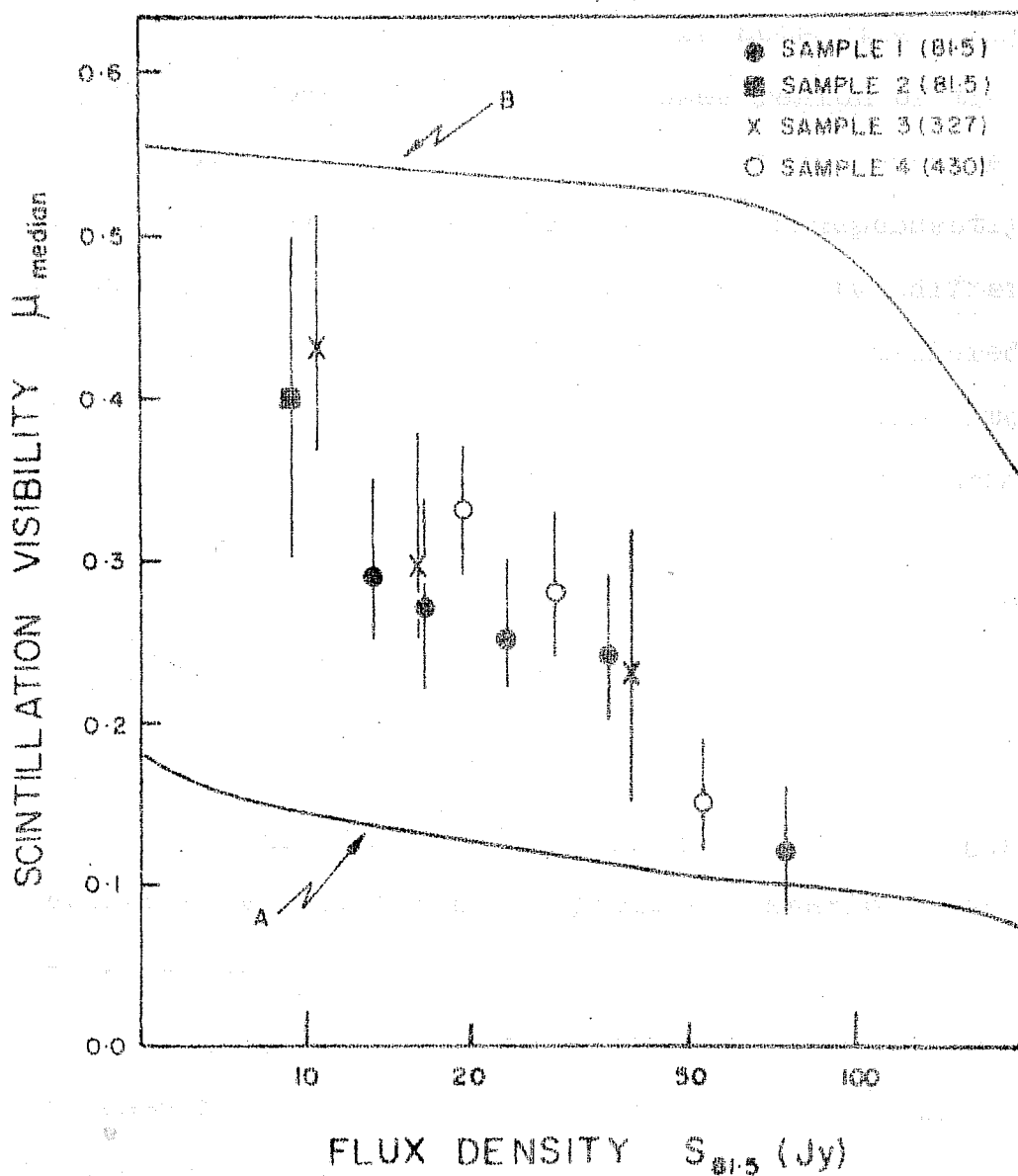
FIG. 5.5   Plot of median values of μ against median values of $S_{81.5}$ for the four samples considered. Curves A and B are expected variations for the models representing Cygnus A and 3C 33 (see text).

At this point it should be noted that Samples 1 and 4 are derived from IPS surveys of same region of the sky and therefore are not independent of each other. However, since their IPS observations were carried out independently at two different frequencies and were analyzed in two different ways to yield μ , these two samples have been considered separately in the μ-S study. We have also separately studied the μ-S correlation for the 3CR sample of stronger sources. A significant correlation was found between μ and S when the analysis is done including as well as excluding the known QSOs in the 3CR sample.

5.3.4 Consideration of Selection Effects:

In the following we discuss important observational selection effects which might produce a spurious correlation between μ and S.

(i) As a result of the limited sensitivity of the telescope used for the IPS survey , it may not be possible to detect scintillations if the flux density of the scintillating component falls below the sensitivity limit. This effect will be more serious for weak sources since the total flux of the source itself is small. In such cases it is only possible to put an upper limit, based on the system noise, on the flux in the scintillating component and hence on the scintillation visibility μ . This effect is seen in Figures 5.1 and 5.2 where more and more upper limits on μ appear at low flux density levels. These sources are usually termed non-scintillators.

Further, since the observed scintillation index depends on the solar elongation of the source the scintillations are observed at a reduced level for sources located away from the ecliptic. Therefore the percentage of sources which can be detected as 'scintillators' with a given sensitivity (instrument) will decrease as the ecliptic latitude increases beyond about 30° for observations at meter wavelengths. This was in fact observed by Little and Hewish (1968) for 3C sources, and a similar effect is most likely to be present, especially for weaker sources, in the IPS survey of Readhead and Hewish (1974) where sources as far as 80° or 90° ecliptic latitude have been observed.

Therefore, if μ-S analysis is carried out for scintillating sources alone, then instrumental sensitivity itself will introduce an artificial correlation between μ and S in the same sense as is observed. Only strong scintillators will be detected at weakest flux density levels. On the other hand, if we use data on all sources above a certain flux density limit, irrespective of the efficiency with which their scintillations have been observed, the resulting μ-S correlation will be free of the above observational bias. In other words, we must analyse complete samples of sources, including scintillators as well as non-scintillators. The statistical completeness of the samples can be ensured by carrying out a source count analysis. This procedure has in fact been followed in the analysis of μ-S correlation leading to Figure 5.5.

The inclusion of non-scintillating sources for which a definite value of μ is not known, only adds to the uncertainties in the determination of median value of μ .

(ii)   As seen in Figure 5.1, for a substantial fraction of weak sources in Samples 1 and 2 only a lower limit to μ has been set by the observations of Readhead and Hewish. For these sources it was not possible to estimate the angular size of the scintillating component and the lower limit to μ is derived by comparing the observed scintillation index with that of a point source. Since a substantial fraction of sources have scintillating components which are resolved, the estimated lower limit to μ will, in general, be an underestimate. Determination of definite values of μ for these sources, therefore, is likely to enhance the observed $\mu-S$ correlation.

        The above discussion shows that the observed trend in $\mu-S$ correlation is unlikely to be significantly affected by selection effects. We have used statistically complete samples of radio sources, and we have included uncertainties in estimation of median value of μ arising from the presence of upper and lower limits on μ . Further, it is interesting to note that in Figure 5.5, the median values of μ derived from IPS data at three different frequencies are in reasonable agreement.

5.4 SCINTILLATION VISIBILITY – ANGULAR SIZE(μ-Θ) CORRELATION

For studying the μ-Θ correlation we have restricted our attention to sources in the well known 3CR complete sample, since each of the 200 sources in this sample has been mapped at 1407 MHz with an angular resolution of about 23"x23" (cosec δ) arc using the Cambridge 1-mile telescope (Macdonald et al.1968, Mackay 1969, Elsmore and Mackay 1969). In the case of some of the sources, brightness maps with improved resolutions have recently become available through the use of Cambridge 5-km telescope (Pooley and Henbest 1974) and these have been included. Estimates of the overall angular size Θ ($\equiv$ projected angular separation between the outermost components of the source and same as the largest angular separation (LAS) defined by Miley 1971) are therefore available for most sources.

The '3CR complete sample' consists of 200 sources in the revised 3C catalogue within about 4.2 sterad of the sky defined by $\delta > 10^\circ$, $\left| b^{II} \right| > 10^\circ$ and having $S_{178} \geq 9.0$ Jy (Mackay 1971). The IPS survey of Readhead and Hewish (1974) at 81.5 MHz fully covers this region of the sky and provides a homogenous set of scintillation data for these stronger sources. We have therefore used μ values from Readhead and Hewish(1974) for the μ-Θ analysis.

Out of these 200 sources, we have excluded 13 sources from the analysis of μ-Θ correlation for the following reasons:

i) 3C 326 — as it may be a galactic source (Mackay 1971)

ii) 3C 435.1 and — as these may be chance associations of
     3C 437.1   unrelated, individually weak 4C sources
                        (Longair and Gunn 1975)

iii) 3C 66 and — in each case high resolution observations
     3C 442   indicate the existence of a physically
                      unrelated component (Mackay 1971) and
                      existing IPS observations do not allow a
                      correct estimate of μ . The situation
                      is similar in the case of 3C 225 (Kapahi
                      et al. 1972). Only 3C 225 B should be
                      considered in the 3CR sample as the flux
                      of 3C 225 A is less than the 3CR limit.
                      Unpublished IPS observations at 327 MHz
                      are available for individual components
                      and give $\mu \simeq 0.4$ for 3C 225 B. We have
                      therefore retained 3C 225 B in the sample.

iv) 3C 207,   — as these are QSOs known to contain extremly
     3C 216,   compact components implied by their concave,
     3C 245,   cm excess spectra and variability (Miley
     3C 249.1,   1971, Roger et al. 1973, Conway et al.
     3C 345,   1974).
     3C 380 and
     3C 454.3

v)   3C 371   — since no IPS observations are available
                     for this source.

     We are thus left with 187 extragalactic sources. We
use this sample of 187 sources in the analysis of the μ–Θ
correlation below.

     Figure 5.6 is a scatter plot of scintillation visi-
bility μ at 81.5 MHz against the overall angular size Θ for
the sample defined above. The values of Θ were mostly taken
from the Cambridge observations at 1407 MHz but in some cases
Θ was taken from better and higher resolution observations
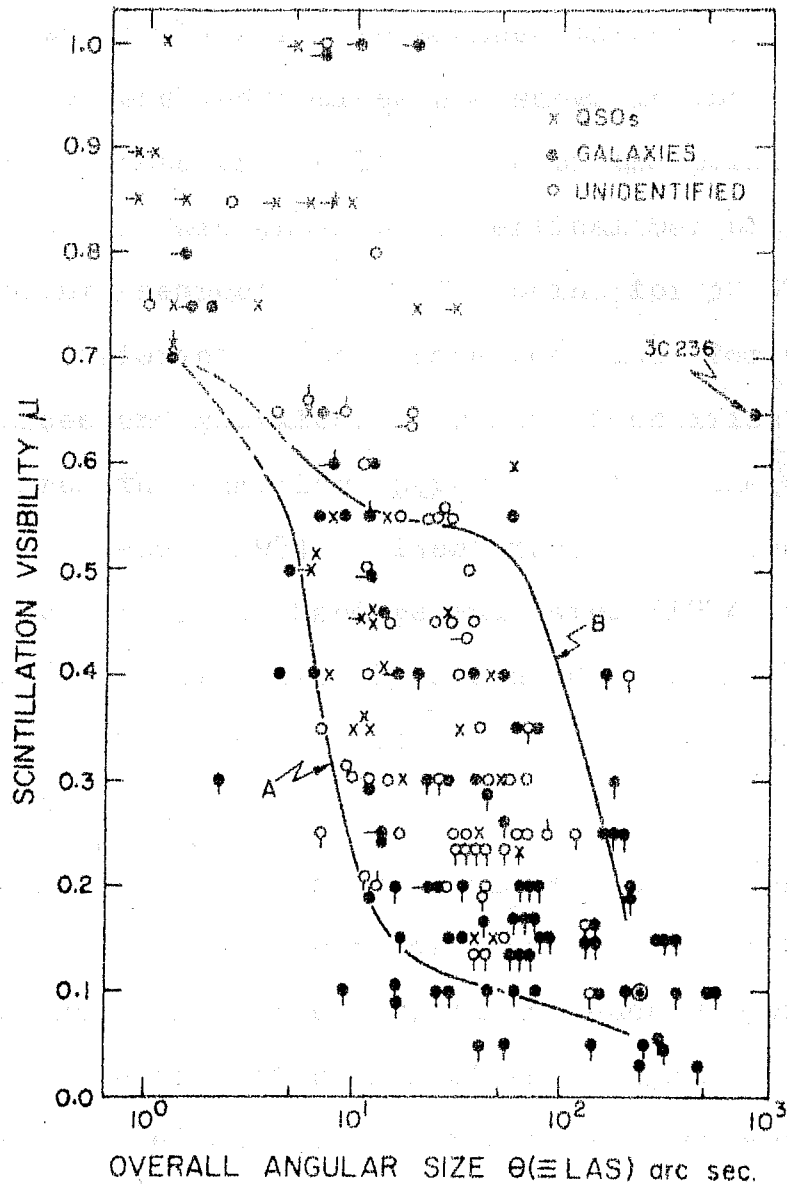
FIG. 5.6 Scatter diagram of scintillation visibility μ against overall angular size θ for the 3CR sample. Horizontal and vertical bars represent limits to θ and μ respectively. Curves A and B show calculated variation for models representing Cygnus A and 3C 33. The point shown encircled near the lower right corner shows the observed value of μ for 3C 33.

made by others (Swarup 1975a and references therein).   Upper
limits to θ for unresolved sources are shown in the figure by
a horizontal bar attached on the left side of the points. Upper
and lower limits to μ are shown by a vertical bar below or
above the data points respectively.   The point for 3C 33 is
shown encircled.   Different symbols have been used for QSOs,
unidentified sources and galaxies.   Optical identification
data were taken from the Cambridge papers and from the compi-
lation by Veron and Veron (1974).   Identifications based on
deep sky surveys by Kristian, Sandage and Katem (1974) and
Longair and Gunn (1975) have also been considered.   All sources
for which identifications are not certain have been plotted as
unidentified sources.

It is seen from the scatter diagram that there is a
clear trend for increasing μ with decreasing θ .   Although
a large amount of scatter is present, the absence of points in
the upper right and lower left region of the diagram is strik-
ing.   QSOs, unidentified sources and radio galaxies appear in
different but overlapping parts of the diagram.   QSOs are dist-
ributed towards regions of smaller θ and higher μ compared
to galaxies and unidentified sources, indicating that QSOs in
general are more compact than other sources.   The μ-θ trend
is present even if all QSOs are removed from the figure.   Most
of the galaxies and unidentified sources (which are most likely
to be similar to radio galaxies) with θ ≲ 30" arc are found to
be moderately strong scintillators while a large majority of

sources with $\Theta > 50''$ arc are non-scintillators with relatively small (0.2 or less) upper limits on μ .

5.5 INTERPRETATION AND DISCUSSION

The observed correlations of scintillation visibility μ with S and Θ in Figures 5.5 and 5.6 show that the strongly scintillating sources in general tend to have smaller flux density and smaller overall angular extents. Recently Swarup (1975a) has also shown that there exists a clear correlation between Θ and S ; Θ decreases statistically with decreasing S approximately as $\Theta \propto S^{\frac{1}{2}}$. These statistical correlations between μ , S and Θ clearly provide a strong evidence that statistically the weaker sources are located farther away than the stronger ones. Decreasing flux and overall angular size associated with increasing μ can simply be interpreted as a geometrical distance effect. This is also supported by the observed correlations between μ and z (Chapter 4, Harris 1973) and between Θ and z (Miley 1971) found for galaxies and QSOs. The correlation between S and z however is not possible to observe due to heavy selection effects present in the determination of redshifts of identified sources and the limited range of S over which redshifts have been measured (Swarup 1975a,b, Kapahi 1975b).

5.5.1 Relation between Compact and Extended Structures:

So far most IPS observations have been carried out at meter wavelengths using single telescopes which,on their own, do not have sufficiently high resolving powers at these

wavelengths to resolve the basic features of the radio source structure. The IPS observations have nevertheless revealed the presence of compact components in radio sources at meter wavelengths. However, the precise location of the scintillating compact components with respect to the overall extended brightness distribution cannot be found. The lunar occultation and aperture synthesis observations, on the other hand, have delineated the overall structure over the whole range of angular sizes down to about a second of arc. From these studies it is known that at meter wavelengths, a large majority of radio sources have their radio emission originating in two extended regions and whenever optical identification exists, these are placed almost symmetrically, one on either side of the associated galaxy or QSO. Only at short cm wavelengths significant emission is found to originate from the region of the optical object.

We have shown in Chapter 4 that in all the IPS surveys more than 50 to 60 % of the sources observed are found to scintillate appreciably, thereby indicating the presence of compact components in them. Since most of the radio sources are double, the scintillating compact components must, in general, be located in one or both of the extended components. Recent high resolution aperture synthesis observations of Cygnus A, 3C 33 and other sources at 5 GHz (Hargrave and Ryle 1974, Hargrave and McEllin 1975) and lunar occultation observations of 3C 33 at 327 MHz (Gopal-Krishna et al. 1976) reveal

the presence of compact high brightness regions located near the outer boundaries of each of the extended components. It is likely that scintillations mainly arise from similar compact regions in most of the radio sources.

The relative importance of compact and extended components in producing scintillation in sources located at different distances can be examined from the observed $\mu-\theta$ correlation. The ratio of the angular size of the scintillating component to the overall size Ψ/θ can be inferred from Figure 5.6. It is seen that most of the scintillating sources in the 3CR sample have values of θ in the range 5-50" arc. Now, in order to scintillate appreciably, some component of the source must have an angular diameter much smaller than the diameter of the first Fresnel zone which is about 2" arc at 81.5 MHz. Hence, for scintillating sources a significant fraction of their total flux density should originate from components with angular sizes $\sim \theta/10$ to $\sim \theta/50$. Interferometric observations at meter wavelengths with resolution comparable to IPS by Wilkinson et al. (1974) have also indicated the presence of similar compact components in many 3CR and Parkes radio sources. In the case of some of the double sources (3C 61.1, 234, 244.1, 263, 325, 380 and 381) a significant flux is found to originate even in components as small as $\theta/100$ (Wilkinson 1972). The presence of a scintillating component in the widely separated double source 3C 33 (Harris and Hardebeck 1969, Gopal-Krishna et al. 1976) having $\theta \sim 250"$ arc, implies structures on angular scales reaching $\sim \theta/700$. This is in addition to the components with

~ $\Theta/50$ and ~ $\Theta/25$ etc. discussed below. From these observations it is clear that even at meter wavelengths, fine structure in radio sources exists over a wide range of angular sizes. It is interesting to examine whether the multi-component structure seen in the strong nearby radio sources e.g. Cygnus A and 3C 33, can explain the observed correlations between μ, Θ and S , under the assumption that the source morphology is preserved over the range of angular sizes and flux densities involved. This assumption seems to be justified from the fact that observations of a large number of weak radio sources (also having small Θ at 327 MHz) by the lunar occultation technique with a resolution of a few seconds of arc, also reveal morphological structures similar to those found for the strong nearby sources (Kapahi 1975b).

Let us consider the high resolution structure of Cygnus A and 3C 33, both of which are strong and nearby radio galaxies with redshift z ~ 0.06. These sources have been mapped at 5 GHz with a resolution of a few seconds of arc (Hargrave and Ryle 1974, Hargrave and McEllin 1975). 3C 33 has also been observed at 327 MHz and its structure has been studied with a resolution of 3" arc using the lunar occultation technique (Gopal-Krishna et al. 1976). In addition to the usual extended double structure, these studies reveal the presence of highly compact 'heads' of emission located at the outer edges of the two main components. For the purpose of illustration we have reproduced in Figure 5.7 the brightness distribution map of Cygnus A at 5 GHz from Hargrave and Ryle (1974). It has been
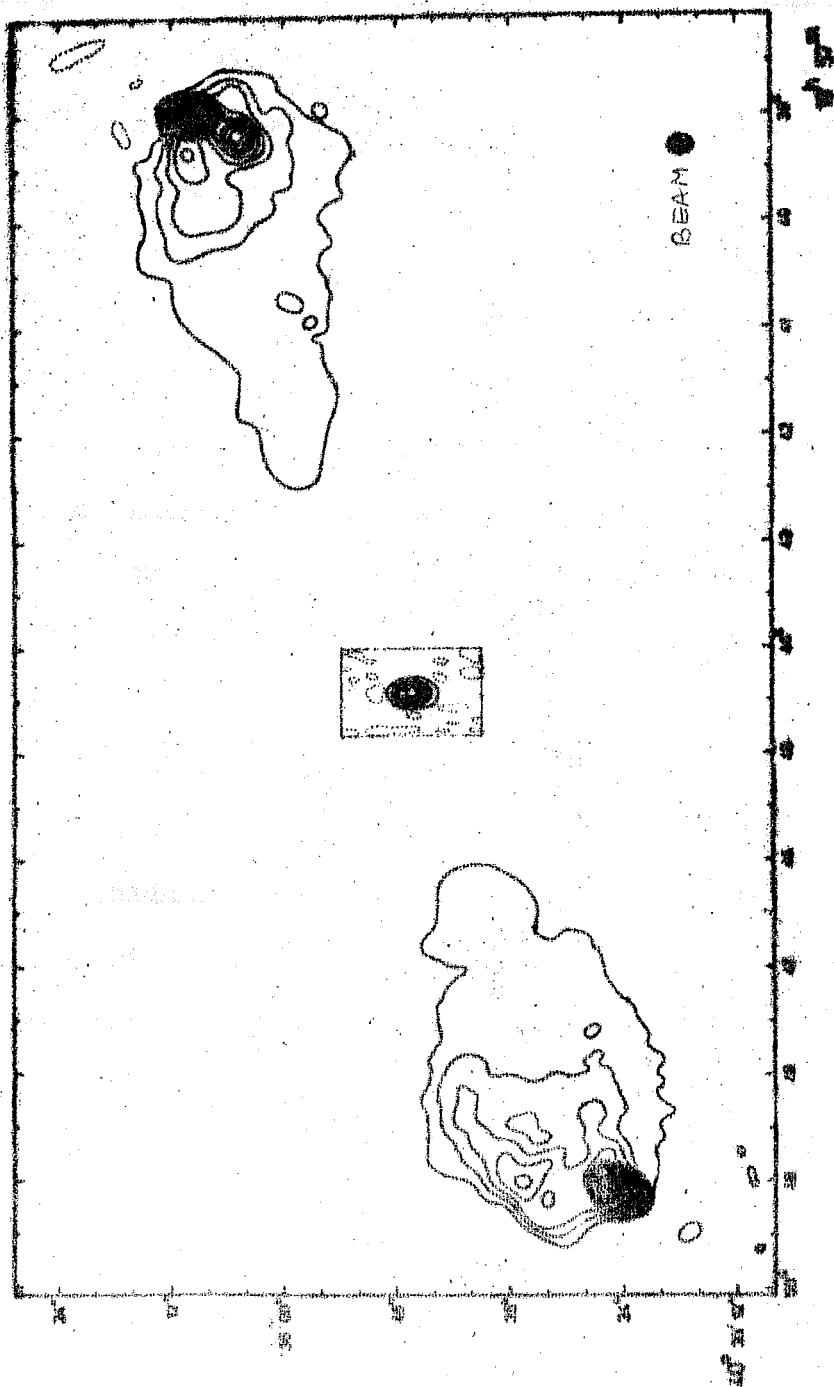
FIG.5.7 Brightness distribution map of Cygnus A at 5 GHz, taken from
Hargrave and Ryle (1974). 'Head-body-tail' type structure in
both components is clearly seen. The weak central component
has a flat spectrum and is not observed at meter wavelengths.

suggested that scintillations of radio sources arise from the
compact 'heads' of linear size 2-6 kpc, similar to those seen
in Cygnus A (Fig.5.7), and that in strongly scintillating radio
sources a substantial fraction of the source flux must origi-
nate in these compact 'heads' (Hewish et al. 1974, Kapahi 1975b).
However the above mentioned observations of Cygnus A, 3C 33 and
many other radio sources, recently mapped at 5 GHz (Pooley and
Henbest 1974, Longair 1975) show that a considerable part of
the emission of these sources also arise from the main 'body'
of each component (having an angular size nearly the same as
that of the source along its minor axis) and diffused tails or
bridges connecting the two components. If Cygnus A and 3C 33
were located much farther away, so that Θ becomes less than
$\sim 15''$ arc, these extended components would also contribute to
scintillations in addition to the compact heads. Since most of
the scintillating sources in the 3CR sample (Fig.5.6) have Θ
in the range of 5-50" arc and since average ratio of component
separation to the size of the 'body' subcomponent is about 8
(Mackay 1971, Swarup 1975b), it is likely that in many of these
sources the extended components would also be smaller than 2"
arc and would give rise to scintillations.

5.5.2 Model Calculations:

In order to explain the observed correlations
between μ, Θ and S we have approximated the observed bright-
ness distributions of Cygnus A and 3C 33 by a symmetrical double
model in which each component consists of 3 concentric gaussian

Table 5.4   Parameters of Models representing Cygnus A and 3C 33 at 81.5 MHz

| Model | Source | Separation/Sub-component size | | | Sub-component flux/Total flux | | |
		θ/ψ_1	θ/ψ_2	θ/ψ_3	α_1	α_2	α_3
A	Cygnus A	75	7.5	3	0.15	0.25	0.60
B	3C 33	55	25	3	0.56	0.22	0.22

Subscripts 1, 2 and 3 to ψ (half power diameter) and α refer to sub-components head, body and tail respectively;

Observed component separations for Cygnus A and 3C 33 are 124" and 250" arc corresponding to linear separations of 186 and 392 kpc respectively.

sub-components; a compact head, a less compact body and a diffused tail. The relative flux densities of each of the sub-components at 81.5 MHz were estimated from high frequency measurements using spectral information provided in the studies mentioned above. The ratio of angular separation to sub-component sizes (θ/γ_n) and the fractional flux densities in the sub-components α_n used to represent Cygnus A and 3C 33 are given in Table 5.4.

Calculations to derive model $\mu-\theta$ curves were made following the IPS theory of Readhead (1971) which was employed by Readhead and Hewish (1974) to interpret their 81.5 MHz IPS data. From the m-p curves given in Figure 8 of Readhead (1971) for different angular diameters of the scintillating components, we first estimate the scintillation index m at elongations of 35° and 90° that would be observed for each sub-component separately. These m-p curves are reproduced here in Figure 5.8. As shown in Chapter 2 (Sec.2.4), the observed scintillation index m_t for a source with three concentric gaussian components of angular size γ_1, γ_2 and γ_3 and containing fractional flux densities α_1, α_2 and α_3 respectively, is given by

$$m_t{}^2 = \alpha_1{}^2 m_1{}^2 + \alpha_2{}^2 m_2{}^2 + \alpha_3{}^2 m_3{}^2 + 2(\alpha_1 \alpha_2 m_{12}^2 + \alpha_2 \alpha_3 m_{23}^2 + \alpha_3 \alpha_1 m_{31}^2)$$

where m_1, m_2 and m_3 are scintillation indices for individual sub-components of size γ_1, γ_2 and γ_3 respectively, and m_{xy} are
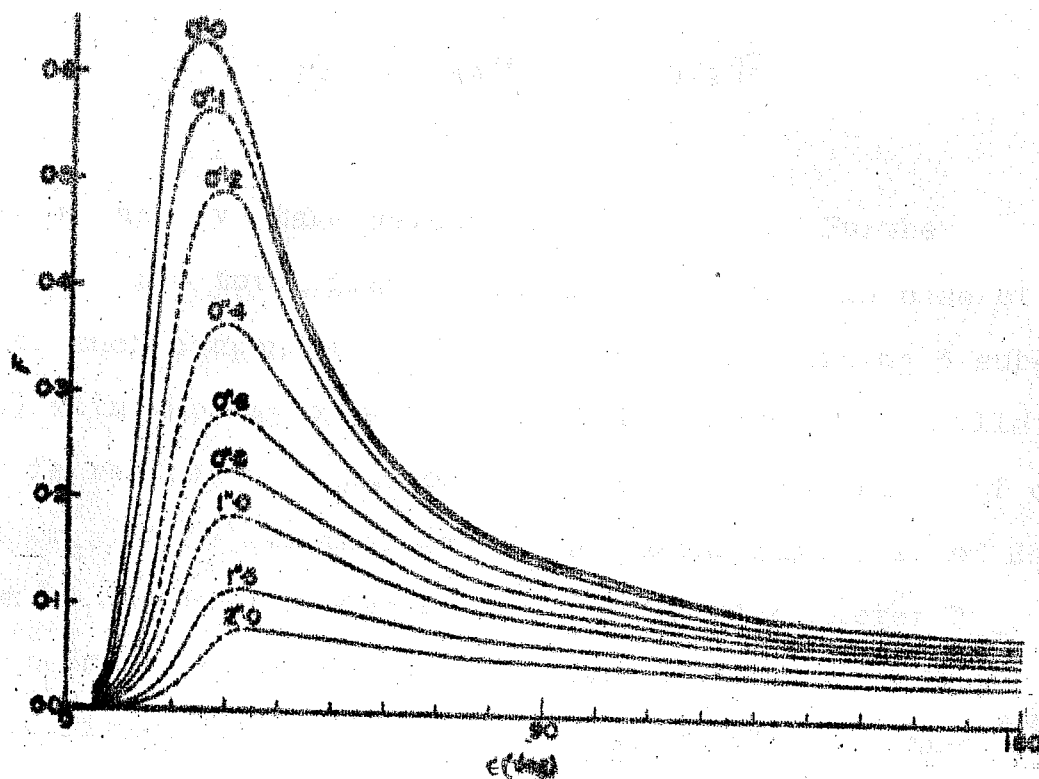
FIG. 5.8 Variation of scintillation index m with
elongation for sources with different
angular sizes at 81.5 MHz. This figure
is taken from Readhead (1971). The angu-
lar diameter values marked refer to (1/e)
diameters, $2\theta_0$ of the gaussian.

indices for components having equivalent sizes

$$\gamma_{xy} = [(\gamma_x^2 + \gamma_y^2)/2]^{\frac{1}{2}}$$

where x and y take values of 1, 2 and 3. Further $\alpha_1 + \alpha_2 + \alpha_3 = 1 =$ total flux of the source. Now, in case of a pair of such components (each component containing 3 sub-components) with separation $\Theta \gtrsim 2''$ arc, the observed scintillation index is reduced by a factor of $\sqrt{2}$. From the ratio of calculated m_t at 35° to that at 90° and using Figure 10 of Readhead (shown in Fig.5.9) we derive the equivalent diameter γ_{eq} that would be measured by Readhead and Hewish (1974). We then go back to Figure 5.8 and read off the value of m_{eq} that would be observed for an angular size of γ_{eq} at an elongation of 35°. The expected scintillation visibility for the model source under consideration can be found by taking the ratio of m_t to m_{eq} for 35° elongation. Using this procedure we have derived the expected values of μ for decreasing values of Θ for the models representing Cygnus A and 3C 33. It must be noted that for simplicity, we have assumed that the ratio of angular size of the sub-components to angular separation i.e. γ_n/Θ and fractional flux densities of the sub-components α_n are independent of Θ. The derived $\mu-\Theta$ curves are shown in Figure 5.6. These $\mu-\Theta$ curves are then combined with the observed $\Theta-S$ relation given by the best-fit parabolic curve of Swarup (1975a) shown in Figure 5.10. The $\mu-S$ curves so
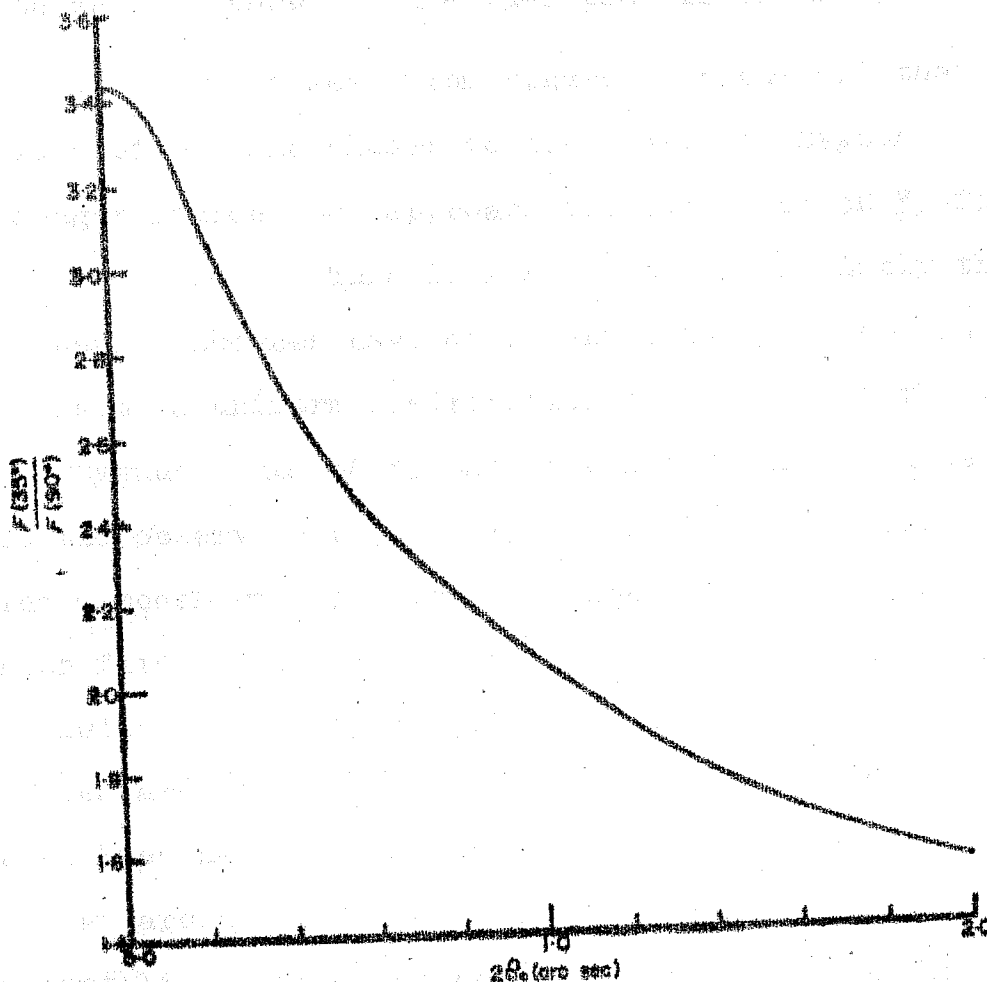
FIG. 5.9   The ratio m(35°)/m(90°) as a function of
source size at 81.5 MHz. This figure is
also taken from Readhead (1971).

obtained are shown in the μ-S plot in Figure 5.5.

It is seen from Figures 5.5 and 5.6 that the median values of μ lie closer to the model for Cygnus A for the stronger sources but approach the curve for 3C 33 for the weaker sources. This does not necessarily imply that stronger and weaker sources have different sub-structures in them. If we assume a uniform distribution of sources of the type ranging from Cygnus A to 3C 33 the calculated median values do not fit the observed points very well. It is possible however to find a model with arbitrarily chosen values of α_n and γ_n/θ which fits the observations but the model is neither unique nor realistic. From Figure 5.6, in which the data for 187 3CR sources are plotted, it is seen that the curve for Cygnus A model lies near the lower bound of data points. This indicates that at around 80 MHz the diffused features, although present, are not likely to be as prominent as assumed by us for Cygnus A.

5.6 CONCLUSIONS

With the availability of large scale IPS surveys carried out at Arecibo, Cambridge and Ooty it has become possible to define statistically complete samples of radio sources for the purpose of studying the dependence of scintillation visibility on flux density and overall angular extent of radio sources. Although large statistical uncertainties are present, we have shown that a clear correlation exists between median values of μ and S , which is free from observational selection effects.
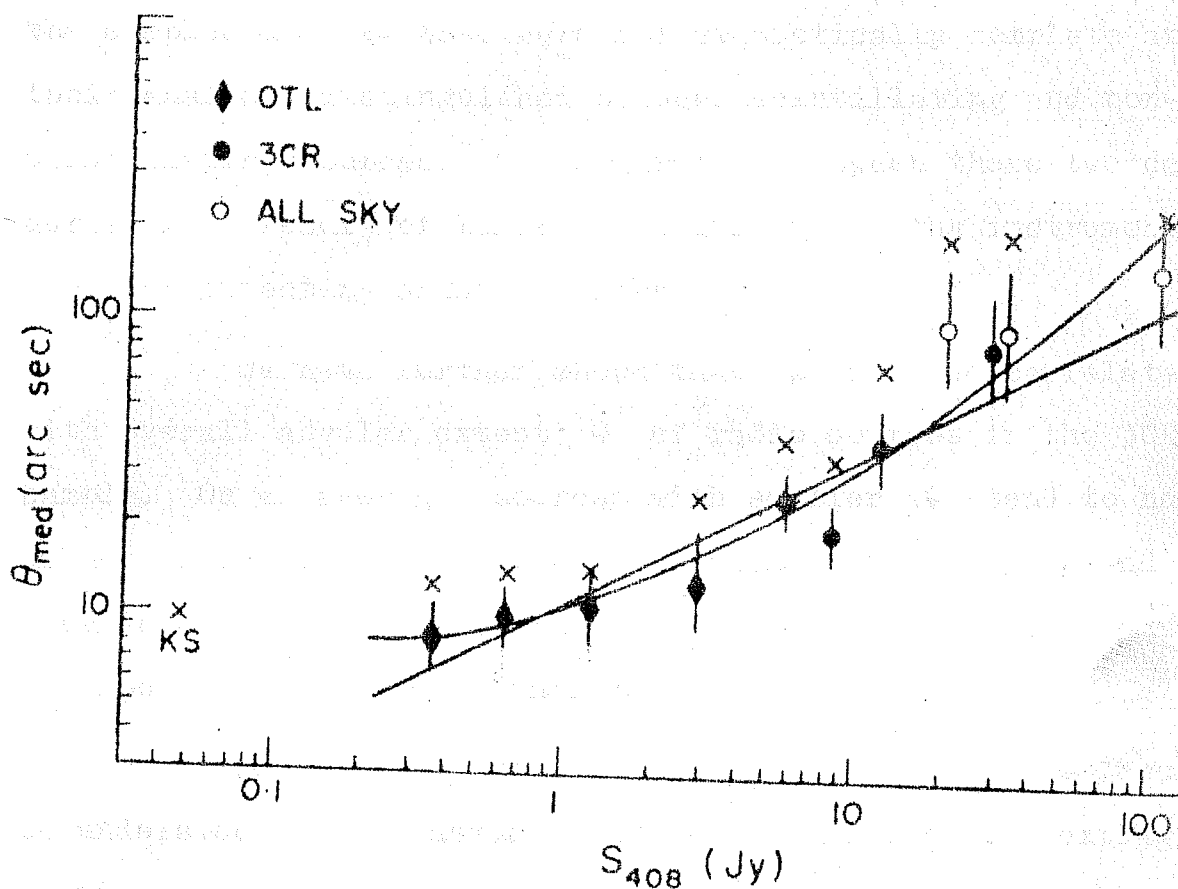
FIG. 5.10 Correlation between θ and S. Median values of θ are plotted against S_{408} for sources from Ooty lunar occultation (OTL), 3CR and All-Sky catalogues as described in Swarup (1975a) from which this figure is reproduced.

Earlier studies of the $\mu-S$ correlation by Harris and Hardebeck (1969) did not show any significant correlation perhaps because the samples used by them were not statistically complete and their analysis distinguished between scintillating and non-scintillating sources. The separation between these two categories is a result of limited sensitivity of the instrument used for detecting scintillations.

We have further shown that μ is also correlated with overall angular extent Θ of radio sources in the 3CR sample. On an average, sources with smaller Θ tend to have higher μ . These statistical relations between μ, Θ and S provide a strong evidence that statistically, the weaker sources are located farther away than the stronger ones.

The observed correlation between μ and Θ could be understood on the assumption that (a) most of the extragalactic radio sources have multi-component structures intermediate between those found in Cygnus A and 3C 33 and (b) the values of α_n and ψ_n/Θ are independent of Θ . The models used to represent Cygnus A and 3C 33 are considerably simplified but broadly explain the observed correlations and imply that a significant fraction of the flux density of many radio sources originates from components having angular sizes as small as (1/10)th to (1/50)th of the overall size Θ . Detailed high resolution observations of a large number of radio sources, providing information on the sizes and flux densities of individual sub-components are necessary to find representative *values of*

α_n and γ_n/θ and to investigate whether these depend on flux density or angular extent of radio sources.

CHAPTER 6

ANGULAR SIZE OF SCINTILLATING RADIO SOURCES AND COSMOLOGY

6.1 INTRODUCTION

Observations of interplanetary scintillations provide two parameters of the compact components in radio sources, the scintillation visibility and the angular size of the scintillating component. In Chapters 4 and 5 we have restricted our attention to the scintillation visibility parameter for studying the variation of scintillation properties of radio sources with distance i.e. with flux density, angular extent and redshift of radio sources. The scintillation visibility was found to increase statistically with decreasing flux density S, decreasing overall angular extent Θ and in case of identified sources with increasing redshift z . This indicated that weaker sources on the average are located farther away than the stronger ones and that scintillation visibility may also be used as a statistical distance indicator for radio sources. However, in these correlations a large amount of scatter was present and it was not possible to derive any cosmological inferences from the scintillation data.

Measurement of angular sizes of radio sources and their variation with redshift provide an important and direct means of studying cosmology. In this chapter we discuss the problems associated with the measurement of

angular sizes by the method of IPS and critically examine the use of angular size of scintillating components in radio sources for studying the geometry of the Universe. In particular we point out that the presence of multicomponent structure in radio sources would introduce an important selection effect in the measurement of angular sizes of the scintillating components by IPS technique.

Section 6.2 summarizes results of observational tests of cosmological theories based on angular size data and Sections 6.3 and 6.4 describe and discuss the use of angular size of scintillating components as 'rigid rods' for cosmological studies.

6.2 COSMOLOGY FROM ANGULAR SIZE DATA ON RADIO SOURCES

It is well known that the expected variation of angle subtended by an object of constant linear size with distance (redshift) is different in different cosmological models. For small redshifts, all models predict a linear decrease of angular size with redshift similar to that expected in Euclidean case. Beyond about $z \approx 1$ the angular size predicted by different cosmological models become significantly different. In relativistic cosmologies the angle subtended continues to decrease up to some redshift and then increases with redshift thereafter. This produces a minimum in the angular diameter – redshift relation in all Friedmann cosmologies. In the Steady State theory, on the other hand, the angular size first decreases with redshift and finally

approaches a constant value. Thus, as pointed out by Hoyle (1959), the observational detection of a minimum in the angular size - redshift relation for extragalactic objects provides a means of discriminating between the Steady State and relativistic models and to determine the value of deceleration parameter q_O of the Universe.

The basic requirement is to search for certain feature of extragalactic objects (e.g. linear sizes or separations of components) which does not have much intrinsic scatter associated with it and then study the variation of the corresponding observed angular size with redshift. It should also be possible to observe these objects to large redshifts say $z \sim 1$ or greater, where sufficiently large differences appear in the predictions of different cosmological models. However, because of difficulties in measuring the angular diameters of faint optical galaxies and clusters of galaxies, the data do not extend beyond about $z = 0.5$ and it has not been possible to determine the deceleration parameter q_O satisfactorily.

Through the use of modern, large and sensitive radio telescopes and interferometers it is now possible to detect and measure angular sizes of a large number of radio galaxies and QSOs extending to very high redshifts. While this makes radio sources promising candidates for cosmological studies, difficulties arise from the fact that radio sources are characterised by a large spread in physical sizes and it has not been possible to find any intrinsic size measure which can serve as

a satisfactory rigid rod. Miley(1971) made an attempt to use the angular separation Θ between the components of double radio galaxies and QSOs, having steep spectra, as a rigid rod and studied the dependence of Θ on z. The $\Theta - z$ relation has been discussed earlier (Sec.5.2). Although a large scatter was present, the $\Theta - z$ plot was found to display a definite upper envelope showing $\Theta \propto 1/z$, as expected in Euclidean geometry. This apparent Euclidean behaviour extended beyond $z \approx 2$ (Wardle and Miley 1974) contrary to the expectations of any of the reasonable cosmological models. The static Euclidean behaviour at large z was explained as due to the presence of evolution in the linear size of QSOs with cosmic epoch. A similar situation persists in the study of Swarup (1975b) who studied the correlation of angular sizes of individual components ($\omega_{\shortparallel}$ and $\omega_{\perp}$) of double radio sources, instead of their separation, with redshift. The evolution in the linear sizes of radio sources has also been inferred from a study of the angular size – flux density correlation and the angular size counts of radio sources (Kapahi 1975a).

Although these results do not support the Steady State theory, the angular size and separation of components of double radio sources do not lead to a unique estimate of q_0 either. This is because the evolutionary effects seem large and are difficult to estimate precisely. Furthermore the analysis is made difficult due to large dispersion in the intrinsic size of radio sources even when selected by certain criteria,e.g. radio

spectrum or structure, which are helpful in reducing the scatter in their properties.

Due to the above difficulties the component separation and component size of extragalactic double radio sources do not serve as satisfactory rigid rods for cosmological studies. One must therefore look for some other feature of the structure of radio sources which is expected to have little intrinsic scatter and which is relatively free of evolutionary effects.

6.3 STRONGLY SCINTILLATING RADIO SOURCES AS A RIGID ROD

Recently Hewish et al. (1974) suggested that the physical sizes of compact features that are located in the outer regions of strongly scintillating radio galaxies and QSOs ,   similar to the 'hot spots' found in Cygnus A, appear to provide the best approximation to a rigid rod for cosmological tests.   Angular size information on the scintillating components in a large number of 3C sources provided by the Cambridge IPS survey at 81.5 MHz (Readhead and Hewish 1974) was used by Hewish et al. for studying the angular size – redshift relation. Several selection criteria were employed to obtain a sample of 23 strongly scintillating sources from the well-known 3CR complete sample contained in the 81.5 MHz IPS survey.   The sources selected were expected to be

  i)   strongly scintillating sources ($\mu > 0.4$) for which Readhead and Hewish have obtained high quality data (denoted as class A sources in their IPS catalogue),

ii)   located at high galactic latitudes   ($|b^{II}| > 20^{\circ}$),

iii) non-variable, steep spectrum sources having typical double morphology with overall angular extent not less than a second of arc and

iv)   optically identified with magnitudes and redshifts measured.

Hewish et al. suggest that with these specifications they obtain a closely defined range of objects suitable for cosmological studies[†] since

a)   Non-variable, steep spectrum radio galaxies and QSOs generally have morphological structure similar to that of Cygnus A and the linear size of the hot spots located in their outer regions seem to have a narrow range of about 2 to 5 kpc. The aperture synthesis maps of brightness distribution of many sources at 5 GHz also show that the morphological characteristics e.g. the component sizes to separation ratios etc. are preserved over a wide range of overall angular sizes, and

b)   strongly scintillating sources are from the highest luminosity class of sources (Readhead and Longair 1975).

---

†   At this stage it may be worthwhile to point out that their sample of 23 sources (Prof. G. Swarup, private communication) does not seem to be quite uniform as some of the selection criteria seem to be only marginally satisfied. For example i) Two sources (3C 99, 237) are not part of the 3CR complete sample, (ii) three sources have $|b^{II}| < 20^{\circ}$, (iii) in the case of seven sources no redshift measurements are available in literature and for these redshifts indirectly estimated from magnitudes have been used. In three cases (3C 67,153 and 455) values of redshift used by them differs from those available in literature (e.g. Kraus and Gearhart 1975), (iv) some of the sources have their LAS close to 1" arc and (v) the examples cited by them to illustrate the selection/rejection criteria are of sources from outside the 3CR complete sample being considered.

The distribution of the angular sizes Υ of the scintillating components determined by the method of IPS (Readhead and Hewish 1974) in these 23 sources has been studied by Hewish et al. They found that there is a peak in the distribution around $0.''4$ arc. The paucity of sources with $\Upsilon \lesssim 0.''3$ arc in their sample is quite evident. The absence of small diameter sources could not be explained due to broadening of intrinsic angular diameter by interstellar scattering (ISS). Their 151 MHz IPS observation of some of the sources have been used to show that the measured IPS diameters at 81.5 MHz are largely unaffected by ISS.

Another selection effect that has been considered by them is that when a source is located far away so that the diameter of its compact component is $< 0.''3$ arc, its scintillating flux density may become very small and the scintillation data may not be of high quality due to poor S/N ratio. The source will then get removed from the sample. This was considered unlikely by Hewish et al. since it would have implied a correlation between angular size and flux density which was not known at the time of their study. Recently a positive correlation between flux density and overall angular size has been observed (Swarup 1975a). However, the effect of such a correlation on the Hewish et al. sample may not be severe in view of the fact that decrease of flux density and angular size with distance

This, coupled with the smallness of the sample, used by Hewish et al., makes it rather difficult to know how unbiased and representative their sample is of the general radio source population. In what follows, however, we consider only those selection effects which are independent of the non uniformities of the sample considered above.

simultaneously involves an increase in scintillation visibility (scintillating flux) of the source as shown in Chapter 5.

In order to understand the cause of the peak in the γ-distribution Hewish et al. plotted the angular size of scintillating components in these sources against their redshift. The γ-z plot (Fig.3 in the paper by Hewish et al.) appears more or less like a scatter diagram without any significant trend. However, when the data are compared with the expected variation of the angular size of a rigid rod of 3.5 kpc in different cosmological models over a range of values of q_0, a significant deficiency of sources with $\gamma < 0.3$ arc emerges for $0.7 < z < 1.6$. They consider this as real and conclude that the observations are consistent with non-Euclidean world models with q_0 in the range 0.5 to 2.0. Even higher values of q_0 would be obtained if evolution in the size of scintillating components, similar to that observed for overall linear size of radio sources, is included.

6.4 DIFFICULTIES WITH THE COSMOLOGICAL INTERPRETATION OF THE OBSERVED γ-z RELATION

The suggestion by Hewish et al. (1974) that the 'hot spots' in strongly scintillating radio sources serve as a reliable rigid rod has important implications for cosmological studies and needs critical examination. In the following we consider some of the problems in associating the angular sizes of scintillating components measured by the method of Readhead and Hewish(1974) with the angular size of 'hot spots' alone.

One of the basic problems involved in using the measured value of the angular size of scintillating component Ψ, by the method of Readhead and Hewish (1974), as representing the angle subtended by a given linear feature of a radio source(e.g. hot spots) arises mainly because of the fact that the occurrence of IPS is sensitive to angular, rather than linear size. A source will not scintillate at 81.5 MHz unless some component of it subtends an angle less than ~ 2" arc. With increasing distance, i.e. at larger redshifts, components of larger and larger linear sizes contribute to observed scintillations (at least up to a distance where cosmological broadening is not significant). The angular size measured by IPS method therefore may not correspond to the same linear feature in radio sources located at different redshifts. This characteristic property of IPS, therefore, introduces difficulties in the use of angular size of scintillating components as rigid rods for cosmological studies. It should be noted at this point that such a difficulty does not arise when the largest angular separation Θ ($\equiv$ LAS) is used for the purpose, since at all distances the measured Θ refers to the total linear extent of the source.

Furthermore, in the presence of multicomponent structure in radio sources (Hargrave and Ryle 1974, Pooley and Henbest 1974, Hewish et al. 1974), the above property of the IPS phenomenon of being sensitive only to angular scales smaller than a certain limit, provides a possible non-cosmological explanation of the observed lack of small diameter (< 0".3 arc) scintillating components. In order to illustrate how the angular sizes

measured by Readhead and Hewish (1974) are affected by the
simultaneous presence of more than one scintillating component,
let us consider a simplified head-body-tail structure for radio
sources (see Sec.5.5.2). When the source is located nearby, no
component subtends an angle < 2" arc and it does not produce
scintillations. With increasing distance the head component
starts scintillating and as long as the angle subtended by the
body component does not become small enough to scintillate, IPS
observations will correctly reveal the flux and the angular
size of the scintillating head component. Beyond that distance,
both the head and the body components scintillate and as shown
in Section 5.5.2 the angular size measured using the ratio
m $(35^{\circ})/m$ (90°) will be an equivalent size Ψ_{eq}, intermediate
between the size of head and body components. The actual value
of Ψ_{eq} will depend on the relative angular sizes and flux den-
sities of the scintillating components. In the terminology of
Section 5.5.2 let us consider a source with $\alpha_1 = \alpha_2 = 0.5$ (and
$\alpha_3 = 0$ i.e. no extended tail component) and $\Psi_2 = 10\,\Psi_1$. Now
if the source is located at such a distance that $\Psi_1 = 0.4$ arc
and $\Psi_2 = 4.0$ arc, then the measured size Ψ_{eq} will be ~ 0.4
arc since there is no contribution to scintillation from the
body component. At progressively larger distances i.e. when
Ψ_1 and Ψ_2 are, say, 0.3 & 3.0, 0.2 & 2.0 and 0.1 & 1.0 arc
the angular sizes Ψ_{eq} derived by Readhead and Hewish (1974),
based on the method of Readhead (1971) and explained in Chapter
5 would be 0.37, 0.34 and 0.30 arc respectively. This illust-
rates that with increasing distance, when Ψ_1 has decreased

linearly, the measured size γ_{eq} has remained at quite a high value.   In other words, when the size of the head component has decreased by a factor of 4, the measured size has decreased only by a factor ~ 1.3.   This is due to the presence of a larger body component, which contributes to scintillations only at larger distances.   Since the IPS method measures γ_{eq} and not γ_1, we do not expect to observe a continuous linear decrease of the measured angular size with distance.   This could explain the observed behaviour of the γ-z plot of Hewish et al. (1974).

Many of the 23 sources chosen by Hewish et al. with $\mu > 0.4$ have their largest angular extent θ considerably smaller than 30" arc, as can be seen from Figure 5.6.   As discussed earlier the average ratio of the size of body subcomponent to separation is $\sim 1/10$ or $1/8$ and the compact head subcomponent has a size almost an order of magnitude smaller (Hooley 1974, Hargrave and Ryle 1974).   These subcomponents together are likely to constitute a major fraction of the total flux of the source for the strongly scintillating 3CR sources considered by Hewish et al.   In the case of sources with overall angular extents $\theta < 10"$ arc, which are largely QSOs, all the three components (i.e. the whole source) may be effective in producing scintillations.   The IPS measurements would lead to γ_{eq} which is intermediate between γ_1 and γ_2.   Now since γ_{eq} is greater than γ_1, observed sizes will be larger than expected thereby explaining the observed deficiency of small diameter scintillating components, especially at high z.

With a sufficiently accurate knowledge of the fine structure of the radio source in question, however, it may be possible to interpret the observed m-p curves differently and obtain some idea of ψ_1 and ψ_2 individually. Such an interpretation of the IPS observation has been attempted earlier by Cambridge workers for 3C 273. We have chosen to mention the case of 3C 273 since it is known to have multicomponent structure at low frequencies and since its IPS observations at 81.5 MHz at Cambridge have been interpreted in two different ways:

i)   From interferometric and lunar occultation studies 3C 273 is known to consist of a compact and an extended component at meter wavelengths. Utilising this information Bell and Hewish (1969) interpreted the observed m-p curve at 81.5 MHz as showing the presence of two components. They could explain their observations satisfactorily by assuming a two component model for the source comprising of (a) a 0.17 arc component containing 40 % of the total flux and (b) a 1.7 arc component containing the remaining 60 % of the flux, consistent with the interferometric observations (Bell and Hewish 1969 and references therein).

ii)   When no consideration is given to the known structure of the source an equivalent size ψ_{eq} is determined for the scintillating component from the measured m-p curve at 81.5 MHz. Readhead and Hewish (1974) determine the ratio $m(35^{\circ})/m(90^{\circ})$ and using the method of Readhead (1971) routinely arrive at an angular size of 0.85 arc (quoted as 0.55 arc in Readhead (1972)) for the scintillating component in 3C 273.

This clearly indicates that the determination of angular size of the scintillating component in a radio source, based on the observed slope of the m-p curve (Readhead 1971), provides an answer which is a weighted average of the sizes of all the scintillating compact components present in the source.

Not much information is available on the detailed fine structure of radio sources at meter wavelengths with resolution comparable to that of IPS in order to investigate the role of various compact components in the scintillation studies. Recently some limited VLBI measurements at low frequencies have become available. Resch (1974) has studied compact components in a number of strong sources at 74 MHz using the VLBI technique and compared the measured angular sizes with those obtained from IPS studies at 81.5 MHz by Readhead and Hewish (1974). Direct comparison was possible in the case of only 10 3CR sources. Scintillation diameters were found to be significantly higher than the corresponding VLBI diameters in the case of 6 sources. Resch (1974) concluded that "the angular diameters measured by Readhead and Hewish were either too large by an amount of 0.1 to 0.3 arc compared to VLBI diameters, or that the presence of source structure confused the determination of angular sizes in one or both of the techniques". This result is consistent with our suggestion that the angular diameters measured by Readhead and Hewish using IPS refer to the weighted angular size of the compact head and diffused body subcomponents in extragalactic radio sources.

CHAPTER 7

CONCLUSIONS

In this chapter we summarize the main conclusions of our investigations on the characteristics of compact sub-arc second angular structures in extragalactic radio sources revealed by their IPS observations at meter wavelengths.

In view of the lack of quantitative IPS data on compact components in southern radio sources, we carried out an IPS survey of about 500 radio sources located between 0° and -30° declinations, at 327 MHz using the Ooty Radio Telescope. The results on the **derived** angular sizes Υ and fractional flux densities μ of compact scintillating components in 188 sources observed during the first part of the Ooty survey are presented. This survey extends and complements the existing IPS studies of northern sky sources at 430 MHz by the Arecibo IPS group. Simultaneously with our survey, results of an extensive 81.5 MHz IPS survey were published by the Cambridge group. Together these surveys provide valuable high resolution information in more than 1800 radio sources stronger than a few Jy at meter wavelengths. In this thesis we have studied the role of compact scintillating components in extended extragalactic radio sources by combining the high resolution information obtained from IPS and the overall structure and morphology known from extensive interferometric and aperture synthesis studies.

Determination of the fine structure of radio sources using IPS technique is necessarily indirect and depends on a number of assumptions regarding the IPM and the radio sources. By making IPS observations on compact point-like radio sources, a self-consistent model of average characteristics of the plasma density irregularities responsible for IPS is derived and used in estimating the fine structure of extended radio sources. In the present work, as well as in other IPS surveys, it has been assumed that the electron density irregularities in the IPM have a gaussian spatial wavenumber spectrum for which a correlation scale can be defined. The temporal spectra of scintillations for 5 compact sources observed at 327 MHz were approximately gaussian in shape and the measured width f_2 of these spectra were used to estimate the irregularity size. This was found to be $\simeq 100$ km for $0.25 \lesssim p \lesssim 0.7$ a.u. (Rao, Bhandari and Ananthakrishnan 1974).

Spacecraft in-situ measurements of the interplanetary plasma, on the other hand, have indicated that the density fluctuations in the IPM over the entire range of scales from $\sim 10^6$ km to ~ 10 km, follow a power-law spectrum with index close to the Kolmogorov value (Jokipii and Hollweg 1970, Jokipii 1973). Information concerning the shape of the irregularity spectrum in the high wavenumber region applicable to IPS, is contained in the observed scintillation spectrum. Recently it has been shown that the high frequency portion of the observed IPS spectra are better fitted

by a power law (Coles et al. 1974, Milne 1976, Pynzar et al. 1976). Also, numerical computations of the scintillation index-elongation curve by Marians (1975) based on the strong scattering theory of Rumsey (1975) and a power law model for the interplanetary irregularities provide a good fit to the complete m vs. p curve for several sources, including the crab pulsar, at 74 MHz (Sime 1976). However, the density spectrum inferred from IPS as well as the spacecraft measurements show significant flattening near wavenumber corresponding to proton gyroradius in the IPM (Unti et al. 1973, Coles et al. 1974). In addition, spacecraft measurements frequently reveal the presence of a small but statistically significant enhancement at the proton gyroradius (Neugebauer 1975). Power law indices vary from day to day and on the average, the spacecraft spectrum is significantly steeper than that found from IPS (Rickett 1973, Coles et al. 1974, Lotova 1975). Thus the spectrum of density irregularities in the range of scales applicable to IPS, departs significantly from the overall background power law spectrum in such a way that the scales near the proton gyroradius which is about 100 km near 1 a.u., are most affective.

Hewish (1972) supported the gaussian spectrum on the basis of the observed $m \propto \lambda$ dependence from IPS observations over a large range of wavelengths and elongations. The power law spectrum predicts $m \propto \lambda^{1.25}$ or a steeper dependence on wavelength and Hollweg and Jokipii (1972) have stressed that

the existing IPS observations, made on different sources under different solar-interplanetary conditions, do not rule this out. Simultaneous multifrequency observations of IPS of well-studied compact radio sources are needed to establish the dependence of m on λ precisely.

Effect of the assumed form of irregularity spectrum on the derived values of μ and ψ from scintillation data has been studied recently by Sime (1976) and Armstrong and Coles (1978). It is shown that the diameters of the scintillating components derived on the basis of power law model and Rumsey-Marians theory at 74 MHz are in reasonable agreement with those estimated by Readhead and Hewish (1974) at a nearby frequency of 81.5 MHz assuming a gaussian spectrum. Power law model was however found to lead to scintillating fluxes or scintillation visibility μ about a factor of 1.5 smaller than those derived by Readhead and Hewish.

It must be noted that in both the Arecibo and the Ooty IPS surveys CTA 21 was assumed to represent an ideal point source even though the maximum observed value of m for it was ≤ 0.6. Recent IPS observations of PKS 1148-00 and a few other compact ($\psi \leq 0".02$ arc) sources (PKS 0019-00, 0056-00, CTA 21 and 2203-18) at 408 MHz at Molonglo (Milne 1976) and of PKS 1148-00 at 327 MHz at Ooty (Swarup 1978) have indicated significantly higher values of m of 0.8 or 0.9. The large difference in observed peak values of m for two sources, namely CTA 21 and 2203-18, which are common between

Molonglo and Ooty needs to be investigated carefully when detailed scintillation index measurements from Molonglo become available. If more, detailed and systematic, observations confirm higher observed values of m, the estimated values of μ will have to be decreased by a factor of ~ 1.5. Such a downward bias is also indicated by the maximum interferometric fringe visibilities of many compact radio sources at 430 MHz when normalised using a pulsar for a point source (Broderick and Condon 1975). Being a constant bias this will not affect our analysis since we have mainly concerned ourselves with the relative properties of compact features in radio sources of different types and at different levels of flux density etc. With these remarks on the estimation of structure of radio sources from IPS we now summarize and discuss the results obtained in the preceding chapters.

In Chapter 4, we have studied the occurrence of scintillating compact structures in a statistically unbiased and random sample of 149 sources with $S_{327} \geqslant 2.5$ Jy selected from Ooty IPS data. From this study we have shown that:

(i)   Compact sub-arc second components are a common feature of radio source structure at meter wavelengths. More than 50 to 60% of all sources contain appreciable scintillating components with angular sizes $\leqslant 0.5$ arc.

(ii)   The average scintillation properties show a progression from radio galaxies to unidentified sources to QSOs.

While most galaxies scintillate weakly, QSOs in general have more pronounced compact features. Unidentified sources show intermediate properties consistent with the hypothesis that these are mostly powerful radio galaxies located at greater distances.

(iii)   Flat spectrum sources in general are characterized by high μ and their scintillating components are extremely compact ($\psi \lesssim 0\overset{"}{.}15$ arc). This is more pronounced in the case of QSOs. All QSOs with spectral index $\alpha < 0.4$ in our sample show $\mu = 1.0$. Since flat and steep spectrum QSOs are observed over similar ranges of redshift and flux density, it also implies that flat spectrum QSOs in general have smaller physical sizes.

(iv)   Combining all available IPS measurements on identified radio sources with measured redshift z and excluding flat or inverted spectrum sources, we have studied the dependence of μ on z. Using data on 104 radio galaxies and 88 QSOs having normal steep spectra we have shown that μ increases statistically with increasing z. At higher redshifts, large percentage of sources are strong scintillators.

These results are in agreement with several high resolution IPS and interferometric studies of compact features in independent samples of radio sources at a number of frequencies (Harris and Hardebeck 1969, Broderick and Condon 1975, Bentley et al. 1976, Readhead and Hewish 1976, Warwick 1977, Jenkins and McEllin 1977).

In Chapter 5 we have investigated the correlation bet-
ween scintillation visibility μ and flux density S of extra-
galactic radio sources using large, statistically complete and
unbiased samples drawn from the three IPS surveys covering a
wide range of flux density. Although large statistical and
estimation uncertainties are present due to upper and lower
limits on μ for many sources, we have shown, for the first
time, that a clear correlation exists between median values
of μ and S. Down to the flux density limit of the samples,
of about 7 Jy at 81.5 MHz (or about 2.5 Jy at 408 MHz) μ is
observed to increase statistically with decreasing S. The
median value of μ is found to increase from about 0.12 at
median $S_{81.5} \sim 75$ Jy to about 0.4 at $S_{81.5} \sim 10$ Jy.

We have also established a strong inverse correlation
between μ and overall angular extent $\theta (\equiv LAS)$ of radio sources
in the 3CR sample using data from the Cambridge IPS and aper-
ture synthesis surveys. With decreasing θ, larger and
larger fraction of total flux density of radio sources is
found to originate in compact scintillating components.
Though the number of galaxies, QSOs and unidentified sources
in this sample are small, the $\mu - \theta$ correlation seems to hold
individually for the three classes of radio sources. Most
scintillating sources, for which definite values of θ are
available, have θ in the range ~ 5 to 50" arc. This sug-
gests that even at meter wavelengths, appreciable fraction

of flux density of many 3CR sources originates from components with sizes (1/10) to (1/50)th of the overall size. Readhead and Hewish (1976) have confirmed the above correlation between μ and θ and have further shown that μ is also closely related to the overall linear size; strongly scintillating radio galaxies and QSOs have total linear extents smaller than about 200 kpc.

The observed increase of μ with decreasing S and θ, in conjunction with the observed statistical correlation between θ and S (Swarup 1975a), provides a strong evidence that weaker sources on the average are more distant than stronger ones.

We have attempted to explain the $\mu - \theta - S$ correlations as a geometrical distance effect in terms of the observed structure and morphology of two well-resolved and well-studied nearby radio sources, 3C 33 and Cygnus A. We have considered a highly simplified 3 sub-component structure for each of the components in these double sources. Fractional flux densities α_n and angular sizes ψ_r/θ of the sub-components were derived from various observations and were assumed to be independent of θ and S. Computations of the expected μ and ψ for the models representing the two sources were made following the procedure described in Chapter 2. Euclidean geometry was assumed and μ was

calculated at smaller and smaller θ and S. A comparison of computed $\mu - \theta$ and $\mu - S$ curves for the two sources with the observed values shows that the average compactness of 3CR sources is intermediate between that of 3C 33 and Cygnus A. In general, diffused features do not seem to be as prominent as those observed in Cygnus A.

Recently, long baseline interferometers sensitive to structures $\leqslant 1''$ arc have been used at Jodrell Bank to investigate the occurrence of compact components in different samples of radio sources covering a much wider range of flux density than has been possible through IPS (Speed 1976, Warwick 1977). Anderson et al. (1978) and Speed and Warwick (1978) have reported the observed variation of the fraction p of sources with maximum interferometer fringe visibility $\gamma_m > 0.5$ over the range of flux densities from about 25 mJy to ~ 100 Jy at 408 MHz. The parameter γ_m provides a measure of the fraction of total flux density of the source arising from regions $\leqslant 1''$ arc and is comparable to scintillation visibility μ estimated from IPS observations. The fraction p is observed to increase from 0.11 ± 0.08 at median $S_{408} \sim 29$ Jy to 0.39 ± 0.1 near $S_{408} \sim 1.5$ Jy. They have also estimated the median value of γ_m which is found to increase from about 0.05 for most intense sources to ~ 0.30 at $S_{408} \sim 1$ Jy. Within the errors

of estimation these results are fully consistent with the μ - S correlation observed by us. Between 1 Jy and 25 mJy, where no IPS observations are available, p remains constant at about 0.3 or possibly decreases slightly with decreasing flux density. Calculations to predict γ_m distribution at different flux density levels, based on the observed γ_m distribution for the most intense sample of 3CR sources studied using the same interferometer, have been made by Speed and Warwick (1978). They have shown that the observed behaviour of γ - S relation is difficult to explain in any standard cosmological model unless strong evolution in space density as well as an evolution in linear sizes of radio sources with redshift are incorporated. A reasonable fit to the observed p- S trend could be obtained by adopting convent-ional forms for density ($\rho = \rho_0(1+z)^6$) and size ($l = l_0(1+z)^{-1}$) evolutions. Similar density evolution was also suggested by Readhead and Longair (1975) for explaining the non-uniform space distribution of strongly scintillating high luminosity sources in the 3CR sample. The $(1+z)^{-1}$ evolution of the overall linear size of radio sources has been invoked earlier to explain the observed θ - z and θ - S relations (Wardle and Miley 1974, Kapahi 1975a). The important thing revealed by the higher resolution interferometric and IPS studies of (γ/μ - S) relation is that the linear sizes of the compact ($\lesssim 1''$ arc) structures in radio sources should also evolve

in a similar fashion. This implies that the ratios of sub-component sizes to component separation ψ_n/θ remain nearly independent of z, justifying the assumption made in our computations of expected μ as a function of θ.

The implications of the use of angular diameters ψ of compact scintillating components in radio sources, estimated from their IPS observations at 81.5 MHz, in cosmological angular size-redshift relation and for models of evolution of double radio sources have been considered by Hewish et al. (1974) and Readhead and Hewish (1976). In a complete sample of appreciably scintillating ($\mu \gtrsim 0.25$) 3CR sources they observed a significant deficit of sources with $\psi \lesssim 0".3$ arc, specially at redshift $z > 0.7$. Hewish et al. conjectured that compact features in high luminosity radio sources that scintillate strongly are morphologically identical to the compact (a few kpc in size) hot-spots observed in the outer components of nearby powerful double radio sources e.g. Cygnus A and due to their small size dispersion hot-spots could serve as a reliable 'rigid-rod' for cosmological studies. Under the assumption that the measured diameter ψ for strongly scintillating high luminosity sources provides a direct measure of the hot-spot size, they compared the observed ψ-z relation with that expected for a rigid-rod of size 3.5 kpc in cosmological models with different values of

the deceleration parameter q_o. The observed deficit of small diameter components in high redshift sources was attributed to a high positive value of q_o, between 0.5 and 2.0. If q_o is to be smaller than about 0.5, the observations would imply that the average linear size of compact scintillating components increases with z. These results are in conflict with the $(1+z)^{-1}$ evolution in linear sizes of compact $\lesssim 1''$ arc structures suggested by the recent γ-S studies described above.

In Chapter 6 we have suggested a possible non-cosmological explanation of the observed lack of decrease of γ with increasing redshift z, in terms of an observational bias which arises when radio sources with multiple sub-component morphology of the type observed in 3C33 and Cygnus A are investigated by IPS. In nearby sources, only the most compact hot-spots are small enough to scintillate and the estimated values of μ and γ correctly represent the fractional flux density and angular size, respectively, of hot-spots. However, when such sources are observed at high z, the hot spots as well as the intermediate size ($\sim$ 10 to 20 kpc) subcomponents are likely to contribute to observed scintillations. The estimated μ and γ in this case will be weighted averages of the corresponding values for the individual scintillating sub-components. Since with increasing z, larger and larger

substructures contribute to IPS, the resultant μ and γ will be overestimates of the flux and angular size of hot-spots, in particular for sources at high z.

On the basis of the aperture synthesis observations of the brightness distribution of identified 3CR sources which are close enough to be mapped in some detail at 5 GHz, Hewish and Readhead (1976) have recently argued that the extended outer components that are present are too large (>20 kpc) to scintillate. Furthermore, from the observed value of $\mu > 0.7$ for most powerful sources at high z they imply that these extended components do not contain enough flux to cause significant overestimation of the angular size of hot-spots suggested by us.

It must however be noted that their interpretation of the observed $\gamma - z$ relation in terms of a high value of q_0 is based on strongly scintillating ($\mu > 0.7$) 3CR sources of high luminosity ($P_{178} \gtrsim 10^{27}$ Watts Hz^{-1} Str^{-1}) at high redshift ($z > 0.7$). These sources, due to their high redshift, are all QSOs. From the $\mu - \theta$ diagram for the 3CR sample (Fig. 5.6) it is clear that sources with $\mu > 0.7$ have overall angular extent $\theta < 10''$ arc and in many cases θ is even less than $2''$ arc. Readhead and Hewish (1976) have also shown that in high luminosity sources, in general, the extended components remain unresolved with the 5 km telescope

and have linear sizes $\leq$ 20 kpc. In some cases (viz. 3C 138, 286, 287, and 454.3) IPS as well as other high resolution interferometric observations indicate that even the total extent of the source is < 10 kpc. Presently it is not possible to resolve and map the structure and morphology of high luminosity sources in any detail.

If it is assumed that these sources have morphological characteristics, such as the ratios of component sizes to their separation , similar to those obtained directly from mapping the larger sources (Hewish et al. 1974) then it is clear that, in addition to the hot-spots, the extended components will also scintillate. Furthermore, when the overall extent of the source is < 10 kpc, IPS observations at 81.5 MHz can not distinguish individual scintillating components in the source. Since all the scintillating components of the source lie within $\sim$1" arc, μ is close to 1 and the estimated ψ will be grossly determined by the angular extent of the source rather than by the size of compact hot-spots embedded within it. This qualitatively explains the observed behaviour of ψ-z relation at high z.

It is also possible that the structure and morphology of the high luminosity QSOs differ somewhat from those of nearby sources e.g. Cygnus A which, as seen from μ-θ-S studies presented in Chapter 5, does not seem quite typical

of highly scintillating radio sources. Strongly scintillating 3CR sources are in general more compact. Morphological characteristics of high luminosity 3CR sources have been investigated by Fanaroff and Riley (1974) and Riley and Jenkins (1977). Although it was shown by Fanaroff and Riley that sources with $P_{178} \gtrsim 2 \times 10^{25}$ Watts Hz^{-1} Str^{-1} have symmetrical double morphology similar to Cygnus A with compact hot-spots located near the outer boundaries of the source, their study included very few QSOs. On the other hand, Riley and Jenkins (1977) have compared the structures of high luminosity ($P_{178} \gtrsim 10^{26}$ Watts Hz^{-1} Str^{-1}) radio galaxies and QSOs using the complete sample of 3CR sources mapped at 5 GHz. They have found that, unlike galaxies, an appreciable fraction of QSOs appear to possess an asymmetric double (D2 type) structure and their central components are in general much more luminous than those associated with galaxies. In an investigation of the fine structure of a complete sample of Parkes QSOs, Bentley et al. (1976) have also noted that, even amongst steep spectrum QSOs, a sizable fraction display D2 type morphology. It is likely that in some high luminosity high redshift sources the scintillating component may be associated with the compact radio components associated with the optical object rather than with the outer hot-spots.

Due to these difficulties, the angular size ψ esti-
mated from IPS observations does not unambiguously measure
the size of a distinct structural feature, e.g. hot-spots, in
radio sources at all redshifts. Furthermore, it is also
necessary to understand (and apply correction for) the
precise nature and form of the possible evolution in the
linear sizes of compact scintillating components with cosmic
epoch, before using the observed $\psi - z$ relation for inferring
the geometry of the Universe.

REFERENCES

AARONS,J.   1975   PROC.BEACON SAT.
                                                     INVESTIGATIONS
                                                     OF THE IONOSP-
                                                     HERIC STRUCTURE
                                                     NOV. 1974
                                                     1, 184.

ALTSCHULER,D.R. AND WARDLE,J.F.C   1975   NATURE 255,306.

ANANTHAKRISHNAN,S.   1976   PH.D. THESIS,UNI
                                                     OF BOMBAY.

ANDERSON,B. ET AL.   1978   NATURE 271, 636.

ANDREWS,P.J. ET AL.   1974   MNRAS 167,7P.

ARMSTRONG,J.W.   1977   ASTR.AP. 61, 313.

ARMSTRONG,J.W. AND COLES,W.A.   1978   UCSD PREPRINT

BELL,M.B. AND FORT,D.N.   1973   AP.J. 186,1.

BELL,S.J. AND HEWISH,A.   1969   AP.LETT. 4,211.

BENTLEY,M. ET AL.   1976   MNRAS 176, 275.

BIRAUD,F.   1971   NATURE 232, 178.

BLANDFORD,R.D. AND REES,M.J.   1975   CONTEMP.PHY.16,1.

BLUM,E.J.   1959   ANN. D'AP. 22,
                                                     140.

BOLTON,J.G.   1966   NATURE 211, 917.

BOND,H.E.   1971   AP.J.(L),167,79.

BOURGOIS,G. AND CHEYNET,C.   1972   ASTR.AP. 21, 25.

BRACCESI,A. ET AL.   1970   ASTR. AP. 6, 268.

BRACEWELL,R.N.   1965   THE FOURIER TRA-
                                                     NSFORM AND ITS
                                                     APPLICATIONS
                                                     (MCGRAW HILL,
                                                     N.Y.) PP110.

BRAMLEY,E.N.   1954   PROC.ROY.SOC.(A)
                                                     225, 515.

BRAMLEY,E.N. AND YOUNG,M. 1967 PROC. IEE 114, 553.

BRODERIC,J.J. AND CONDON,J.J. 1975 AP.J. 202, 596.

BROTEN,N.W. ET AL. 1967 SCIENCE 156,1592.

BROTEN,N.W. ET AL. 1969 MNRAS 146, 313.

BUCKLEY,R. 1975 J.ATMO.TERR.PHYS. 37, 1431.

BURBIDGE,G.R. 1967 NATURE 216, 1287.

BURBIDGE,G.R. AND O'DELL,S.R. 1972 AP.J. 178, 583.

CHRISTIANSEN,W.A. ET AL. 1976 NATURE 266, 593.

CLARK,T.A. AND ERICKSON,W.C. 1973 PROC. IEEE 61, 1230.

CLARK,B.G. ET AL. 1968 AP.J.(L),153, 67.

CLARKE,R.W. ET AL. 1969 MNRAS 146, 381.

COHEN,M.H. 1969 ANN. REV. ASTR. AP. 7, 619.

COHEN,M.H. AND GUNDERMANN,E.J. 1969 AP.J. 155,645.

COHEN,M.H. ET AL. 1967A AP.J. 147,449.

COHEN,M.H. ET AL. 1967B AP.J. 150, 767.

COLES,W.A. AND RICKETT,B.J. 1976 J.GEOPHYS.RES. 81, 4797.

COLES,W.A. ET AL. 1974 PROC.SOLAR WIND 3 ED.RUSSELL 351.

COLLINS,R.A. AND SCOTT,P.F. 1969 MNRAS 142, 317.

CONWAY,R.G AND STANNARD,D. 1972 MNRAS 160, 31P.

CONWAY,R.G. ET AL. 1974 MNRAS 168, 137.

COOLEY,J.W. AND TUKEY,J.W. 1965 MATH.COMP. 19, 297.

COOLEY,J.W. ET AL. 1970 J.SOUND VIB. 12. 315.

CRITCHLEY,J. ET AL.   1972   MNRAS 160, 271.

DE YOUNG,D.S.   1976   ANN. REV. ASTR.
                                                         AP. 14, 447.

DISNEY,M.J. ET AL.   1974   AP.J.(L), 194,
                                                         79.

DUFFETT-SMITH,P.J. AND   1976   MNRAS 174, 7.
   READHEAD,A.C.S.

EKERS,J.A. (ED); PARKES CAT.   1969   AUST.J.PHYS.AP.
   OF RADIO SOURCES   SUPPL.NO.7.

EKERS,R.D.   1967   PH.D. THESIS,
                                                         AUST. NAT. UNI.

EKERS,R.D. AND EKERS,J.A.   1973   ASTR. AP. 24,
                                                         247.

ELSMORE,B. AND MACKAY,C.D.   1969   MNRAS 146, 361.

FANAROFF,B.L. AND LONGAIR,M.S.   1972   MNRAS 159,119.

FANAROFF,B.L. AND RILEY,J.M.   1974   MNRAS 167, 31P.

FLASAR,F. AND MORRISION,P.   1976   AP.J. 204, 352.

FOMALONT,E.B. AND MILEY,G.K.   1975   NATURE 257, 99.

FRYE,G.M. ET AL.   1971   NATURE 233, 466.

GARDNER,F.F. ET AL.   1969   AUST.J.PHY.22,79.

GOPAL-KRISHNA   1977   NATURE 269, 780.

GOPAL-KRISHNA ET AL.   1976   AP.LETT.17, 11.

GOWER,J.F.R ET AL.   1967   MEM.RAS 71, 49.

GUELIN,M.   1973   PROC.IEEE 61,
                                                         1298.

HARGRAVE,P.J. AND MCELLIN,M.   1975   MNRAS 173, 37.

HARGRAVE,P.J. AND RYLE,M.   1974   MNRAS 166, 305.

HARGRAVE,P.J. AND RYLE,M.   1976   MNRAS 175,481.

HARRIS,D.E.   1973   ASTR.J. 78, 369.

HARRIS,D.E.   1974   ASTR.J. 79, 1211.

HARRIS,D.E. AND HARDEBECK,E.G.   1969   AP.J.(SUPPL),
                                                   19, 115.

HAZARD,C. AND SUTTON,J.   1971   ASTR.J. 76, 609.

HEWISH,A.   1972   PROC.SOLAR WIND 2
                                                   NASA SP-308,
                                                   477.

HEWISH,A. AND SYMONDS,M.D.   1969   PLANET. SP. SC.
                                                   17, 313.

HEWISH,A. AND READHEAD,A.C.S.   1976   AP.LETT. 18,1.

HEWISH,A. ET AL.   1964   NATURE 203,1214.

HEWISH,A. ET AL.   1974   NATURE 252, 657.

HOLLWEG,J.V. AND JOKIPII,J.R.   1972   PROC.SOLAR WIND 2
                                                   NASA SP-308,494

HOOLEY,T.   1974   MNRAS 166,259.

HOYLE,F.   1959   PARIS SYMPOSIUM
                                                   ON RADIO ASTR.
                                                   ED. BRACEWELL,
                                                   PP.529.

HUNSTEAD,R.W.   1971   NATURE 233, 401.

HUNSTEAD,R.W. AND JAUNCEY,D.L.   1970   MNRAS 149,91.

JAUNCEY,D.L. ET AL.   1970   AP.J. 160, 337.

JENKINS,C.J. AND MC ELLIN,M.   1977   MNRAS 180, 219.

JENKINS,C.J. ET AL.   1977   MEM.RAS 84, 61.

JOKIPII,J.R.   1973   ANN. REV. ASTR.
                                                   AP. 11, 1.

JOKIPII,J.R. AND HOLLWEG,J.V.   1970   AP.J. 160, 745.

JOKIPII,J.R. AND LEE,L.C.   1973   AP.J. 182, 317.

KAKINUMA,T. AND WATANABE,T.   1976   SP.SC.REV. 19,
                                                   611.

KAPAHI,V.K.   1971   NATURE 234, 49.

KAPAHI,V.K.   1975A   MNRAS 172,513.

KAPAHI,V.K.   1975B   PH.D. THESIS,UNI
                                                      OF BOMBAY

KAPAHI,V.K.ET AL.   1972   AP.LETT.11, 155.

KAPAHI,V.K. ET AL.   1975   J.INST.ELEC.TELC
                                                      ENGG. 21,117.

KELLERMANN,K.I. ET AL.   1968   AP.J.(L),153,209.

KELLERMANN,K.I. ET AL.   1969   AP.J. 157, 1.

KELLERMANN,K.I. ET AL.   1975   AP.J.(L),197,113.

KRAUS,J.D. AND GEARHART,M.   1975   ASTR.J. 80, 1.

KRISTIAN,J ET AL.   1974   AP.J. 191, 43.

LEGG,T.H.   1970   NATURE 226,65.

LITTLE,L.T.   1968   PLANET.SP.SC. 16,
                                                      749.

LITTLE,L.T.   1976   METHODS OF EXPTL.
                                                      PHYS. (ACAD.
                                                      PRESS) 12, 118.

LITTLE,L.T. AND HEWISH,A.   1966   MNRAS 134,221.

LITTLE,L.T. AND HEWISH,A.   1968   MNARS 138, 393.

LONGAIR,M.S.   1966   MNRAS 133,421.

LONGAIR,M.S.   1971   REP.PROGR. IN
                                                      PHYS.34, 1125.

LONGAIR,M.S.   1975   MNRAS 173, 309.

LONGAIR,M.S. AND GUNN,J.E.   1975   MNRAS 170, 121.

LONGAIR,M.S. AND POOLEY,G.G.   1969   MNRAS 145,121.

LONGAIR,M.S. ET AL.   1973   MNRAS 164, 243.

LOTOVA,N.A.   1975   SOV.PHYS.-USP.
                                                      18, 292.

LYNE,A.G.   1972   MNRAS 158, 431.

MACDONALD,G.H. ET AL.	1968	MNRAS 138, 259.
MACKAY,C.D.	1969	MNRAS 145, 31.
MACKAY,C.D.	1971	MNRAS 154, 209.
MARIANS,M.	1975	RAD.SC. 10, 115.
MENON,T.K.	1975	AP.J.(L) 199,161.
MERCIER,R.P.	1962	PROC.CAMB.PHIL. SOC. 58,382.
MILEY,G.K.	1971	MNRAS 152, 477.
MILLER,J.S.	1975	AP.J.(L). 200, 55.
MILLER,H.R. ET AL.	1974	ASTR.J. 79, 1352.
MILNE,R.G.	1975	AUST.J.PHYS. 28, 621.
MILNE,R.G.	1976	AUST.J.PHYS. 29, 201.
MUNRO,R.E.B.	1971A	AUST.J.PHYS. 24, 263.
MUNRO,R.E.B.	1971B	AUST.J.PHYS. 24, 617.
MUNRO,R.E.B.	1971C	AUST.J.PHYS. 24, 743.
MUNRO,R.E.B.	1972	AUST.J.PHYS. AP. SUPPL.NO.22
NEUGEBAUER,M.	1975	J.GEOPHYS.RES. 80, 998.
NICOLSON,G.D.	1971	NATURE 233, 155
OKE,J.B. AND GUNN,J.E.	1974	AP.J.(L),189,5.
PACHOLCZYK,A.G. AND SCOTT,J.S.	1976	AP.J. 203, 313.
PAULINY-TOTH,I.I.K. ET AL.	1976	NATURE 259, 17.
POOLEY,G.G. AND HENBEST,S.N.	1974	MNRAS 169, 477.

POOLEY,G.G. AND RYLE,M.   1968   MNRAS 139, 515.

PURCELL,G.H.   1973   PH.D. THESIS,
                                                 CALIFORNIA INST
                                                 OF TECHNOLOGY

PYNZAR,A.V. ET AL.   1976   SOV.ASTR. 19,711.

RAO,A. PRAMESH   1975   PH.D. THESIS,UNI.
                                                 OF BOMBAY

RAO,A. PRAMESH ET AL.   1974   AUST.J. PHY.27,
                                                 105.

RATCLIFFE,J.A.   1956   REP.PROG.PHYS.
                                                 19, 188.

READHEAD,A.C.S.   1971   MNRAS 155, 185.

READHEAD,A.C.S.   1972   PH.D.THESIS
                                                 UNIV. OF
                                                 CAMBRIDGE

READHEAD,A.C.S. AND HEWISH,A.   1972   NATURE 236, 440.

READHEAD,A.C.S. AND HEWISH,A.   1974   MEM.RAS 78, 1.

READHEAD,A.C.S. AND HEWISH,A.   1976   MNRAS 176, 571.

READHEAD,A.C.S. AND LONGAIR,M.S.   1975   MNRAS 170, 393.

REES,M.J.   1971   NATURE 229, 312.

REES,M.J.   1976   COMM. AP. 6, 113.

REES,M.J. AND SASLAW,W.C.   1975   MNRAS 171, 53.

RESCH,G.M.   1974   PH.D. THESIS,UNI.
                                                 OF FLORIDA-NASA
                                                 GSFC X-693-74-
                                                 324.

RICKETT,B.J.   1973   J.GEOPHYS.RES.
                                                 78, 1543.

RICKETT,B.J.   1977   ANN. REV. ASTR.
                                                 AP. 15, 479.

RICKETT,B.J. ET AL.   1976   J.GEOPHYS.RES.
                                                 81, 3845.

RILEY, J.M. AND JENKINS, C.J.   1977   RADIO ASTR. AND
                                                 COSMOLOGY (IAU#74)
                                                 ED. JAUNCEY, 237.

ROGER.S. ET AL.   1973   ASTR.J. 78, 1030.

RUMSEY,V.H.   1975   RAD. SC. 10, 107.

SALPETER,E.E.   1967   AP.J. 147,433.

SANDAGE,A.R.   1973   AP.J. 180, 687.

SARMA,N.V.G. ET AL.   1975   J.INST.ELEC.TELC
                                                   ENGG. 21,110.

SASLAW,W.C. ET AL.   1974   AP.J. 190, 253.

SCHMIDT,M.   1968   AP.J. 151, 393.

SCHMIDT,M.   1972   AP.J. 176, 273.

SCHMIDT,M.   1974   CONF.ON RES. PR-
                                                   OG.FOR NEW LA-
                                                   RGE TELESCOPES.
                                                   ED.A.REIZ.,253.

SCOTT,M.A.   1977   MNRAS 179, 377.

SCOTT,P.F. AND SHAKESHAFT,J.R.   1971   MNRAS 154, 19P.

SETTI,G. AND WOLTZER,L.   1973   AP.J.(L) 181, 61.

SIME,D.G.   1976   PH.D. THESIS,UNI.
                                                   OF CALIFORNIA

SLEE,O.B. AND HIGGINS,C.S.   1973   AUST.J. PHYS. AP.
                                                   SUPPL. NO. 27.

SPEED,B.   1976   MNRAS 177,137.

SPEED,B. AND WARWICK,R.S.   1978   JODRELL BANK
                                                   PREPRINT

STRITTMATTER,P.A. ET AL.   1972   AP.J.(L),175, 7.

SWARUP,G.   1975A   MNRAS 172, 501.

SWARUP,G.   1975B   BULL. ASTR. SOC.
                                                   INDIA, 3, 24.

SWARUP,G.   1978   PROC.SP.SC.SYMP.
                                                   TRIVANDRUM
                                                   INDIA,1977

SWARUP,G. ET AL.   1971   NATURE 230,185

UNTI,T.W. ET AL.   1973   AP.J. 180, 591.

VERCN,M.P. AND VERON,P.   1974   ASTR. AP.(SUPPL)
                                                        18, 309.

WALL,J.V.   1972   AUST.J. PHYS. AP.
                                                        SUPPL.NO.24.

WARDLE,J.F.C. AND MILEY,G.K.   1974   ASTR. AP. 30,305.

WARWICK,R.S.   1977   MNRAS 179, 1.

WATANABE,T. ET AL.   1974   J.GEOPHYS.RES.
                                                        79, 3841.

WESTERLUND,B.E. AND WALL,J.V.   1969   ASTR.J. 74, 335.

WILKINSON,P.N.   1972   MNRAS 160, 305.

WILKINSON,P.N. ET AL.   1974   MNRAS 168, 515.

WILLS,D.   1974   CCNF.CN RES. PR-
                                                        OG. FOR NEW
                                                        LARGE TELESCO-
                                                        PES ED.A.REIZ,
                                                        275.

WRAITH,P.K.   1972   MNRAS 160, 283.

YULE,U.G. AND KENDAL,M.G.   1950   AN INTRODUCTION
                                                        TO THE THEORY
                                                        OF STATISTICS
                                                        (CHARLES GRIF-
                                                        FIN AND CO.
                                                        LONDCN), 425.